XLPR MODELS SUBGROUP REPORT

CRACK GROWTH AND COALESCENCE

PROBABILISTIC FRACTURE MECHANICS CODE

DISCLAIMER

THIS PUBLICATION WAS PREPARED AS AN ACCOUNT OF WORK JOINTLY SPONSORED BY THE ELECTRIC POWER RESEARCH INSTITUTE (EPRI) AND AN AGENCY OF THE U.S. GOVERNMENT. NEITHER EPRI NOR THE U.S. GOVERNMENT NOR ANY AGENCY THEREOF, NOR ANY EMPLOYEE OF ANY OF THE FOREGOING, MAKES ANY WARRANTY, EXPRESSED OR IMPLIED, OR ASSUMES ANY LEGAL LIABILITY OR RESPONSIBILITY FOR ANY THIRD PARTY'S USE, OR THE RESULTS OF SUCH USE, OF ANY INFORMATION, APPARATUS, PRODUCT, OR PROCESS DISCLOSED IN THIS PUBLICATION, OR REPRESENTS THAT ITS USE BY SUCH THIRD PARTY COMPLIES WITH APPLICABLE LAW.

EPRI RETAINS COPYRIGHT IN EPRI-GENERATED MATERIALS CONTAINED IN THIS PUBLICATION.

THIS PUBLICATION DOES NOT CONTAIN OR IMPLY LEGALLY BINDING REQUIREMENTS. NOR DOES THIS PUBLICATION ESTABLISH OR MODIFY ANY REGULATORY GUIDANCE OR POSITIONS OF THE U.S. NUCLEAR REGULATORY COMMISSION AND IS NOT BINDING ON THE COMMISSION.

xLPR Models Subgroup Report

Crack Growth and Coalescence

xLPR-MSGR-CGR Version 1.0	
Author Signature	**Date**
Kyle Schmitt Kyle Schmitt Crack Growth Subgroup Member	06/29/16
Reviewer Signatures	**Date**
Glenn White Glenn White Crack Growth Subgroup Lead	06/18/16
Dilip Dedhia Dilip Dedhia Crack Growth Subgroup Member	06/23/16
Bruce Bishop Bruce Bishop PIB Member	06/29/16
Approver Signatures	**Date**
Marjorie Erickson Marjorie Erickson, PEAI xLPR Models Group Lead	06/16/16
Craig Harrington Craig Harrington, EPRI xLPR Code Development Lead	06/28/16

THE TECHNICAL CONTENTS OF THIS DOCUMENT WERE <u>NOT</u> PREPARED IN
ACCORDANCE WITH THE XLPR SOFTWARE QUALITY ASSURANCE PLAN.

Revision History

Version Number	Description of Changes	Issue Date
1.0	Initial Issue	06/29/16
	The U.S. Nuclear Regulatory Commission Office of Nuclear Regulatory Research's and the Electric Power Research Institute's xLPR Project Contacts approved an administrative update in 2021 to support public release of this document without incrementing the version number or issue date. The administrative updates included: (a) title changed from "PWSCC & Fatigue Crack Growth and Coalescence Module Development" to "xLPR Models Subgroup Report—Crack Growth and Coalescence" throughout the document, (b) cover and title pages updated accordingly, (c) disclaimer statement added, and (d) statement that the document was not prepared in accordance with the xLPR Software Quality Assurance Plan added.	

EXECUTIVE SUMMARY

The Crack Growth Subgroup within the xLPR Models Group is responsible for selecting and implementing models for predicting the growth and coalescence of cracks in normal pressurized water reactor (PWR) environments under constant and cyclic loading conditions.

This report presents the following information related to the Crack Growth Subgroup's efforts:

- Development of models for predicting PWSCC crack growth rate in Alloy 600 and Alloys 82/182/132, including technical bases, underlying assumptions, and mathematical descriptions.

- Development of models for predicting fatigue crack growth rate in nickel-based alloys, austenitic stainless steels, and ferritic steels, including technical bases, underlying assumptions, and mathematical descriptions.

- Quantification and characterization of uncertainty for crack growth rate models.

- Development of conventions for integrating crack growth rates to predict crack shape and location as a function of time.

- Validation of PWSCC and fatigue growth rate models with independent field and laboratory experience.

- Development of simple conventions for approximating crack interaction and coalescence for partial through-wall flaws and through-wall flaws.

- Validation of simple conventions for crack interaction and coalescence using high-fidelity modeling or controlled experimentation.

- Implementation of crack growth and coalescence models, including requirements, design, specification of inputs and outputs, and verification testing.

- Recommendations for future work related to crack growth and coalescence modeling.

PWSCC crack growth rate, fatigue crack growth rate, and coalescence model parameters are provided for various materials subject to PWR environments. The user of xLPR Version 2.0 may adopt the parameter recommendations and the documented technical bases of this report.

TABLE OF CONTENTS

LIST OF FIGURES

LIST OF TABLES

NOMENCLATURE/LIST OF SYMBOLS

Symbols

a	Crack depth
$\dot{a}$	Crack growth rate
a_{ctsm}	Load ratio constant for custom fatigue growth model
A_{env}	Environmental factor for Ni-based alloy fatigue growth model
b_{cstm}	Load ratio exponent for custom fatigue growth model
c	Peak width for SCC growth model
C_1	TCF environmental factor for ferritic steel fatigue growth model
C_2	Medium-sulfur EAC environmental factor for ferritic steel fatigue growth model
C_3	High-sulfur EAC environmental factor for ferritic steel fatigue growth model
C_{cstm}	Scaling constant for custom fatigue growth model
C_{env}	Generic environmental factor for ferritic steel fatigue growth model
C_{Kb}	Upper EAC threshold scaling factor for ferritic steel fatigue growth model
C_{Kth}	Stress intensity factor range threshold for fatigue growth model
C_{Ni}	Scaling constant for Ni-based alloy fatigue growth model
C_{SS}	Scaling constant for austenitic SS fatigue growth model
$\dfrac{da}{dN}$	Per cycle fatigue rate including environmental conditions
$\left.\dfrac{da}{dN}\right|_{air}$	Per cycle fatigue rate in air
f_{alloy}	Alloy factor for SCC growth model
f_{H_2}	Hydrogen factor for SCC growth model
f_{comp}	Component-to-component factor for SCC growth model
f_{flaw}	Flaw-to-flaw factor for SCC growth model

f_{heat}	Heat-to-heat factor for SCC growth model
f_{orient}	Orientation factor for SCC growth model
F_R	Load ratio effect for austenitic SS fatigue growth model
F_T	Temperature effect for austenitic SS fatigue growth model
F_τ	Rise time effect for austenitic SS fatigue growth model
f_{weld}	Weld-to-weld factor for SCC growth model
f_{wh}	Within-heat factor for SCC growth model
f_{ww}	Within-weld factor for SCC growth model
$[H_2]$	Concentration of dissolved hydrogen in the primary water
$[H_2]_{Ni/NiO}$	Concentration of dissolved hydrogen corresponding to nickel metal/nickel oxide transition at location of crack
IF	Improvement factor for SCC growth model
$I_{material}$	Material group
$I_{mechanism}$	Mechanism type flag
I_{tip}	Crack tip index
K	Crack-tip stress intensity factor
K_{th}	Crack-tip stress intensity factor threshold
m_{cstm}	Paris law exponent for custom fatigue growth model
N_{cyc}	Number of cycles per transient component
n_{env}	Environmental exponent for Ni-based alloy fatigue growth model
n_{fer}	Paris power-law exponent for ferritic steel fatigue growth model
n_{Ni}	Paris power-law exponent for Ni-based alloy fatigue growth model
n_R	Load ratio exponent for ferritic steel fatigue growth model
n_{SS}	Paris power-law exponent for austenitic SS fatigue growth model
NTS	Number of transient components
P	Peak-to-valley ratio for SCC growth model

p_{cstm}	Rise time exponent for custom fatigue growth model
Q_g	Thermal activation energy
R	Load ratio
R_{gas}	Universal gas constant
S	Sulfur content
T	Absolute temperature
T_{ref}	Absolute reference temperature
V_{trans}	Critical velocity at crack tip for ferritic steel fatigue growth model
α	Scaling constant for SCC growth model
β	Stress intensity factor exponent
$\Delta ECP_{Ni/NiO}$	Difference in ECP between the Ni/NiO transition and the ECP at the current concentration of hydrogen
ΔK	Cyclic stress intensity factor range
ΔK_b	Stress intensity factor range at which transition from EAC to TCF begins
ΔK_b	Stress intensity factor range at which TCF susceptibility is maintained
ΔK_{th}	Stress intensity factor range threshold for PWSCC growth
Δt	Duration of time step
τ_r	Loading rise time of transient component

ABBREVIATIONS

ANL	Argonne National Laboratory
ASME	American Society of Mechanical Engineers
B&W	Babcock & Wilcox
BWR	Boiling Water Reactor
CEA	Alternative Energies and Atomic Energy Commission
CGR	Crack Growth Rate
CIEMAT	Centro de Investigaciones Energéticas, Medioambientales y Tecnológicas
CRDM	Control Rod Drive Mechanism
DLL	Dynamic Link Library
EAC	Environmentally Assisted Cracking
ECP	Electrochemical Corrosion Potential
EDEAC	EPRI Database for Environmentally Assisted Cracking
EDF	Électricité de France
EPRI	Electric Power Research Institute
HAZ	Heat Affected Zone
ID	Inner Diameter
IGSCC	Intergranular Stress Corrosion Cracking
JSME	Japan Society of Mechanical Engineers
LWR	Light Water Reactor
MHI	Mitsubishi Heavy Industries, Ltd.
MRP	Materials Reliability Program
MVR	Module Validation Report
OD	Outer Diameter
ODE	Ordinary Differential Equation
PNNL	Pacific Northwest National Laboratory
PWR	Pressurized Water Reactor
PWSCC	Primary Water Stress Corrosion Cracking
RCS	Reactor Coolant System
SS	Stainless Steel
TCF	True Corrosion Fatigue

TIFFANY   Thermal Stress Intensity Factor for Any Coolant History

TW   Through Wall

UK   United Kingdom

US   United States

V&V   Verification and Validation

xLPR   eXtremely Low Probability of Rupture

1. INTRODUCTION

1.1 Crack Growth Subgroup Objectives

The first responsibility of the Crack Growth Subgroup assembled for the development of Extremely Low Probability of Rupture (xLPR) Version 2.0 was to identify appropriate models for predicting the growth and coalescence of cracks in normal pressurized water reactor (PWR) environments under constant and cyclic loading conditions and from these to select the best models for use. Among the criteria for selection were: (a) comprehensive treatment of important independent variables, (b) ability to account for uncertainties, (c) agreement with crack growth rates (CGRs) observed in field or laboratory settings, (d) ease of implementation, and (e) technical and industry precedence.

The Crack Growth Subgroup was further responsible for developing selected *models* as programmed *modules* that could be integrated within the xLPR Version 2.0 Framework. As part of module development, the Crack Growth Subgroup produced requirements documentation, design documentation, source code, and verification and validation (V&V) documentation.

Specific responsibilities of the Crack Growth Subgroup, as originally captured in the Crack Growth Subgroup Work Plan [1], are stated below and are discussed as they relate to the final work products presented in this report:

(1). *Review the xLPR Version 1.0 ("Pilot Study") PWSCC growth models, including treatment of uncertainties.* The primary water stress corrosion cracking (PWSCC) growth models of xLPR Version 1.0 were deemed largely acceptable through careful assessment. Refinements to the PWSCC growth module implemented for xLPR Version 2.0 are discussed as Task 2 below.

(2). *Implement enhancements to the PWSCC growth models.* Enhancements to the PWSCC growth module include parameterization to improve flexibility and inclusion of weld-to-weld CGR variability. All enhancements are covered in this report.

(3). *Determine whether and how to implement fatigue growth.* The Crack Growth Subgroup—in collaboration with the K-Calculation Models Subgroup, the Inputs Group, and the Framework Group—developed within the xLPR Framework a structure to enable the treatment of fatigue growth, including the definition of loading transients, conversion of loading transients to stress intensity factor transients, and calculation of fatigue CGRs. The last is detailed in this report.

(4). *Implement the fatigue CGR models.* The Crack Growth Subgroup implemented three material-specific fatigue CGR models applicable to PWR environments. This implementation is detailed in this report.

(5). *Investigate intergranular stress corrosion crack (IGSCC) growth rate models for austenitic stainless steel (SS) in boiling water reactor (BWR) environments.* The development of an IGSCC CGR model was not performed for Version 2.0 of xLPR and as such is not discussed in this report. The scope of xLPR Version 2.0 is limited to PWR environments.

(6). *Investigate and implement PWSCC CGR models for Alloys 52 and 152.* The PWSCC CGR module was developed to be flexibly parameterized to accommodate materials

other than Alloy 600 (and its associated weld metals), provided that appropriate model parameter inputs are developed. For instance, the module includes a factor of improvement term commonly used to adjust a reference model to represent different, but related, materials or environments. The effort to develop appropriate and validated model parameter inputs for PWSCC in Alloys 52 and 152 is ongoing outside of the xLPR Project.

(7).   *Perform module-level V&V.* Extensive V&V was performed to ensure correct implementation of the Crack Growth Subgroup modules (relative to documented requirements) and to demonstrate agreement with CGRs observed in field or laboratory environments.

(8).   *Implement a crack coalescence module.* Crack coalescence was implemented in the crack coalescence module. The model and module are detailed in this report.

1.2 Models and Inputs

The Crack Growth Subgroup was responsible for developing models for predicting PWSCC growth, fatigue crack growth, and crack coalescence. A brief overview of each model is given below.

The foundation of the PWSCC growth model is a module that predicts PWSCC *growth rate* as a function of important environmental and loading variables and includes appropriate uncertainties. This module is leveraged within the xLPR Framework, in accordance with rules prescribed by the Crack Growth Subgroup, to yield predictions for crack growth (i.e., location, shape, and size) over time. The Crack Growth Subgroup has provided model parameter recommendations for PWSCC CGR predictions in Alloy 600 and its associated weld metals (Alloys 82, 182, and 132[1]) in normal PWR environments. Model parameters appropriate for other materials or environments have not been prescribed; however, there is ample evidence that PWSCC in other common primary-side component materials—such as Alloys 52 or 152, austenitic SS base metals and welds, and ferritic steels—does not occur or occurs at substantially reduced rate relative to Alloy 600 in normal PWR environments.

Like the PWSCC growth model, the foundation of the fatigue growth model is a module that predicts fatigue *growth rate* as a function of important environmental and loading variables and includes appropriate uncertainties. CGR predictions for PWSCC and fatigue mechanisms are summed and utilized by the xLPR Framework to yield predictions for crack growth. Distinct submodels have been developed for fatigue CGR predictions in three different material classes: Ni-based alloys, austenitic SS, and ferritic steels. The Crack Growth Subgroup has provided model parameter recommendations to span the different materials common in primary-side pressure boundary components, including the primary piping system.

---

[1] Alloy 132, which is similar in composition to Alloy 182, was generally used rather than Alloy 182 for dissimilar metal piping welds in Japanese PWRs.

The coalescence model is implemented as a module that predicts the combination of cracks of engineering significance.[2] This module uses rule-based criteria to simulate coalescence of coplanar circumferential cracks of engineering significance based on their type, geometry, and location. This simulation is intended to account for mechanisms that lead to crack extension on a time-scale significantly faster than that predicted for PWSCC and fatigue growth of a single crack, including crack tip interaction that can lead to intensified stress intensity factors and plastic collapse of a ligament separating two cracks. The Crack Growth Subgroup has provided general coalescence model parameters and has validated them against laboratory studies and fracture mechanics modeling.

1.3 Scope

The objective of the Crack Growth Module of xLPR 2.0 is to predict SCC and fatigue CGRs in normal PWR primary water environment of materials commonly located in PWR primary piping systems, including dissimilar metal welds and similar metal welds.

The objective of the Coalescence Module of xLPR 2.0 is to predict the combination of idealized cracks of the types modeled within the xLPR 2.0 framework.

1.4 Report Organization

This report is organized as follows:

- Section 1 provides an overview of the Crack Growth Subgroup roles, responsibilities, and models.

- Section 2 details the PWSCC and fatigue crack growth models including their technical bases, underlying assumptions, and mathematical descriptions.

- Section 3 discusses the implementation of the CGR modules, including design, integration, and V&V.

- Section 4 details the coalescence growth model.

- Section 5 discusses the implementation of the coalescence module.

- Section 6 provides recommendations for future work.

- Section 7 provides a list of references cited in this report.

---

[2] As detailed later, the term "cracks of engineering significance" is used to differentiate macro-sized cracks (e.g., 1-3 mm or more in depth) from micro-sized fissures and defects. The process of micro-flaw incubation, formation, and coalescence is not within the scope of xLPR Version 2.0.

2. CRACK GROWTH MODELS

This section describes the models that enable the prediction of crack growth within the xLPR Version 2.0 framework. This section is organized as follows:

- Section 2.1 presents an overview of the growth model.

- Section 2.2 describes the mathematical equations, development efforts, and technical bases related to the PWSCC CGR models.

- Section 2.3 describes the mathematical equations, development efforts, and technical bases related to the fatigue CGR models.

- Section 2.4 describes the additional modeling steps required to integrate CGR predictions to yield predictions for crack location, shape, and size versus time.

- Section 2.5 catalogues the primary assumptions and simplifications that are part of the crack growth model.

- Section 3 complements this section with a description of the CGR modules that support implementation of the crack growth models.

2.1 Model Overview

The crack growth model (1) predicts CGRs due to PWSCC and fatigue degradation in common primary side materials in normal PWR environments and (2) integrates these CGR predictions to predict crack growth versus time. The CGR model, as implemented in the CGR module detailed in Section 3, accepts environmental and loading conditions at a single point in time at a single location on an advancing crack front and returns a growth rate. The CGR models incorporate functional dependencies to account for the predominant drivers of crack growth: Mode (I) stress intensity factor, temperature, water chemistry, material conditions, and loading characteristics. Time integration is performed to convert CGR to crack extension versus time. Certain conventions, which are detailed in Section 2.4, are applied to relate the crack extension at a finite number of crack locations to crack shape and size.

The PWSCC CGR model is based primarily on investigations performed under the Electric Power Research Institute (EPRI) Materials Reliability Program (MRP). These investigations selected appropriate model forms, derived model parameters and uncertainties, and presented statistical validation. These models are semi-empirical in that they incorporate theoretical dependencies, but use laboratory data to estimate parameters and uncertainties that fully define the corresponding CGR equation. As part of work for xLPR Version 2.0, these model forms have been validated with field and laboratory data independent from those data used for model development.

The fatigue CGR model includes distinct model forms for three material classes: Ni-based alloys (Alloys 600, 690, and their associated weld metals), wrought and cast austenitic SS (Types 304, 304L, 304LE, 316, 316L, 316NG, and 316LN; and Grades CF8, CF8M, CF3, and CF3M) and associated weld metals, and general ferritic steels (e.g., carbon steel and low-alloy steel). The origins of these three model forms are different, as detailed in Section 2.3. Like the PWSCC models, the fatigue models were developed semi-empirically using data from controlled laboratory

studies. The fatigue models have been validated with independent laboratory data and other existing model forms.

2.2 PWSCC Model Development

This section describes the development and technical bases for the PWSCC CGR models for thick-wall Alloy 600, Alloys 82/182/132, and other materials common in PWR primary side components. In general, the sections are separated into submodel-specific subsections that discuss the mathematical description of the model form, the development and technical justification of model parameters, the treatment of uncertainty, and model validation.

2.2.1 Alloy 600

This section presents the thick-wall wrought Alloy 600 PWSCC CGR model. Briefly, the technical bases for the selected model are:

- The model form is the product of consensus of an international panel of experts in the area of PWSCC, as documented in MRP-55 [2]. It is simple and parametrically accounts for important and quantifiable influences on PWSCC CGR.

- Model development was based on a screened laboratory database of 158 CGR measurements from tests performed by Westinghouse, Studsvik, Électricité de France (EDF), the Alternative Energies and Atomic Energy Commission (CEA), and CIEMAT. The laboratories confirmed that their test procedures took account of the key technical issues to ensure data quality.

- A deterministic equivalent (i.e., a 75th percentile model) has been applied in numerous industry studies and was adopted in Section XI Nonmandatory Appendices C and O of the American Society of Mechanical Engineers (ASME) Boiler and Pressure Vessel Code for flaw evaluation [3].

- Independent validation performed for xLPR confirmed acceptable agreement relative to field experience and independent laboratory data.

2.2.1.1 Mathematical Description

The Alloy 600 PWSCC CGR model, based on MRP-55 [2], is a function of temperature and stress intensity factor as given below:

$$\dot{a} = \begin{cases} \exp\left[-\dfrac{Q_g}{R_{gas}}\left(\dfrac{1}{T}-\dfrac{1}{T_{ref}}\right)\right]\alpha f_{heat}f_{wh}\left(K-K_{th}\right)^{\beta} & K > K_{th} \\[2em] 0 & K \leq K_{th} \end{cases} \qquad \text{[Eqn. 2-1]}$$

where:

$\dot{a}$	=	CGR
Q_g	=	thermal activation energy for crack growth
R_{gas}	=	universal gas constant

T = temperature at location of crack (absolute)
T_{ref} = reference temperature (absolute)
α = scaling constant
f_{heat} = common factor applied to all specimens fabricated from the same material heat to account for variation in susceptibility of a given heat
f_{wh} = within heat factor that accounts for the variability in CGR for different specimens fabricated from the same material heat
K = crack-tip stress intensity factor
K_{th} = crack-tip stress intensity factor threshold
β = stress intensity factor exponent

A key feature of the CGR curve for Alloy 600 is the dependence on the Mode (I) stress intensity factor. The functional form for this dependence was adopted from the Scott equation [4], which was originally developed using inspection data for axial cracks in the roll transitions of steam generator tubes, comprising a database of hundreds of tubes and many tens of susceptible heats. In this regard, MRP-55 states that the data used to develop [Eqn. 2-1] reflected stress intensity factors no less than about 15 MPa√m (14 ksi√in), so the dependence of CGR on K for thick-wall material was not specifically verified for lower K values. Thus, the impact of this limitation should be considered when applying [Eqn. 2-1] in this form. A second key feature of the CGR curve for Alloy 600 is the temperature dependence, implemented as the classical Arrhenius model for thermally activated processes. Finally, other scaling constants are available for normalization, heat-to-heat variation, and within-heat variation.

2.2.1.2 Model Development

In 2002, the EPRI Materials Reliability Program (MRP) developed a recommended CGR curve for PWSCC of thick-wall components fabricated from Alloy 600 base material, such as reactor vessel head nozzles. The curve was presented in MRP-55 [2], which was compiled from the input of an international panel of experts in the area of PWSCC. The curve can be applied directly to disposition detected PWSCC in Alloy 600 wrought material and provide guidance on inspection intervals and repair or mitigation options. It has been applied in numerous industry studies and was adopted in Section XI Nonmandatory Appendices C and O of the ASME Boiler and Pressure Vessel Code for flaw evaluation.

The MRP-55 curve was developed from a database of laboratory CGR measurements screened to eliminate non-representative test conditions and was validated against instances of PWSCC growth rate estimation in field components. This database spanned temperatures from 290 to 363°C, stress intensity factors from ~15 to ~50 MPa√m, and various product forms/manufacturers; it is noted that specimens with intentionally added cold work were not included for this development effort. The remainder of this section describes the model parameters derived using this database.

The adoption of the Scott equation for stress intensity factor dependency originally resulted in a power-law exponent of β = 1.16 and a stress intensity factor threshold, K_{th} = 9 MPa√m [2]. While there is an EPRI-sponsored effort currently underway to revisit the Alloy 600 CGR model, including consideration of the value assumed for the stress intensity factor threshold, the current model form offers flexibility to adopt prevailing or forthcoming recommendations for the model parameters including the stress intensity factor threshold.

The best-estimate activation energy for PWSCC in Alloy 600 is 130 kJ/mol based on laboratory CGR data [2]. A reference temperature of 325°C should be used in accordance with industry-standard PWSCC CGR models like that developed in MRP-55.

With stress intensity factor and temperature modeling terms set, analysis was performed in MRP-55 to estimate an appropriate scaling constant, α, to reflect CGRs observed in the laboratory CGR database, resulting in a best-estimate of 1.34E-12 (m/s)/(MPa√m)$^{1.16}$.[3]

While analysis presented in MRP-263 [5] suggests some modest hydrogen effect for PWSCC in Alloy 600, analysis that is more rigorous would be necessary to refit other model parameters and uncertainties. A recommendation for an Alloy 600 PWSCC CGR model that includes the effect of dissolved hydrogen concentration is not made in this report. Such an analysis was not made a priority for xLPR Version 2.0 given that there are relatively few Alloy 600 safe ends installed in existing PWR primary piping system applications, given that Alloy 600 is not used in new plant applications, and given that the hydrogen effect observed for Alloy 600 is smaller than that for the Alloys 82/182/132 weld metals. The addition of a hydrogen effect for Alloy 600 is left as an open area for research.

Finally, data on the beneficial effect of zinc on Alloy 600 CGR are mixed. The laboratory data vary from a substantial reduction in CGR[4] to no effect and therefore no zinc effect is included in the CGR model for xLPR. On the other hand, the results of laboratory testing clearly indicate a benefit of zinc addition in mitigating the initiation of PWSCC in Alloys 600/82/182, and this effect is thus included in the initiation model for xLPR.

2.2.1.3 Treatment of Uncertainty

Uncertainty in the CGR models results from several factors including: a) unmodeled effects, b) incorrectly modeled effects, c) error or uncertainty in the laboratory measurements that support the laboratory database from which the model was developed, and d) unpredictable variation or randomness. Several model parameters are treated as random variables in order to characterize uncertainty.

A predominant uncertainty in CGR prediction for Alloy 600 is due to heat-to-heat variability in material processing and fabrication. Since it is impractical to model this variation explicitly (due, for instance, to unavailability of processing details in practice), this uncertainty is captured through the heat-to-heat variability term, f_{heat}. As part of an MRP effort to model PWSCC probabilistically in reactor vessel head penetration nozzles [6], a heat-to-heat variability factor distribution was derived using the MRP-55 database, which comprises 158 measurements across 26 different material heats. Based on this work, heat-to-heat variability can be represented using a log-normal distributed heat-to-heat variability term with a median of 1, a 5th percentile of 0.19, and a 95th percentile of 5.32.[5] This uncertainty is regarded as epistemic based on the conclusion that it is

---

[3] For producing a single deterministic disposition curve in MRP-55, the 75th percentile scaling factor was recommended. This is the origin of the commonly reported value of 2.67E-12(m/s)/(MPa√m)$^{1.16}$.

[4] For instance, based on laboratory data, MRP-263 [5] concludes that a factor of improvement of ~1.8 may be applied to PWSCC growth rates in Alloy 600 for stress intensity factors below 15 ksi√in (16.5 MPa√m).

[5] Log-normal distributions in this report are described using median, 5th percentile, and 95th percentile. It is acknowledged that only two of these quantities are required to describe the two-parameter distribution fully, but all three are given for information. The log-μ parameter is the natural logarithm of the median. The log-

due to quantifiable differences between heats (e.g., detailed manufacturing specifications) that have not been incorporated in modeling and that they may be in large part explainable with refinements in modeling, more precise data collection and analysis, and additional laboratory testing.

In addition to heat-to-heat variability, there exists variability in PWSCC susceptibility within a single heat, as exhibited by different CGR measurements in the same heat of material. This variability is due to microstructural variation or local material composition. This uncertainty is captured with the within-heat variability term, f_{wh}. Again, based on analysis of the MRP-55 database [6], within-heat variability is represented as a log-normal distributed scaling parameter with a median of 1, a 5th percentile of 0.39, and a 95th percentile of 2.55. This uncertainty is regarded as aleatory given that it is not considered reducible in practice.

Uncertainty in the thermal activation energy is treated separately. It is reasonable to treat the uncertainty in the temperature effect as independent of the heat-to-heat variability used to model the effect of basic material susceptibility because the uncertainty modeled using the f_{heat} input tends to dominate the uncertainty in the thermal activation parameter. The uncertainty in thermal activation energy is believed to reflect the combination of experimental uncertainty and heat-to-heat variation in temperature sensitivity—that is, controlled testing on a single specimen generally yields precise estimates for activation energy, whereas investigations of different Alloy 600 or Alloys 82/182 specimens have yielded a range of different estimates. A normally distributed uncertainty about the best-estimate of 130 kJ/mol, with a standard deviation of 5 kJ/mol, is recommended to represent this variability. This uncertainty is informed from a range of activation energy values reported by different investigators testing with different material heats. This uncertainty is treated as epistemic as it represents uncertainty that is at least partially reducible in practice.

2.2.1.4 Model Validation

As part of the module-level validation for xLPR [7], the Alloy 600 CGR model was compared against independent CGR data including:

- EDF-reported PWSCC growth experience recorded between 1991 and 1996 at Alloy 600 reactor vessel head penetration nozzles (e.g., see Figure 2-1);

- U.S. plant PWSCC growth experience recorded between 1994 and present day at Alloy 600 control rod drive mechanism (CRDM) penetration nozzles;

- Laboratory PWSCC CGR testing in Alloy 600 separate from data used in the MRP-55 modeling efforts (e.g., see Figure 2-2).

This validation investigated the overall agreement between probabilistic CGR predictions and data (e.g., by investigating the ability of CGR confidence intervals to bound data scatter), but also investigated the agreement between modeled effects and data trends.

In the conclusion of this work, the Alloy 600 PWSCC CGR model was shown to provide CGR predictions that are generally consistent with the extensive database of laboratory PWSCC

σ parameter can be calculated by taking the natural logarithm of the ratio of the 95th percentile and the median, and then scaling that quantity by 0.608.

simulation separate from the MRP-55 database and mostly acquired since 2004 and instances of PWSCC in field components. There exist a minority of instances in which the model generally under-predicts data for certain heats, i.e., Babcock and Wilcox (B&W) Tubular Products and French top head penetration nozzles, measured via both field and laboratory experience. These instances reflect material heats with relatively high susceptibility to PWSCC—for instance, this is demonstrated by the relatively high occurrence of cracking detected in nozzles fabricated using these heats—such that general under-prediction by the median CGR model for these heats is expected. Argonne National Laboratory (ANL) measured [8] a CGR percentile of 95% for one heat of ex-service CRDM nozzle material supplied by B&W Tubular Products. It is also noted that the French top head penetration nozzle material is a forged Alloy 600 material that is not directly relevant to U.S. PWRs.

This model validation applies for stress intensity factors between 10-80 MPa√m and operating temperatures between 280-350°C.
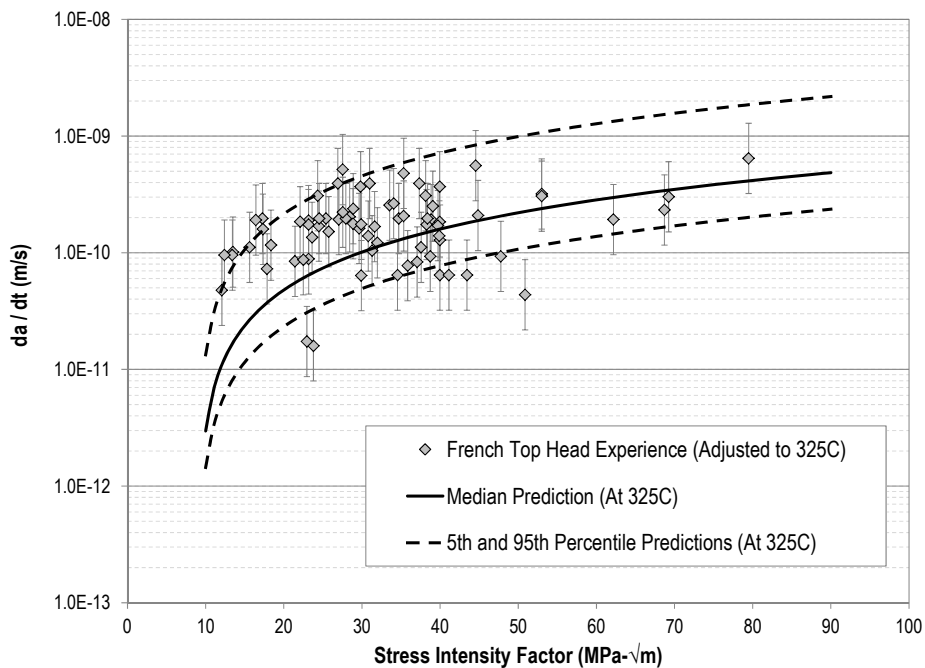
Figure 2-1.   Comparison of 5-95th Percentile[6] Alloy 600 CGR Model to French Top Head Experience

---

[6] The confidence intervals shown (5th percentile, median, 95th percentile) reflect those associated with the upper half (i.e., the upper two quartiles) of the MRP-55 model. This convention is used for validation because of the known high material susceptibility of materials used in French top heads in the 1990s. In other words, the confidence intervals are conditional on the knowledge the material is of the worse half in terms of material susceptibility.
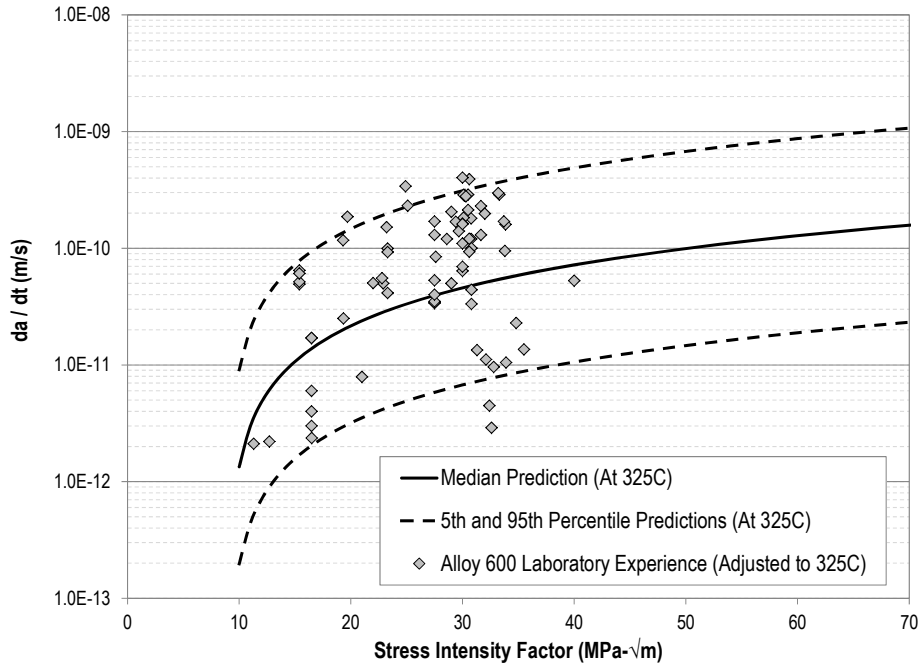
Figure 2-2.   Comparison of Alloy 600 CGR Model to Independent Laboratory Experience

2.2.2 Alloys 82/182/132 (Excluding the Effect of Dissolved Hydrogen Concentration)

This section presents the Alloys 82/182/132 PWSCC CGR model without inclusion of a dissolved hydrogen effect. Briefly, the technical bases for the selected model are:

- The model form was developed with the input and participation of an international PWSCC expert panel organized by EPRI, as documented in MRP-115 [9]. It is simple and parametrically accounts for important and quantifiable influences on the PWSCC CGR in Alloys 82/182/132 weld material.

- Model development was based on a screened laboratory database of 77 CGR measurements across 19 unique test welds. The panel developed screening criteria that were applied to the collected laboratory data to ensure the data applied to calculate the model parameters satisfied key data quality criteria.

- A deterministic equivalent (i.e., a 75th percentile model) has been applied in numerous industry studies and was adopted in Section XI Nonmandatory Appendices C and O of the ASME Boiler and Pressure Vessel Code for flaw evaluation.

- Independent validation performed for xLPR confirmed acceptable agreement relative to field experience and independent laboratory data.

2.2.2.1   Mathematical Description

The Alloys 82/182/132 PWSCC CGR model, based on MRP-115, is a function of temperature and stress intensity factor as given below:

$$\dot{a} = \begin{cases} \exp\left[-\dfrac{Q_g}{R_{gas}}\left(\dfrac{1}{T}-\dfrac{1}{T_{ref}}\right)\right]\alpha f_{weld}\,f_{ww}\,f_{alloy}\,f_{orient}\left(K-K_{th}\right)^{\beta} & K > K_{th} \\[2ex] 0 & K \le K_{th} \end{cases}$$

[Eqn. 2-2]

where:

f_{weld} = common factor applied to each unique weld to account for weld wire/stick heat processing and for weld fabrication

f_{ww} = within-weld factor that accounts for the variability in CGR at different locations within a unique weld

f_{alloy} = alloy factor

f_{orient} = crack orientation factor

Note that this equation is similar to the Alloy 600 equation, but includes an alloy factor to account for the reduced PWSCC susceptibility of Alloy 82 versus Alloys 182/132 (due to differences in chromium content) and an orientation factor to account for the influence of crack orientation (i.e., parallel or perpendicular to dendrite growth direction).

2.2.2.2   Model Development

In 2004, EPRI published MRP-115 [9], which documents the development of complementary MRP CGR curves for weld metals that are commonly selected for use with Alloy 600 base material (Alloys 82, 182, and 132), e.g., as "J-groove" partial penetration welds attaching various penetration nozzles and in piping dissimilar metal butt welds found at numerous locations in the PWR primary circuit. The MRP-115 curve has been adopted in Section XI Nonmandatory Appendices C and O of the ASME Boiler and Pressure Vessel Code for flaw evaluation. MRP-115 also proposes parameter uncertainties, thus constituting the development of a probabilistic CGR model. Key aspects of MRP-115 model development are described below.

For the MRP-115 effort, an international expert panel was first formed and subsequently collected detailed laboratory test data for the relevant set of worldwide laboratory CGR tests using pre-cracked fracture mechanics specimens. The expert panel developed screening criteria to qualify data for use in the development of a deterministic CGR model for Alloys 82, 182, and 132 weld metals. The screening criteria were based upon the criteria previously applied to thick-wall Alloy 600 wrought material in MRP-55, but were extended to cover the special test considerations associated with the weld metal materials. For instance, a special criterion was developed to screen out instances of low "engagement" to IGSCC across the specimen width and over the test duration. The resulting database spanned temperatures from 316 to 360°C, stress intensity factors from ~20 to ~60 MPa√m, hydrogen concentrations from 25 to 50 cc(STP)/kg, and various welds/manufacturers.

While the expert panel adopted the power-law stress intensity factor term of MRP-55, they concluded that there were insufficient data available to include a nonzero stress intensity factor threshold. The expert panel also adopted the Arrhenius temperature model that had been used

in MRP-55. The model form also included an alloy factor to treat differences between Alloy 82 and Alloys 182/132 (which have different nominal chromium concentrations) and an orientation factor to treat differences in growth parallel or perpendicular to the weld dendrites. It was judged that insufficient data were available at the time to include the effects of dissolved hydrogen concentration (i.e., electrochemical potential).

In MRP-115, the best-estimate activation energy for PWSCC in Alloys 82/182/132 was assumed to be 130 kJ/mol, consistent with Alloy 600. With the activation energy fixed at this value, a linearized multiple regression statistical model was fit to the screened database to estimate other model parameters. The fitted power-law constant was 1.6, resulting in very similar stress intensity factor dependence for K values greater than 20 MPa√m (relative to the Alloy 600 model). The alloy factor was determined to be unity for Alloys 182/132 and 0.385 (or an improvement factor of 1/0.385 = 2.6) for Alloy 82.[7] The orientation factor was determined to be unity for growth parallel to dendrite growth and 0.5 for growth perpendicular to weld dendrites. However, this orientation factor is not used in practice in the model because the dendrite growth direction at any given location in the weldment is usually not reliably known, especially given the potential for pre-service weld repairs. The best-estimate scaling factor for the fitted model was estimated as 9.82E-13 (m/s)/(MPa√m)$^{1.6}$.[8]

2.2.2.3 Treatment of Uncertainty

Similar to the Alloy 600 CGR model, a predominant uncertainty in CGR prediction for Alloys 82/182/132 is due to weld-to-weld variability. This uncertainty is captured with the weld-to-weld variability term, f_{weld}. Per analysis of the 77 measurements across 19 unique test welds in the MRP-115 database (see Figure 2-3), weld-to-weld variability can be represented as a log-normal distributed weld-to-weld variability term with a median of 1, a 5th percentile of 0.38, and a 95th percentile of 2.64 [10]. This uncertainty is regarded as epistemic based on reasoning given in Section 2.2.1.3. It is noted that this variability is roughly half that of the probabilistic Alloy 600 PWSCC CGR model. At the upper end of PWSCC growth susceptibility, the Alloy 182 weld metal has a similar susceptibility as the Alloy 600 base metal. However, the Alloy 182 weld material most resistant to PWSCC growth tends not to be as resistant as the most resistant Alloy 600 wrought material.

Within-weld variability is represented as a log-normal distributed within-weld variability factor, f_{ww}, with a median of 1, a 5th percentile of 0.45, and a 95th percentile of 2.20 (see Figure 2-4) [10]. This uncertainty arises from spatial variations in microstructure and composition such as with respect to grain boundary angle/energy or dendrite alignment and is treated as aleatory.

---

[7] Alloy 182 was often used for the filler metal and weld butter of Alloys 82/182 PWR piping butt welds, but Alloy 82 was often used for root passes of the weld. (In some cases the Alloy 82 root passes were subsequently machined away as part of the weld joint design.) Furthermore, pre-service weld repairs may be present from plant construction that applied Alloy 82 or 182 weld metal. Because Alloy 182 tends to have a higher PWSCC CGR than Alloy 82, typically Alloy 182 CGRs are assumed to apply for all the nickel-based weld metal in the joint. Hence, the improvement factor for Alloy 82 of 2.6 should only be applied in the unusual case in which it is confirmed that the PWSCC as modeled is exclusively located in Alloy 82 material.

[8] For the purpose of producing a single deterministic disposition curve in MRP-115, the 75th percentile scaling factor was recommended. This is the origin of the commonly reported value of 1.5E-12(m/s)/(MPa√m)$^{1.6}$.

Finally, a normally distributed uncertainty about the best-estimate thermal activation energy, with a standard deviation of 20 kJ/mol, is recommended [7]. This standard deviation, which is larger in comparison to the recommended Alloy 600 value, is a rough recommendation considered appropriate to account for a) the fact that the 130 kJ/mol apparent activation energy is predominately based on testing of Alloy 600 and thus may include some bias in relation to Alloys 82/182/132, b) the observation that Alloys 82/182/132 are more sensitive to changes in (temperature-dependent) electrochemical potential than Alloy 600, and c) a larger range of values reported by various investigators. This uncertainty is considered to be epistemic.
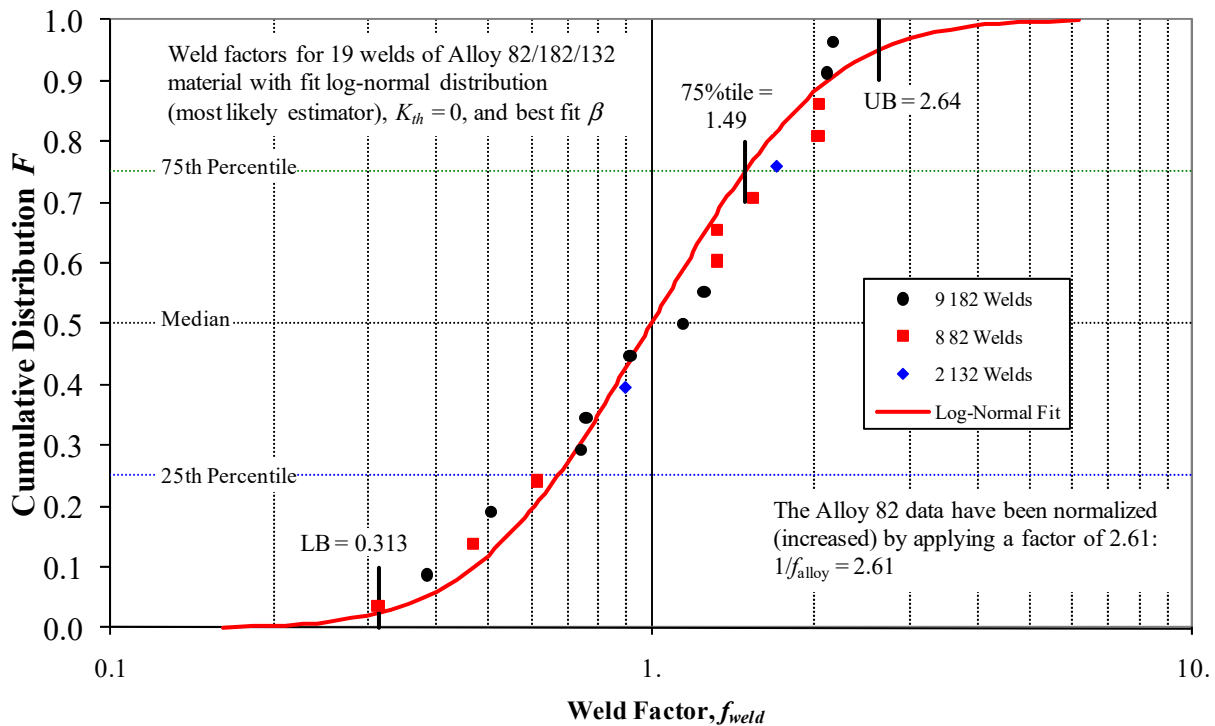
Figure 2-3. **MRP-115 Weld-to-Weld Variability Distribution with Log-Normal Fit for Alloys 82/182/132 [9]**
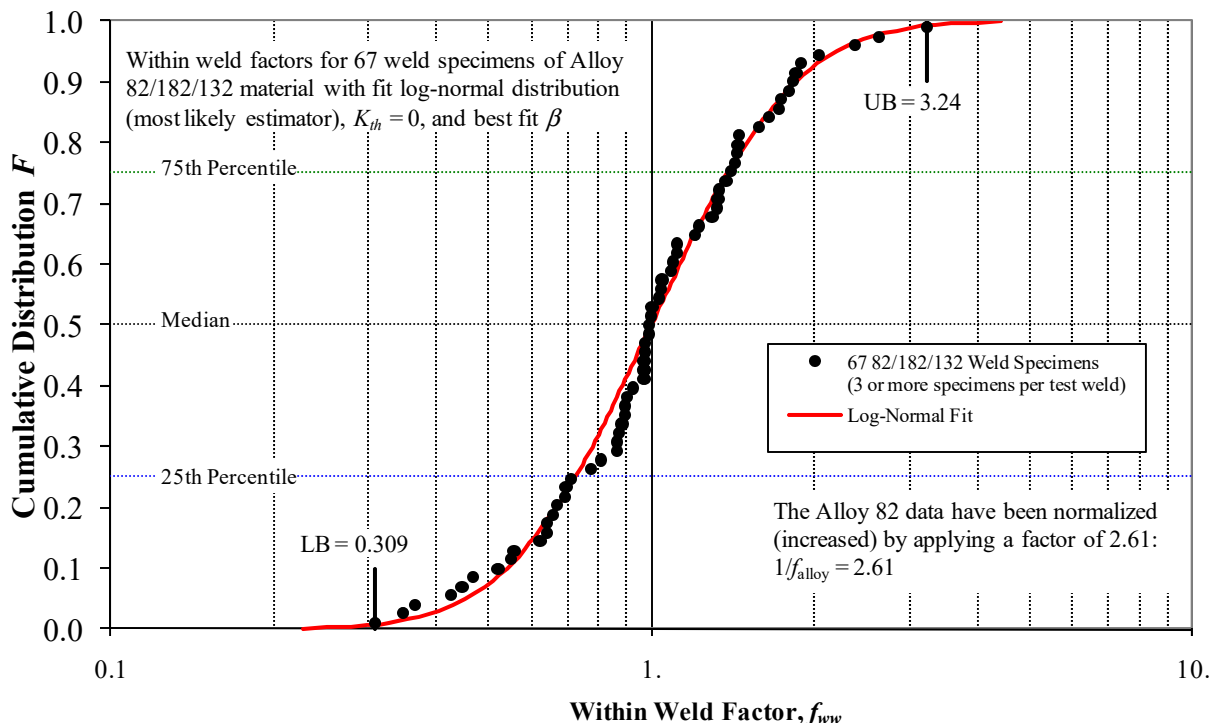
Figure 2-4.   MRP-115 Within-Weld Variability Distribution with Log-Normal Fit for Alloys 82/182/132 [10]

2.2.2.4   Model Validation

In MRP-115, detailed comparisons were performed against worldwide laboratory CGR data that were not included in its final screened database. These comparisons validated the robustness of the MRP-115 model.

As part of the module-level validation for xLPR [7], the Alloy 82 and Alloys 182/132 CGR models were compared against other independent CGR data including:

- Ringhals 3 PWSCC growth experience recorded between 2000 and 2001 at a reactor vessel outlet nozzle-to-safe-end Alloy 182 butt weld (e.g., see Figure 2-5);

- Laboratory PWSCC CGR testing in Alloys 82/182/132 separate from data used in the MRP-115 modeling efforts (e.g., see Figure 2-6 and Figure 2-7).

This validation investigated the overall agreement between probabilistic CGR predictions and data as well as the agreement between modeled effects and data trends.

In conclusion, the Alloys 82/182/132 PWSCC CGR model provides CGR predictions that are in agreement with the limited PWSCC CGR measurements in field components. While there is some indication that the MRP-115 model predicts CGRs that are on average higher than measurements obtained in laboratory weld specimens since 2004, the model is recommended without exception given its agreement with the screened database used for MRP-115. This model validation applies for stress intensity factors between 10-80 MPa√m and operating temperatures between 280-350°C.
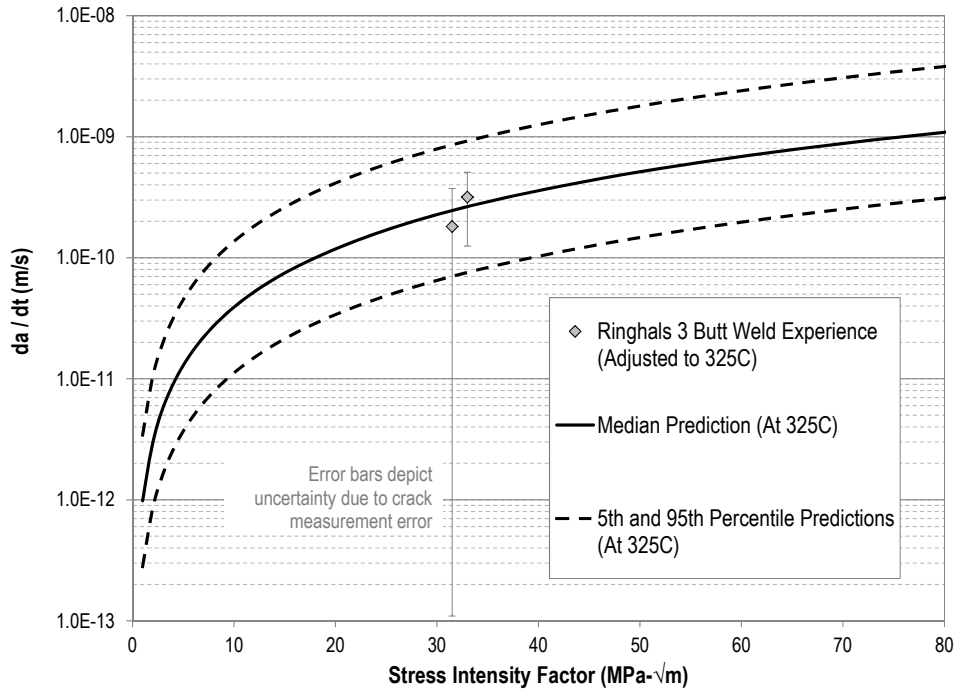
Figure 2-5. **Comparison of Alloy 182 CGR Model (Without Hydrogen Effect) to Ringhals Unit 3 Reactor Vessel Hot Leg Safe End Butt Weld Experience**
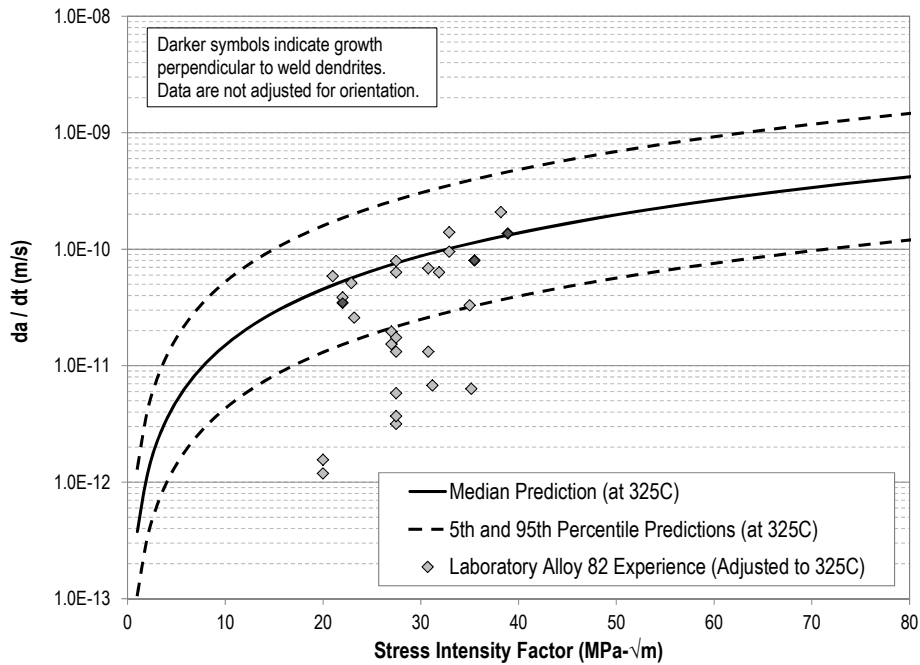
Figure 2-6. **Comparison of Alloy 82 CGR Model (without Hydrogen Effect) to Laboratory Experience**
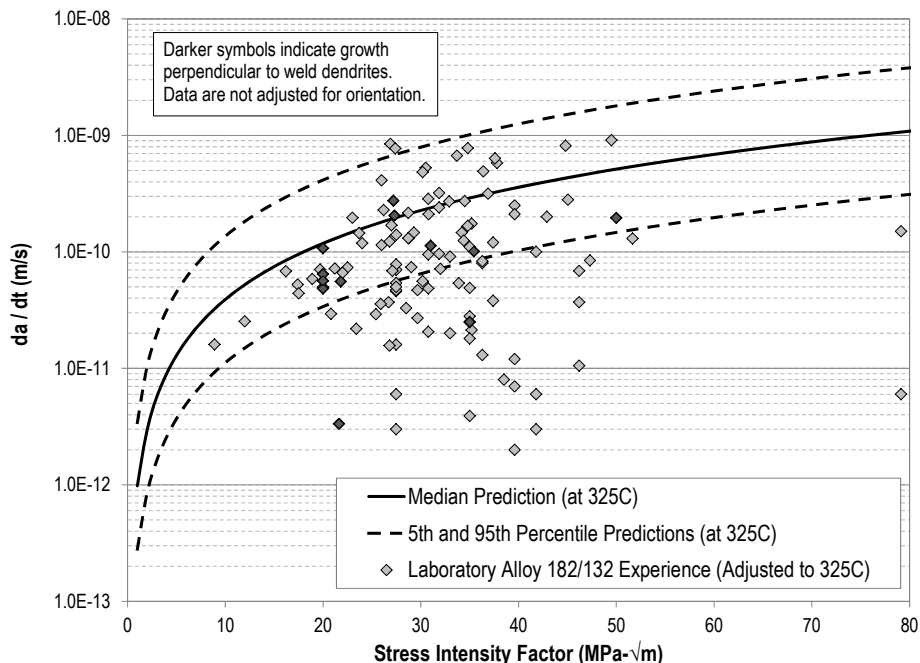
Figure 2-7.   Comparison of Alloys 182/132 CGR Model (without Hydrogen Effect) to Laboratory Experience

2.2.3 Alloys 82/182/132 (Including the Effect of Dissolved Hydrogen Concentration)

This section presents the Alloys 82/182/132 PWSCC CGR model with a dissolved hydrogen effect. Briefly, the technical bases for the selected model are:

- The inclusion of a hydrogen effect refines the prediction of PWSCC over the range of hydrogen concentrations expected at U.S. PWRs (i.e., 25-50 cc(STP)/kg). Furthermore, it allows the study of operation with elevated dissolved hydrogen concentration, a candidate chemical mitigation method for PWSCC.

- The hydrogen model form is equivalent to some of the others suggested by various investigators to account for the tendency of PWSCC growth to moderate away from the Ni/NiO equilibrium transition point. Prior to publication, the modeling in MRP-263 [5] was reviewed by PWSCC experts from major research organizations to ensure that there was expert level agreement on the technical approach to model the effect of hydrogen concentration on PWSCC growth.

- Model development was based on data considered in MRP-115 and data developed later by investigators who had participated in the MRP-115 development effort.

- Model parameter development is presented in MRP-263 [5] and MRP-307 [11]. This is considered the most developed effort available in literature to model the effect of dissolved hydrogen concentration on the PWSCC CGR in Alloys 82/182/132.

- Independent validation performed for xLPR confirmed acceptable agreement relative to independent laboratory data [7].

2.2.3.1 Mathematical Description

The Alloys 82/182/132 PWSCC CGR model with a hydrogen effect, based on MRP-263, has the same model form as that presented in the previous section with the exception that a hydrogen effect scaling term is added:

$$\dot{a} = f_{H_2}\left(\exp\left[-\frac{Q_g}{R_{gas}}\left(\frac{1}{T}-\frac{1}{T_{ref}}\right)\right]\alpha f_{weld} f_{ww} f_{alloy} f_{orient} \left(K-K_{th}\right)^{\beta}\right) \qquad \text{[Eqn. 2-3]}$$

$$f_{H_2} = \left[\frac{1}{P}+\frac{(P-1)}{P}\exp\left(-0.5\left(\frac{\Delta ECP_{Ni/NiO}}{c}\right)^2\right)\right] \qquad \text{[Eqn. 2-4]}$$

where:

$\dot{a}$ = CGR accounting for hydrogen effect

f_{H_2} = hydrogen factor

$\Delta ECP_{Ni/NiO}$ = difference in electrochemical corrosion potential (ECP) between the Ni/NiO transition and the ECP at the current concentration of hydrogen and temperature

P = peak-to-valley ratio

c = peak width parameter

The difference in ECP between the Ni/NiO transition and the ECP at the current concentration of hydrogen is calculated as follows (in units of mV) using the following fit presented in Reference [12]:

$$\Delta ECP_{Ni/NiO} = 29.58 \,[\text{mV}]\cdot\left(\frac{T}{298.15 \,[\text{K}]}\right)\log\left(\frac{[H_2]}{[H_2]_{Ni/NiO}}\right) \qquad \text{[Eqn. 2-5]}$$

where:

$[H_2]$ = concentration of dissolved hydrogen in the primary water (cc/kg at standard temperature and pressure)

$[H_2]_{Ni/NiO}$ = concentration of dissolved hydrogen corresponding to the nickel metal / nickel oxide (Ni/NiO) transition at temperature at location of crack (cc/kg at standard temperature and pressure)

The concentration of dissolved hydrogen corresponding to the potential Ni/NiO transition is temperature dependent, and may be calculated using the following fit presented in Reference [12]:

$$\left[H_2\right]_{Ni/NiO} = 10^{(0.0111T-2.59)}$$

[Eqn. 2-6]

The hydrogen factor accounts for the effect of the hydrogen concentration in the primary system. The term has a Gaussian dependence relative to ECP such that the CGR prediction is reduced at both high and low hydrogen concentrations away from the Ni/NiO transition.

2.2.3.2 Model Development

The effort presented in MRP-263 [4] developed a PWSCC CGR model for Alloys 82/182/132 that included the effect of dissolved hydrogen concentration, with adjustments to other model parameters to maintain consistency with the dataset used in MRP-115.

The exact functional form of the model for the effect of hydrogen on CGR varies in recommendations across the literature (e.g., [13] and [14]). Several models have been developed that use a reference CGR to normalize the data to unity at high and low hydrogen concentrations.[9] The MRP-263 model for hydrogen dependence assumed the following form:

$$CGR = CGR_{max} \left[\frac{1}{P} + \frac{(P-1)}{P} \exp\left(-0.5 \left(\frac{\Delta ECP_{Ni/NiO}}{c} \right)^2 \right) \right]$$

[Eqn. 2-7]

All the modeling presented in MRP-263 used [Eqn. 2-5] and [Eqn. 2-6] for the calculation of, respectively, the ECP difference between the environment and the Ni/NiO transition and the hydrogen concentration at the Ni/NiO transition. Though different forms of these relationships exist in literature, the resulting fit of [Eqn. 2-7] does not differ significantly (when based on the same experimental data set).

Four different estimates of peak-to-valley ratio and peak width based on independent laboratory studies were put forth in MRP-263. These estimates were used in MRP-307 to develop distributions (see Section 2.2.3.3). These studies used Alloys 182 and 132. Very limited data for Alloy 82 analyzed in MRP-263 suggested a roughly Gaussian dependency relative to ECP, but exhibited a shift in the peak CGR from the estimated location of the Ni/NiO transition. Additional testing is required to resolve this apparent discrepancy.

The inclusion of the hydrogen effect, which itself includes a temperature dependence, gives rise to an interesting concept. If the hydrogen effect is not accounted for (such as in modeling described in Section 2.2.2), some of the temperature dependence ascribed to activation energy is in fact due to changes in the ECP relative to the Ni/NiO transition (and not solely the thermal activation of the reaction kinetics). As such, an activation energy derived without hydrogen

---

[9] The first such model developed by Attanasio and Morton [14] fit a three-parameter curve—using a peak-to-valley ratio, a peak width, and a peak offset from the Ni/NiO transition—to the data and required the selection of a baseline CGR [15]. Andresen et al. later modified this curve to approach asymptotically a relative CGR of unity at high and low ECP [15].

adjustment is termed "apparent activation energy." Since testing is often performed over a range of temperatures at a fixed hydrogen concentration, without adjusting for differences in the ECP relative to the Ni/NiO transition, the apparent activation energy is the parameter that is commonly reported. This approach also simplifies CGR predictions for PWRs, which have a variable operating temperature depending on location in the primary system but a single hydrogen concentration in the reactor coolant at a given time.

More detailed experimental investigations of activation energy intentionally vary hydrogen concentration throughout testing to maintain a constant ECP difference relative to the Ni/NiO transition. Activation energy estimated this way is termed "actual activation energy". Appendix G of MRP-263 derives the actual activation energies for several laboratory studies that were featured in the MRP-115 database. The recommended activation energy input when using the Alloys 82/182/132 PWSCC CGR model with hydrogen adjustment (104 kJ/mol) is close to the average actual activation energy across these studies.

2.2.3.3 Treatment of Uncertainty

In MRP-307 [11], a probabilistic model for hydrogen effect was developed with a normally distributed peak width (with a mean and standard deviation of 18.2 mV and 5.5 mV, respectively) and a shifted log-normally distributed[10] peak-to-valley ratio (with a median of 92.8, a 5th percentile of 1.0, and a 95th percentile of 8462). A positive correlation of 0.714 between the underlying normal deviates was used for peak width and peak-to-valley ratio samples. This uncertainty is treated as epistemic as it represents uncertainty that is at least partially reducible in practice.

With the best-fit hydrogen effect model proposed in MRP-263, the scaling factor and CGR variability terms were re-estimated to account for a) the shift in CGR caused by the inclusion of the hydrogen effect (for common hydrogen concentrations and temperatures) and b) the reduction in uncertainty afforded by treatment of the hydrogen effect. Based on this work, the best-estimate scaling factor for the Alloys 182/132 model with the hydrogen effect is 2.01E-12 (m/s)/(MPa√m)$^{1.6}$. Epistemic weld-to-weld variability can be represented as a log-normal distributed scaling parameter with a median of 1, a 5th percentile of 0.45, and a 95th percentile of 2.24 (see Figure 2-8); aleatory within-weld variability can be represented as a log-normal distributed scaling parameter with a median of 1, a 5th percentile of 0.54, and a 95th percentile of 1.85 (see Figure 2-9).

---

[10] A shifted log-normal is a log-normal deviate plus a constant shift. This distribution can be used to model data with large positive skewness, but with a non-zero minimum. In this case, the minimum for the peak-to-valley ratio is 1.
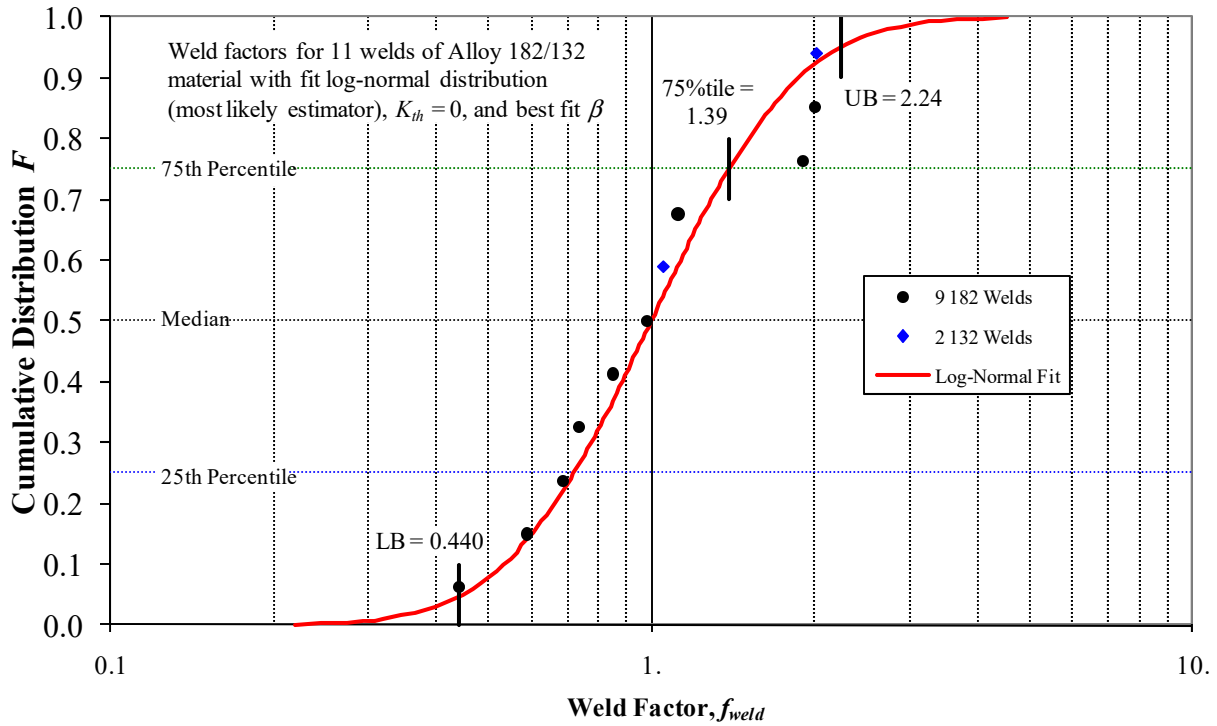
Figure 2-8. **MRP-263 Weld-to-Weld Variability Distribution with Log-Normal Fit for Alloys 182/132 [10]**
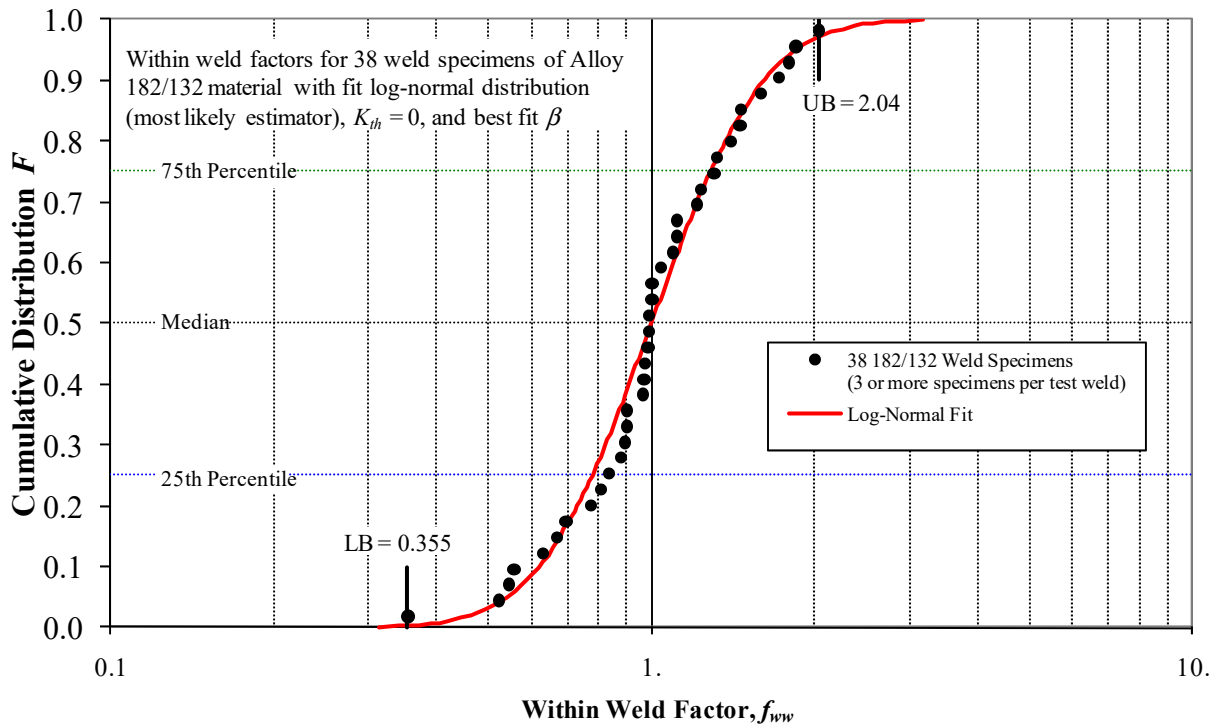
Figure 2-9. **MRP-263 Within-Weld Variability Distribution with Log-Normal Fit for Alloys 182/132 [10]**

36

2.2.3.4 Model Validation

Validation of the hydrogen effect is presented in the SCC Growth Module Validation Report (MVR) [7]. Among the Alloys 82/182/132 data available for validation, there was one study separate from those used directly in MRP-263 for which hydrogen concentration was systematically varied during testing of a single specimen under otherwise similar conditions: the PNNL testing of specimen CT012 reported in Reference [16]. The estimated peak width parameter for these data is 24 mV. This single estimate shows reasonable agreement with the distributed representation given for peak width in the previous section.

As additional validation, the full model form of [Eqn. 2-3] was fit to a database independent from data used in MRP-115[11] (although, overlapping with data used in MRP-263). The peak width estimate from this regression was 24.7 mV, again showing reasonable agreement with the distributed representation given for peak width in the previous section.

Furthermore, five studies independent from both MRP-115 and MRP-263 were identified in which temperature was systematically varied during testing of a single specimen under otherwise similar conditions. Three of these studies varied hydrogen concentration to maintain a constant ECP difference relative to the Ni/NiO transition; for the other two, the CGR data were adjusted to a common ECP difference relative to the Ni/NiO transition. The average actual activation energy derived from the five studies was 114 kJ/mol. This agrees sufficiently with the 104 kJ/mol activation energy derived based on the MRP-263 analysis.

Analysis has not been performed to validate the peak-to-valley ratio against independent data. Laboratory studies on a single test specimen (or on a series of test specimens fabricated from the same test weld and tested by the same laboratory) with a sufficient span of ECP conditions (i.e., on both sides of the Ni/NiO transition), independent from those used in MRP-263, have not been identified.

This model validation applies for stress intensity factors between 10-80 MPa√m, operating temperatures between 280-350°C, and hydrogen concentrations between roughly 1 and 60 cc(STP)/kg.

2.2.4 PWSCC in Other Common Materials

2.2.4.1 Alloys 690/52/152

Because of SCC in Alloy 600/82/182/132 components, repair and replacement applications have displaced these materials with the high-chromium nickel-base alloy wrought Alloy 690. Initially selected for tubing in replacement steam generators, thick-section Alloy 690 material also has been widely used, particularly for nozzle penetrations during replacement of reactor pressure vessel heads and during repairs to other J-groove nozzles in the primary system. Achieving comparable PWSCC resistance in the associated welds has necessitated use of the matching (high chromium) welding Alloys 52 (including variants) and 152, rather than Alloys 82 and 182 that were originally used to weld Alloy 600 components [17]. Furthermore, Alloys 52 and 152 are used for weld mitigation and repair (e.g., overlay, onlay, inlay, etc.).

---

[11] Many of these data were produced after the MRP-115 report was published in 2004; some were available at the time, but not included.

There is an ongoing effort focused on collection, scoring, and analysis of Alloy 690/52/152 data to develop a CGR model that may gain consensus from industry experts assembled by EPRI. While these materials are less susceptible (e.g., by a factor of 10 to 1000) to PWSCC given their increased chromium content, laboratory data suggest that PWSCC rates of engineering significance are possible under aggressive environmental and loading conditions. While at the time of the publication of this report, there is no consensus on a PWSCC CGR model for these materials, it is expected that one of two approaches will be used: a) the application of a (potentially statistically distributed) improvement factor to the Alloys 82/182/132 CGR model, or b) re-estimation of model parameters for a model form similar to [Eqn. 2-2].

2.2.4.2 Other SCC-Resistant Materials

For austenitic SS and ferritic steel, no SCC CGR model was developed to support xLPR Version 2.0. These materials are ordinarily considered not to be susceptible to SCC under normal PWR conditions (especially relative to Alloys 600/82/182/132). For instance:

- Laboratory research and plant experience have demonstrated that ferritic steel base and weld metal materials in their normal material condition are not susceptible to SCC [18]. SCC in ferritic steel requires stresses over yield strength, applied plastic strain, and oxidizing conditions.

- Laboratory research ([18], [19]) and plant experience ([18], [20], [21]) show that low SCC crack growth susceptibility is expected for SS material with relatively low levels of cold work and exposed to low-potential PWR primary coolant.

- The Materials Handbook for Nuclear Plant Pressure Boundary Applications [18] discusses the lack of susceptibility or low susceptibility to SCC in high-chromium nickel-based alloys, austenitic SS, and low-alloy and carbon steels.

Nonetheless, a general material model of the form shown in [Eqn. 2-8] is included in xLPR and could be used to implement SCC CGR models for these materials:

$$\dot{a} = \begin{cases} \alpha f_{comp} f_{flaw} \left(K - K_{th} \right)^{\beta} \exp\left[-\frac{Q_g}{R_{gas}} \left(\frac{1}{T} - \frac{1}{T_{ref}} \right) \right] & K > K_{th} \\ 0 & K \le K_{th} \end{cases} \qquad \text{[Eqn. 2-8]}$$

This equation is modeled after the CGR equations developed in MRP-55 and MRP-115. It includes terms to account for component-to-component variation, within-component variation, a stress intensity factor effect, and a temperature effect.

2.3 Fatigue Model Development

This section describes the model development and technical bases for the fatigue CGR models for general Ni-based alloy, austenitic SS, and ferritic steel. The sections generally are separated into subsections that discuss the mathematical description of the model form, the development and technical justification of model parameters, the treatment of uncertainty, and model validation.

2.3.1   General Considerations

For a given material, the fatigue growth per cycle, *da/dN*, is largely governed by the stress intensity factor range, ΔK, as well as the load ratio, *R*. For cracks exposed to reactor coolant, environmental effects can accelerate the crack growth, and additional factors, such as the frequency of the loading cycle, can become more important. The frequency of the loading cycle is often measured as the loading rise time, denoted as τ_R.

The Crack Growth Subgroup followed the conventional procedure of relating *da/dN* to ΔK, with due consideration of other contributing factors. The correlations between *da/dN* and ΔK, as well as other factors, are based on laboratory measurements, and differ substantially from one material to another. Hence, mathematical models for distinct material classes were developed. This section describes general considerations that apply across all material-specific fatigue models; later sections describe the material-specific models.

Stress intensity factor range: Cyclic loading is readily characterized by the cyclic stress intensity factor range [22], defined as:

$$\Delta K = K_{max} - K_{min} \quad K_{max} > 0$$
$$\Delta K = 0 \quad K_{max} \leq 0$$

[Eqn. 2-9]

By this convention, compressive-compressive cycles do not cause growth; however, fatigue cycles that are mostly compressive, but include a tensile portion, can cause growth. This stress intensity factor range calculation is based on ASME Section XI Appendix A guidance for light water reactor (LWR) environments.

Load ratio: The load ratio calculation is also based on ASME Section XI Appendix A guidance for LWR environments:

$$R = \begin{cases} \dfrac{K_{min}}{K_{max}} & K_{min} > 0 \\ 0 & K_{min} \leq 0 \end{cases}$$

[Eqn. 2-10]

Nominal temperature: The fatigue CGR models for Ni-based alloy and austenitic SS require a temperature input. The temperature effect models for these materials are given in [Eqn. 2-17] and [Eqn. 2-20], respectively. However, no specification is given in source documentation as to how to calculate nominal temperature from cyclically varying temperatures common for reactor transients. To accommodate different possible treatments, the nominal temperature used for fatigue CGR calculation can be set to the minimum, maximum, or average of the temperature cycle, as determined by a user-defined input. Most laboratory data available did not include temperature cycling so the appropriate convention cannot be determined from how model development from these data was performed.

Stress intensity factor range threshold: The mechanical threshold below which the fatigue CGR is negligible is an important parameter in some fatigue problems, e.g., high cycle, low amplitude vibration. The model for stress intensity factor range threshold, or ΔK_{th}, including its dependence on load ratio, is given in [Eqn. 2-11] (in units MPa√m):

$$\Delta K_{th} = C_{Kth} \cdot 5.5 \cdot (1 - 0.8R)$$ [Eqn. 2-11]

This model form is based on ASME Code Case N-643-2 [23], which presents a fatigue CGR curve for ferritic steels in PWR water environments. The stress intensity factor range threshold scaling constant in [Eqn. 2-11], C_{Kth}, allows adjustment to the N-643-2 curve. If C_{Kth} is set to unity, the N-643-2 curve is recovered and the model for the threshold is conservatively low.

Figure 2-10 [22] depicts results from laboratory testing aimed at studying the stress intensity factor range threshold. Note that results for ferritic and austenitic steels appear similar, justifying the use of the same ΔK_{th} model for material classes that are otherwise treated separately.

A least squares linear fit to the data of Figure 2-10 for $R \geq 0.10$ (28 data points) provided the following best-fit equation (in units MPa√m):

$$\Delta K_{th} = 7.0 \cdot (1 - 0.693R)$$ [Eqn. 2-12]

The use of the N-643-2 curve without adjustment results in a ΔK_{th} prediction that is biased low by 30% at low load ratios and by a factor of two at high load ratios, relative to the data in Figure 2-10. A best-estimate for C_{Kth} relative to the data in Figure 2-10 is approximately 1.27.

The prediction residuals of [Eqn. 2-12] relative to data were used to estimate a distribution for C_{Kth}. The parameter C_{Kth} can be represented by a log-normal distribution with a log-σ parameter 0.139.[12] The suitability of this distribution can be seen in Figure 2-11, which shows the 10th, 50th and 90th percentiles of this distribution along with the 28 data points from Figure 2-10 ($R \geq 0.10$).

The extent to which model uncertainty is due to specimen-to-specimen variation, within-specimen variation, material differences, test variation, etc. is not precisely known. The value for the stress intensity factor range threshold should be sampled once per component simulation, reflecting the belief that more variation is due to component-to-component variation than to within-component variation. The uncertainty in the stress intensity factor range threshold is regarded as epistemic because it is believed to be partially reducible with additional data.

---

[12] Upper truncation at the positive 3-σ level (i.e., at 1.517 times the median) should be used to prevent non-conservative values that are not represented in small data set used to fit the recommended distribution.
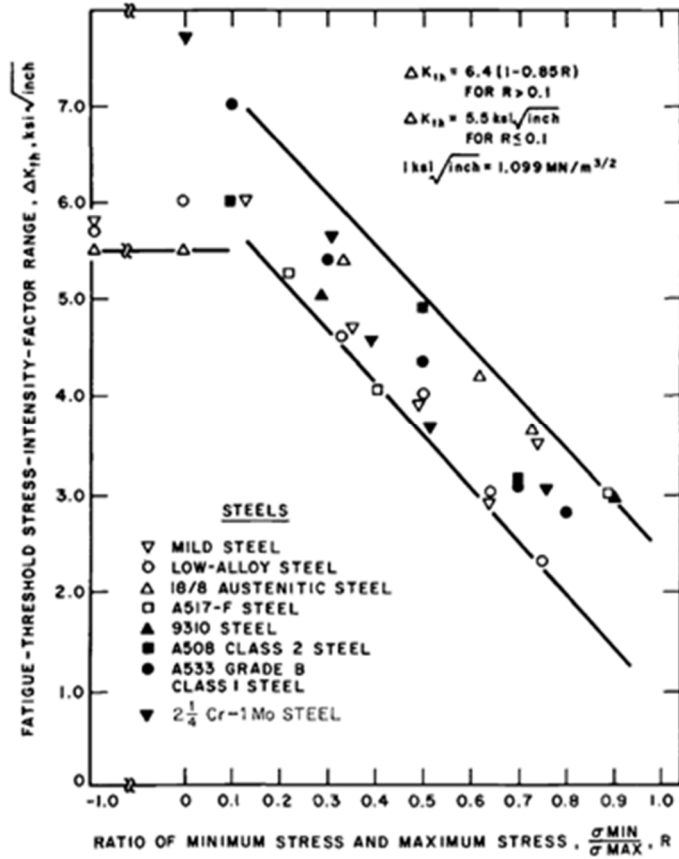
Figure 2-10.   Fatigue Crack Threshold versus Load Ratio for a Variety of Steels [22]
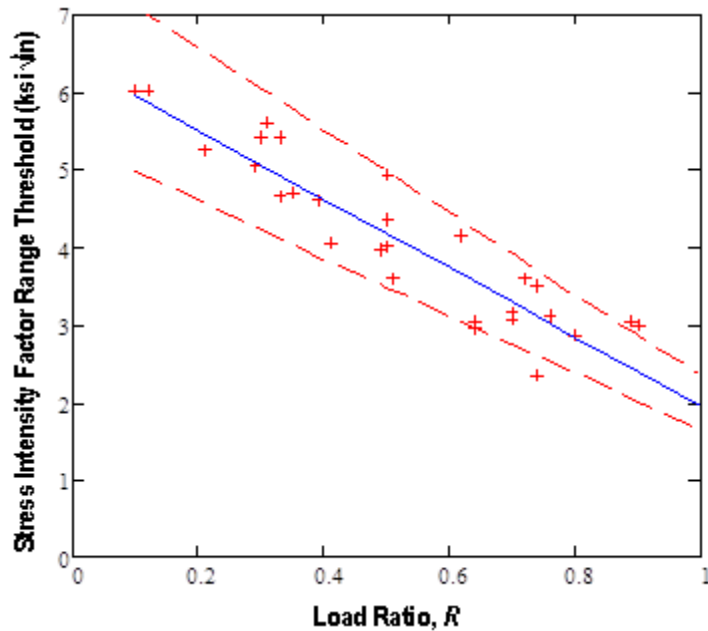
Figure 2-11.   Data Points from Figure 2-10 ($R \geq 0.10$) Along With the 10th, 50th and 90th Percentiles of the Estimated Lognormal Distribution

41

Data concerning the stress intensity factor range threshold for nickel-based alloys are not plentiful. The limited low ΔK data presented by Mills [24] are at high load ratios and are similar to the values reported in Figure 2-10. Therefore, it was selected that the same ΔK_{th} model be used for all three material classes unless additional data that refute this approach are produced or identified.

In summary, it was selected that [Eqn. 2-11] be applied to predict the stress intensity factor range threshold for ferritic steel, austenitic steel and nickel-based alloys. The parameter C_{Kth} may be represented by a log-normally distributed variable with a median of 1.27, a 5th percentile of 1.01, and a 95th percentile of 1.60. Alternatively, to err on the conservative side with respect to fatigue growth susceptibility, a median of 1.0 may be used to recover the ASME N-643-2 Code Case curve.

2.3.2 Nickel-Based Alloys

This section presents the fatigue CGR model for general nickel-based alloys in PWR environments. It is generally applicable to Alloys 600 and 690 and their associated weld metals. The fatigue crack growth characteristics of nickel-based Alloy 600 and related weld materials are extensively reviewed in NUREG/CR-6721 [25]. The representation of the growth relations from that reference are employed for the xLPR Version 2.0 effort.

2.3.2.1 Mathematical Description

Fatigue CGRs for nickel-based alloys are calculated as follows:

$$\frac{da}{dN} = \frac{da}{dN}\bigg|_{air} + A_{env}\left(\frac{da}{dN}\bigg|_{air}\right)^{n_{env}} \tau_r^{1-n_{env}} \qquad \text{[Eqn. 2-13]}$$

$$\frac{da}{dN}\bigg|_{air} = C_{Ni} f_{alloy} F_T F_R \left(\Delta K\right)^{n_{Ni}} \qquad \text{[Eqn. 2-14]}$$

where:

$\dfrac{da}{dN}$	=	per cycle fatigue rate including environmental conditions
$\dfrac{da}{dN}\bigg|_{air}$	=	per cycle fatigue rate in air
A_{env}	=	environmental factor
n_{env}	=	environmental exponent
τ_r	=	loading rise time of transient component
C_{Ni}	=	scaling constant
f_{alloy}	=	alloy factor
F_R	=	load ratio effect
F_T	=	temperature effect
ΔK	=	stress intensity factor range
n_{Ni}	=	Paris power-law exponent

This model includes conventional fatigue dependencies on stress intensity factor range (i.e., Paris power-law) and load ratio. It also includes a projection from air conditions to environmental conditions, which is dependent on the loading rise time of the fatigue cycle[13]. Finally, the model includes the influence of alloy type and temperature, consistent with observations during testing. The alloy factor defines any systematic difference in fatigue behavior between nickel-alloy welds and nickel-alloy base metals:

$$f_{alloy} = \begin{cases} 1 & \text{for} & \text{Alloy 600 or Alloy 690} \\ f_{Ni,weld} & \text{for} & \text{Alloy 182/132/82 or Alloy 152/52} \end{cases}$$
[Eqn. 2-15]

2.3.2.2 Model Development

The fatigue CGR model for nickel-based alloys is based most notably on analysis presented in NUREG/CR-6721. This analysis included a wide range of CGR measurement data, both in air and in a simulated PWR environment, and in base and welds metals of varying chromium content. Testing in air spanned temperatures from room temperature to 538°C; testing in simulated PWR environments spanned temperatures from 240 to 325°C. Loading characteristics were varied to span loading rise times from approximately 0.05 to 800 seconds, load ratios from approximately 0.05 to 0.95, stress intensity factor ranges from 1.4 to 79 MPa√m, and maximum stress intensity factors from 10 to 96 MPa√m.

Fatigue in air: The Paris power-law exponent was derived in NUREG/CR-6721 by fitting the power-law relationship to measured fatigue CGR versus stress intensity factor range data recorded with Alloy 600 specimens in air. Across different load ratio, loading rise times, and temperatures, the exponent varied from 3.5 to 5.5. For the analysis presented in NUREG/CR-6721, a central value of 4.1 was assumed.

In accordance with earlier precedent and to give good agreement with data recorded in air, the load ratio effect was expressed as given in [Eqn. 2-16]:

$$F_R = (1 - b \cdot R)^{-p}$$
[Eqn. 2-16]

Best fits to individual data sets for air fatigue of Alloy 600 in constant temperature environment yielded values of 0.82 and 2.2 for b and p, respectively.

The temperature effect for Alloy 600 and associated weld metals (Alloys 82, 182, and 132) was developed using Alloy 600 fatigue data recorded in air and normalized to a common stress intensity factor range and load ratio using the expressions above. A third-order polynomial fit yielded the following best-estimate temperature effect:

$$F_T = 4.835\text{E-}14 + (1.622\text{E-}16)T - (1.490\text{E-}18)T^2 + (4.355\text{E-}21)T^3$$
[Eqn. 2-17]

---

[13] The environmental enhancement is typically related as an adjustment to the time rate of fatigue in air to attain the time rate of fatigue in environmental conditions. The loading rise time effect arises from the need to relate the per cycle rate of fatigue in air to the per cycle rate of fatigue in environmental conditions.

The roughly 60 tests available for Alloy 690 fatigue CGR in air were not sufficient to support estimation of the Paris power-law model or the load ratio effect. However, the temperature effect was re-estimated for Alloy 690. Again, a third-order polynomial fit yielded the following best-estimate temperature effect:

$$F_T = 5.423\text{E-}14 + (1.830\text{E-}16)T - (1.725\text{E-}18)T^2 + (5.490\text{E-}21)T^3 \qquad \text{[Eqn. 2-18]}$$

For weld metals, the fatigue CGR database in air was composed of results from 35 tests of Alloy 182 between room temperature and 320°C. The results indicated that under similar loading conditions, the fatigue CGRs of Alloy 182 are a factor of roughly two higher than those for Alloy 600. The effect of temperature on growth rates remains similar to that for Alloy 600. Fatigue crack growth data for Alloys 82, 52, and 152 in air were not available. Given this information, it is considered most appropriate to apply the Alloy 600 model to Alloys 82/182/132 and the Alloy 690 model to Alloys 52/152 with the only exception that the alloy factor, f_{alloy}, is set to 2.0 for all of the weld metals.

Fatigue in PWR environment: NUREG/CR-6721 presented environmental fatigue tests performed on Alloy 600 under a variety of conditions including varying water chemistry, material condition, mechanical loading, and temperature. The environment enhancement of fatigue was found to be greater under loading conditions that correspond to smaller fatigue rates in air (e.g., <1E-09 m/s). A least squares fit to data relating air and environmental CGRs for the same specimen under the same loading conditions, recorded in high purity water with 300 ppb dissolved oxygen, yielded best-fit estimates for the environmental factor and environment exponent parameters of 4.4E-07 (m/cyc-s)$^{1-0.33}$ and 0.33, respectively. This degree of environmental enhancement was observed for some specimens in simulated PWR environment (i.e., < 10 ppb dissolved oxygen), namely those with relatively poor grain boundary coverage of carbides or high yield strength.

Limited testing performed with Alloys 82 and 182 in simulated PWR environments demonstrate relative environmental enhancement similar to that of Alloy 600 under loading conditions that correspond to low fatigue rates. However, these tests demonstrate environmental enhancement even under loading conditions that correspond to high fatigue rates (e.g., a factor of four to eight enhancement for conditions expected to yield fatigue rates of 1E-09 to 1E-07 m/s in air). NUREG/CR-6721 is not definitive on whether these results should be trusted.

Limited data for Alloy 690 and its weld metals reveal no environmental enhancement in simulated PWR conditions. However, additional tests are needed to verify these results.

Finally, as detailed in Section 2.3.2.4, the nickel-based alloy model has been validated with independent data from nickel-based alloy fatigue CGR testing performed by Mitsubishi Heavy Industries (MHI). More accurate prediction of the MHI data was attained through the use of an environment exponent of 0.25.

2.3.2.3 Treatment of Uncertainty

To account for uncertainty in the air fatigue crack growth model prediction for nickel-based alloys, the scaling constant, C_{Ni}, in [Eqn. 2-14] can be characterized as a distributed random variable. The median value of C_{Ni} is set to unity to recover the best-fit from NUREG/CR-6721. The dispersion of C_{Ni} is estimated by approximating the number of points that deviate from the best-fit equation by a factor of two or more (as depicted in Figure 2-12). The results from this analysis suggest a 5th and 95th percentile of 0.51 and 1.96, respectively (or a log-σ parameter of 0.408).
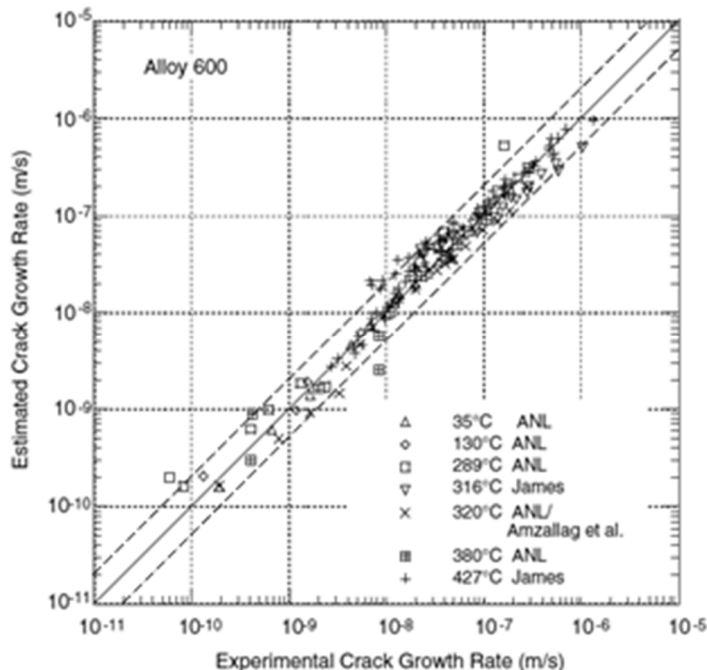
Figure 2-12. **Predicted Versus Measured CGRs for Alloy 600 with Various Environments and Loadings: Solid Line Indicates Best-Fit; Dashed Lines Indicate Factor-of-Two Deviation [25]**

Further uncertainty exists in the environmental effect, as shown in Figure 2-13. In fact, there appears to be bimodality in which some Alloy 600 specimens in PWR environments experience environmental enhancement while others do not, although this determination on a component-specific basis is outside of the scope of the current model.

Uncertainty is roughly accounted for by considering the environmental factor, A_{env}, (in [Eqn. 2-13]) as a distributed random variable. The recommended distribution for the environmental factor is log-distributed with a median of 4.4E-07 (m/cyc-s)$^{1-0.33}$ (corresponding with the best-fit from NUREG/CR-6721) and a log-σ parameter that is determined as a function of fatigue CGR in air, varying linearly from 1.2 at $\log_{10}(CGR_{air})$ = -12 to 0.0 at $\log_{10}(CGR_{air})$ = -8.[14] The model resulting from this fit is shown with red lines in Figure 2-13. Conservatively, this model represents Alloy 600 heats that are susceptible to environmental enhancement.

Absent additional data, the treatment of uncertainty for the air CGR scaling factor and the environmental factor are applied generally for Alloys 82 and 182 as well as for Alloy 690 and its weld metals.

The extent to which the nickel-based alloy fatigue CGR model uncertainty is due to specimen-to-specimen variation, within-specimen variation, material differences, environmental variation, test variation, etc. is not precisely known. The values for the air CGR scaling constant and the

---

[14] An environmental factor distribution parameter that varies as a function of air fatigue CGR cannot be implemented in Version 2.0 of xLPR. Instead, a fixed log-σ parameter of 1.2 is recommended at the risk of incorporating excessive variability at high CGRs. The more detailed treatment is recommended for future work in Section 6.

environmental factor can be sampled once per component simulation, reflecting the belief that more variation is due to component-to-component and environmental variation than to within-component variation. The uncertainties in these parameters are regarded as epistemic because they are believed to be partially reducible with additional data.

Alternatively, some of the uncertainty in the model parameters can be characterized as within-component variation. This might be done to study the sensitivity of the xLPR predictions to how fatigue uncertainty is characterized. If this is done, the portion of uncertainty characterized as within-component variation should be considered aleatory (e.g., due to microstructural variation that cannot be resolved in practice).
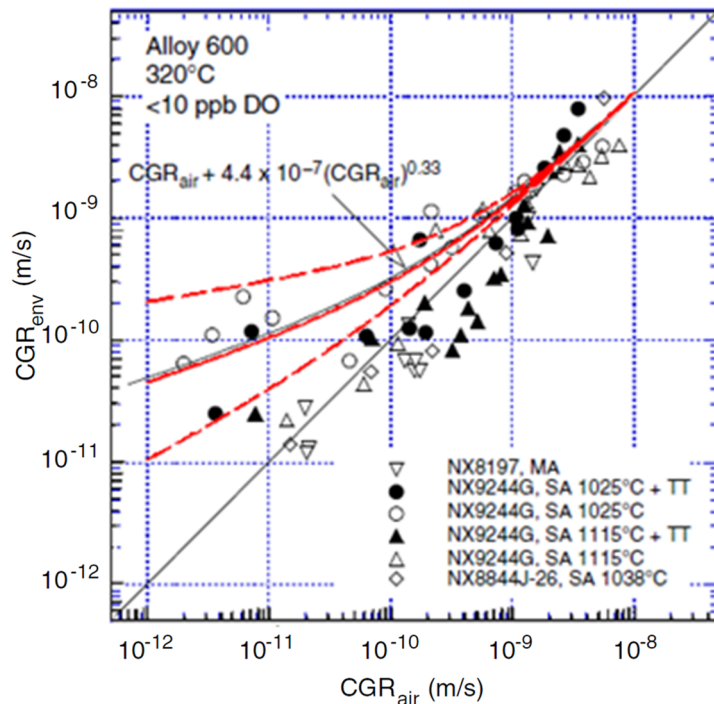
Figure 2-13. Data and Probabilistic Fit for Alloy 600 Environmental Fatigue Enhancement in Simulated PWR Environment [25]

Finally, it is noted that uncertainty is not explicitly treated for other parameters in the nickel-based alloy fatigue model (e.g., the parameters defining the stress intensity factor range or load ratio effects). There is insufficient data to quantify all parameter uncertainties in a unified and comprehensive manner. As such, all model uncertainty is consolidated in the air CGR scaling constant and environmental factor.

2.3.2.4 Model Validation

The nickel-based alloy fatigue CGR model was validated by comparison to laboratory CGR test data recorded by investigators from MHI in support of a reference curve for the Japan Society of Mechanical Engineers (JSME) code [26]. These data comprise testing in Alloy 600, Alloy 690, and their associated weld metals in simulated PWR environments and are completely independent from the database used for model development.

An example comparison between xLPR predictions and the MHI data, for Alloy 600, is shown in Figure 2-14. The xLPR predictions are shown with an environmental exponent of 0.33 and 0.25. Predictions with 0.33—the value derived from ANL data—were generally biased low in comparison to MHI data (across the different alloys and test conditions); predictions with 0.25 were unbiased. The conclusion from this validation effort was to select the range from 0.25 to 0.33 as appropriate for the nickel-based alloy environmental exponent.

In general, the xLPR model predictions were in good agreement with data: a) there was little systematic bias of the median xLPR prediction relative to data, across various conditions, provided the environmental exponent was set to 0.25; b) the xLPR model probabilistic bounds captured the data reasonably; and c) underlying model trends (e.g., versus load ratio) were similar to trends determined empirically with the MHI data.
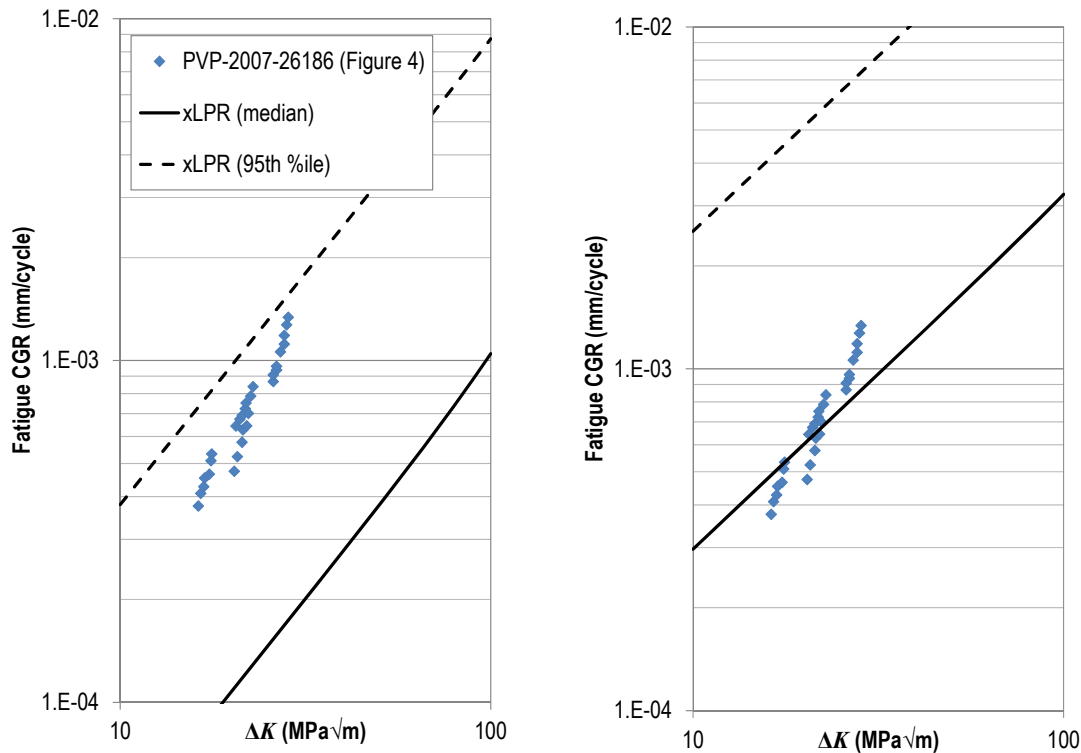
Figure 2-14. **Comparison of xLPR Model and Independent Data [26]: Alloy 600; load ratio 0.7; loading rise time 300 s; environmental exponent of 0.33 (left) or 0.25 (right)**

2.3.3 Austenitic Stainless Steel

This section presents the fatigue CGR model for general austenitic SS in deaerated water, which is applicable to Types 304, 304L, 304LE, 316, and 316L SS and their associated weld metals. It has also been validated for low-carbon variations (Types 316NG and 316LN) and cast materials (Grades CF8, CF8M, CF3, and CF3M). The relations governing fatigue CGRs in austenitic SS in reactor water are based on an extensive compilation of test data provided by Mills [24]. The specified model is in close agreement with the CGR model being developed for ASME Code Case N-809, which has not yet been published, but is described in Reference [27].

2.3.3.1 Mathematical Description

Fatigue CGRs for austenitic SS are calculated as follows:

$$\frac{da}{dN} = C_{SS} \cdot f_{alloy} \cdot F_{\tau} \cdot F_{R} \cdot F_{T} \left(\Delta K \right)^{n_{SS}}$$

[Eqn. 2-19]

where:

$\dfrac{da}{dN}$	=	per cycle fatigue rate including environmental conditions
C_{SS}	=	scaling constant
f_{alloy}	=	alloy factor
F_{τ}	=	loading rise time effect
F_{R}	=	load ratio effect
F_{T}	=	temperature effect
ΔK	=	stress intensity factor range
n_{SS}	=	Paris power-law exponent

Similar to the nickel-based alloy CGR model, this model is founded on the Paris power-law relationship and includes temperature, load ratio, and alloy-specific adjustments. Different from the nickel-based alloy CGR model, the model does not separate fatigue in air and environmental enhancement; instead, the environmental factor is built into the scaling factor, C_{SS}, and the loading rise time effect term.

2.3.3.2 Model Development

The austenitic SS fatigue CGR model is based primarily on analysis supporting the development of forthcoming ASME Code Case N-809, which will present fatigue CGR curves that may be used for crack growth analysis under Appendix C of Section XI for selected austenitic materials exposed to normal PWR environments [27]. This model attempts to capture the primary determinants of air fatigue and environmentally assisted cracking (EAC), including loading characteristics, metallurgical factors, and environmental factors. Testing supporting this analysis was conducted in environments categorized as normal for PWRs with dissolved oxygen less than ~2 ppb, temperatures between room temperature and 371°C, loading rise times of 1 to 30,000 seconds, and load ratios from 0.1 to 0.95. However, data with dissolved oxygen in the range of 5 to 500 ppb were used to validate the N-809 model. Primary investigators included participants from the U.S. (Bettis and General Electric), the U.K., Japan, France, and Sweden.

Stress intensity factor range effect: A Paris power-law exponent of 2.25 was found to be appropriate across a span of different temperatures, load ratios, loading rise times, and alloys. It is noted that this is significantly reduced in comparison to the Paris power-law exponent of roughly 4 observed for fatigue in air.

Temperature effect: Modest temperature sensitivity was evident across the range of temperatures investigated. As anticipated, CGRs increased with increasing temperature between roughly 150°C and 325°C; however, while the physical mechanism is not understood, CGRs increased with decreasing temperature between roughly 90°C and 150°C. The temperature effect model given in [Eqn. 2-20] was fit to available data (where temperature, T, is in units Kelvin).

$$F_T = e^{-2516/T} \max\left\{ 1.0 \ , \ 3.39\text{E}05 \cdot e^{-0.0301 \cdot T} \right\}$$ [Eqn. 2-20]

Load ratio effect: The load ratio effect on environmental fatigue varied markedly from heat to heat and appeared to be correlated to the carbon content. Types 304 and 316 SS with nominal carbon contents (up to 0.08%) exhibited pronounced load ratio effects at load ratios exceeding 0.5, while Types 304L and 316L with lower carbon contents (up to 0.03%) exhibited modest load ratio effects, even at load ratios exceeding 0.8. The load ratio effect model given in [Eqn. 2-21] treats the material differences observed:

$$F_R = \begin{cases} \begin{cases} 1 & R \leq 0.7 \\ 1+1.5(R-0.7) & R > 0.7 \end{cases} & \text{for} \quad \text{Type 304L, 304LE, or 316L} \\ 1+e^{8.02(R-0.748)} & \text{for} \qquad \text{Type 304 or 316} \end{cases}$$ [Eqn. 2-21]

Loading rise time effect: Fatigue CGRs in austenitic SS increased in accordance with a power law relationship relative to loading rise time. A power law exponent of 0.3 was appropriate across a span of different temperatures, load ratios, stress intensity factor ranges, and alloys. The loading rise time is truncated at 1 and 2000 seconds to mitigate large extrapolation error outside of the range of loading rise times available from laboratory testing, resulting in the following loading rise time effect:

$$F_\tau = \tau_r^{\ 0.3}$$

$$\tau_{r,limit} = \begin{cases} 1 & \tau_r < 1 \\ \tau_r & 1 \leq \tau_r \leq 2000 \\ 2000 & \tau_r > 2000 \end{cases}$$ [Eqn. 2-22]

Alloy effect: The alloy factor has two purposes: a) to scale the product of the effect models described above such that the nominal CGR predictions are in agreement with laboratory CGR measurements and b) to differentiate between CGRs for different SS alloys. The best-estimate values for the alloy factor (in units $[\text{m/cyc-s}^{0.3}]/[\text{MPa-}\sqrt{\text{m}}]^{2.25}$) are 1.39E-08 for Type 304L and 304LE, 9.10E-09 for Types 304 and 316L, and 7.28E-09 for Type 316.

2.3.3.3   Treatment of Uncertainty

To account for uncertainty in the fatigue crack growth model prediction for austenitic steels, the scaling constant, C_{SS}, in [Eqn. 2-19] can be characterized as a distributed random variable. The median value of C_{SS} is set to unity to recover the model described in the previous subsection.

The dispersion of C_{SS} has been estimated by digitizing data from Reference [24] (as reproduced in Figure 2-15) and fitting the extreme relative residuals with a log-normal distribution. Of the reported 635 data points shown in Figure 2-15, five extreme relative residuals on each side of the data scatter were used to estimate a 5th and 95th percentile for C_{SS} of 0.5 and 2.0, respectively (i.e., a log-σ parameter of 0.42). For comparison, this uncertainty is equivalent in magnitude to that derived for the CGR prediction of Alloy 600 in air (see Section 2.3.2.3).

Discussion of sampling frequency and characterization of uncertainty (as epistemic or aleatory) given in Section 2.3.2.3 for the nickel-based alloy model is generally applicable to the austenitic SS fatigue CGR model uncertainties.

Finally, similar to the nickel-based alloy model, uncertainty is not explicitly treated for other parameters in the austenitic SS fatigue model. Given the extensive data set reported in Reference [24], it is believed that additional analysis could be performed to estimate all parameter uncertainties in a unified and comprehensive manner. For now, however, all model uncertainty is consolidated in the CGR scaling constant.

304 SS, 304LE SS & 316 SS
Complete Database of Steady State CGRs

$$\frac{da}{dN} = C \left(F_{MAT'L} \; t_R^{0.3} \; F_R \; e^{-5000/R'T} \; F_{T(NA)} \right) \Delta K^{2.3}$$

$F_{MAT'L} = 1$ for 304 SS, 304LE, 304L
$F_{MAT'L} = 0.8$ for 316SS

304LE SS / 304L SS
$C = 6.75 \times 10^{-7}$
$F_R = 1$ $R \le 0.7$
$F_R = 1 + 1.5(R - 0.7)$ $R > 0.7$

304SS / 316 SS
$C = 4.43 \times 10^{-7}$
$F_R = 1 + e^{8.02(R - 0.748)}$

Legend:
◇ UK - 304LE SS
△ Japan - 304 SS
▽ Japan - 316 SS
□ Bettis - 304SS
□ GE - 304L
★ Sweden - 304 SS
○ France - 316 SS
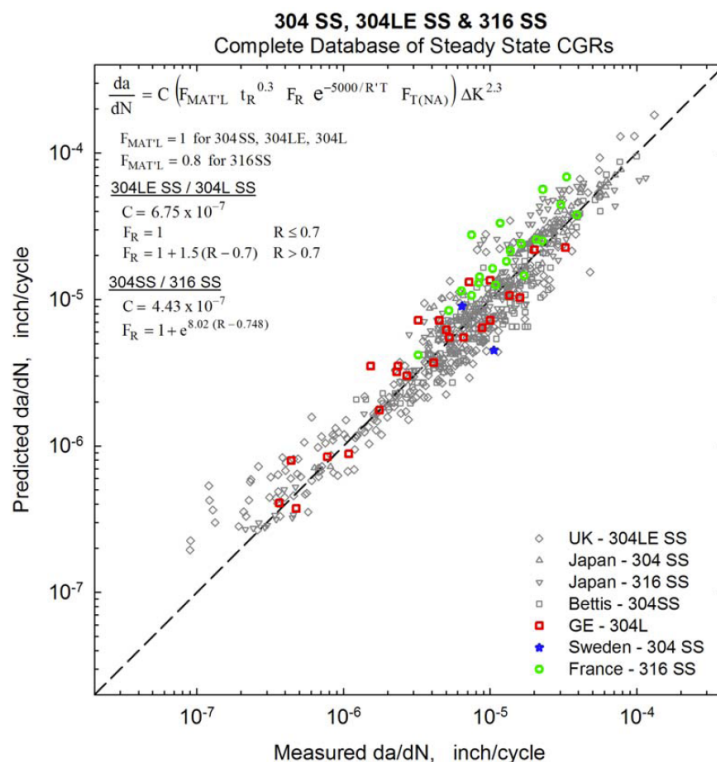
Figure 2-15.   Fatigue Crack Growth Data for Austenitic Steels [24]

2.3.3.4   Model Validation

The austenitic SS fatigue CGR model was first validated by comparison to a database of laboratory testing from ANL [28-32], EPRI [33], and Japan [27], completely independent from the database used for model development. These data comprise testing in nominal Type 304 and 316, low-carbon variations 316NG and 316LN, Alloy 304/316 weld material, and cast equivalents Grades CF8, CF8M, CF3, and CF3M in simulated PWR and BWR environments. An example comparison is shown in Figure 2-16.

This comparison demonstrated acceptable agreement: a) there was little systematic bias of the median xLPR prediction relative to data, across various conditions; b) to the extent that there was a bias, it was conservatively high; c) the xLPR mode probabilistic bounds captured the data reasonably; and d) the xLPR Paris power-law trend was exhibited by the independent data.

The austenitic SS fatigue CGR model was further validated using a model from NUREG/CR-2189 [34]. The NUREG/CR-2189 model was derived as a best-estimate (least-squares) from laboratory

data attained in the late 1970s that are independent from the xLPR development data set and the EPRI/ANL/Japan data set used in the validation described in the above paragraph. The two models were in acceptable agreement: a) the xLPR model generally predicts CGRs higher than or consistent with the NUREG/CR-2189 model (the xLPR model CGR predictions are notably higher for low-carbon SS) and b) while the xLPR model demonstrated a lower Paris power-law exponent and less sensitivity to load ratio, it was considered more accurate, e.g., because the NUREG/CR-2189 model development was based on a much smaller dataset that was available in the 1970s and included some data from BWR environments. The NUREG/CR-2189 model also includes an independently derived model for the stress intensity factor range threshold. The stress intensity factor range threshold prediction of xLPR and NUREG/CR-2189 were in very good agreement, e.g., see Figure 2-17.
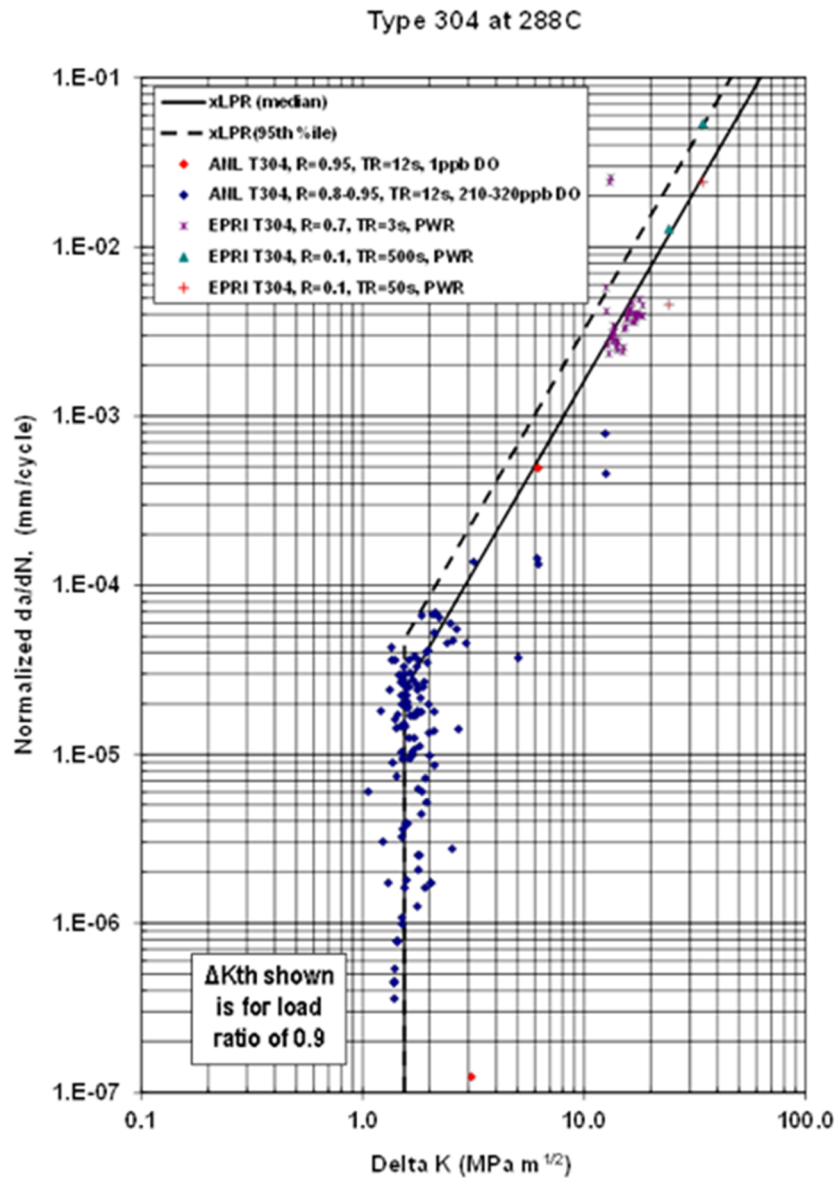
Figure 2-16.   Comparison of xLPR Model and Independent Data [28-33]: Type 304 SS

51
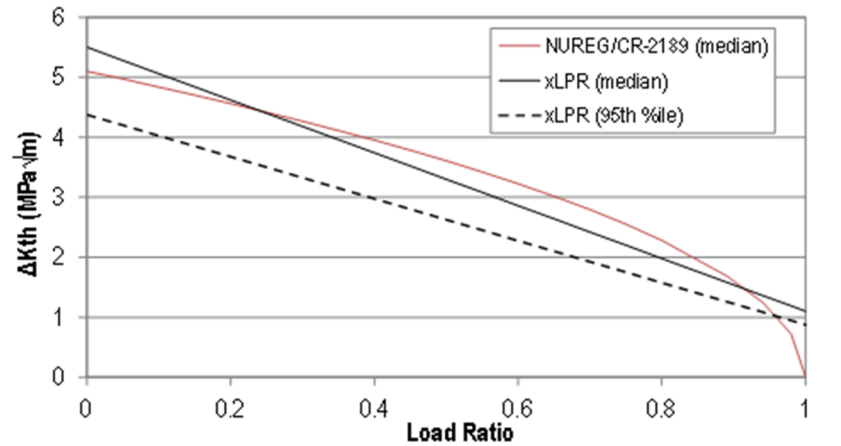
Figure 2-17   Comparison of xLPR model and NUREG-2189 [34]: Stress Intensity Factor Threshold

2.3.4   Ferritic Steels

This section presents the fatigue CGR model for general ferritic steels in PWR environments. It is generally applicable to carbon steels and low-alloy steels and their associated weld metals. The fatigue crack growth characteristics of ferritic steels are extensively reviewed in References [35], [36] and [37]. The specified model is in close agreement with ASME Code Case N-643-2 [23].

2.3.4.1   Mathematical Description

Figure 2-18 presents the flow chart used in calculating fatigue CGRs in ferritic steels in ASME Code Case N-643-2. The logic given for surface cracks is applied to develop the mathematical description for fatigue CGR, including time-dependent transitioning to EAC.

Figure 2-19 depicts example fatigue CGR curves for ferritic steels. As shown, the CGR curve is a function of stress intensity factor range, ΔK; load ratio, R; loading rise time, θ; and the sulfur content of the steel in weight percentage, S. Furthermore, the curves demonstrate different growth regimes for true corrosion fatigue (TCF) and EAC[15], as determined by time-dependent, metallurgical, and environmental conditions.

The different fatigue CGR curves for ferritic steels, such as those depicted in Figure 2-19, can all be calculated using the following general equation form:

$$\frac{da}{dN} = C_{env} \left[\frac{\Delta K}{(2.88 - R)^{n_R}} \right]^{n_{fer}} \qquad \text{[Eqn. 2-23]}$$

---

[15] Per Reference [36], TCF and EAC both describe increased rates of fatigue growth observed in a fluid environment, relative to rates of fatigue growth in air. However, TCF relates to a small (e.g., factor of two) increase while EAC relates to a significantly larger increase (e.g., factor of 10 or more) exhibited for some combinations of loading, metallurgical, and environmental conditions.

where:

$\dfrac{da}{dN}$ = per cycle fatigue rate including environmental conditions

C_{env} = environmental factor

ΔK = stress intensity factor range

R = load ratio

n_{fer} = Paris power-law exponent

n_R = load ratio exponent

As with the other two material-specific fatigue models, this model is founded on a Paris power-law principle and includes a load ratio effect. The environmental factor, Paris power-law exponent, and sulfur-dependent load ratio exponent are varied to represent the different growth regimes, as summarized in Table 2-1 and detailed in the next subsection. A temperature effect has not been included, despite experimental evidence to the contrary. The effect of temperature variation is incorporated as model uncertainty.

Table 2-1.   Parameters Defining Fatigue CGR Model for Ferritic Steel in Different Growth Regimes

Growth Regime	Environmental Factor	Paris Power-Law Exponent	Load Ratio Exponent
	C_{env}	n_{fer}	n_R
Air	7.87E-11 (m/cyc)/(MPa-√m)$^{3.07}$	3.07	1
TCF	2.76E-10 (m/cyc)/(MPa-√m)$^{3.07}$	3.07	1
EAC of medium-sulfur material	1.17E-09 (m/cyc)/(MPa-√m)$^{3.07}$	3.07	1
Nominal EAC of high-sulfur material	1.42E-07 (m/cyc)/(MPa-√m)$^{3.07}$	3.07	2.166
Upper transition of EAC for high-sulfur material	see [Eqn. 2-26]	0.948	1

2.3.4.2 Model Development

The fatigue CGR model for ferritic steels is based on analysis presented in References [35] and [36] and ultimately developed into a model in ASME Code Case N-643-2 [23]. The underlying analysis included a wide range of CGR measurement data spanning temperatures from 130°C to 325°C (although predominantly at 288°C), a diversity of loading rise times (although

predominantly at 30 seconds), and sulfur contents from very low (e.g., 0.004 %wt) to 0.02 %wt.[16] Reference [35] suggests that the application of the ferritic fatigue CGR model—which is developed from forging material—for plate, HAZ, and weld material is conservative with respect to limited data. Until other more specific models are developed, the model form and input recommendations given below are considered acceptable for all forms of ferritic steel found in the primary RCS.

Analysis was largely focused on determining the conditions for which transition to EAC fatigue from TCF is permissible. The following list describes the conditions for which the material is not susceptible to EAC:

- *Low sulfur material:* Sulfur impurities (such as MnS) in the steel have a profound effect on the EAC response. Sulfide ions interfere with the kinetics of repassivation of base metal surfaces and act as a hydrogen recombination poison; atomic hydrogen produced by the corrosion reaction at the bare metal surfaces is retarded from recombining into molecular hydrogen, leaving it available to drive SCC/EAC [38]. Analysis presented in Reference [35] suggests a minimum threshold of 0.004% sulfur content by weight is necessary for EAC to occur in primary water environments.

- *Insufficient rate of sulfide supply to engage EAC:* To transition to EAC from TCF, the crack tip advancement must occur at a rate fast enough such that the sulfide supply to the crack tip is sufficiently high (i.e., such that sulfide inclusions are exposed faster than dissolved sulfur ions are removed by diffusion). Code Case N-643-2 defines the following "critical velocity" that must be achieved before EAC can engage:

$$V_{trans} = \begin{cases} 5.1\text{E-7 [mm/s]} & a \leq 2.5 \text{ [mm]} \\ 5.1\text{E-7 [mm/s]} \cdot \left(2.5\,[\text{mm}]/a\right) & a > 2.5 \text{ [mm]} \end{cases} \qquad \text{[Eqn. 2-24]}$$

  If the sum of PWSCC and fatigue growth rates is below this critical velocity at any given time, fatigue growth cannot transition to EAC.

- *Insufficient exposure to sulfides to transition to EAC:* Furthermore, to transition to EAC, the crack must advance at a rate above the critical velocity for some critical extent. Code Case N-643-2 defines this critical extent as 0.33 mm. In accordance with the Code Case, this extent does not necessarily need to be attained over a single continuous period.

- *Insufficient rate of sulfide supply to maintain EAC:* Currently available data show that rapid transients cause little to no EAC in primary water environments for relatively low material sulfur content. It is hypothesized that this occurs because the rate of sulfide supply is insufficient to maintain EAC. Reference [35] suggests the use of a one second loading rise time and 0.013% sulfur content by weight to separate conditions for which EAC can be maintained. That is, for material with sulfur content below 0.013%, EAC can only be maintained for transients with loading rise times slower than one second.

---

[16] Reference [35] does note that predictions involving the combination of intermediate temperature (200-250°C) and long loading rise time (>1000 s) may be unreliable given the scarcity of applicable data points.

- *High CGRs:* Under particularly aggressive loading conditions, the importance of the environmental effect begins to moderate until, at very aggressive loading conditions, CGR is well-predicted by the TCF model.[17] Specifically, the TCF curve is regained for stress intensity factor ranges above that specified below:

$$\Delta K_c = \left(\frac{C_{upper}}{C_1} \right)^{2.122} \theta^{0.326} \left(2.88 - R \right)$$
[Eqn. 2-25]

where C_1 and C_{upper} are the environmental factors applied for TCF and in the upper transition region for EAC, as defined below.

If any of the conditions that limit EAC are met, fatigue progresses as TCF. The TCF curve recommended in xLPR Version 2.0 is based on data from the EPRI Database for Environmentally Assisted Cracking (EDEAC) in nominal PWR environments with bulk sulfur content less than 0.005% by weight [39]. The median environmental factor (C_{env}) for these data is 2.76E-10 (m/cyc)/(MPa-√m)$^{-3.07}$—equivalent to roughly 3.5 times fatigue in air.[18] The best-fit Paris power-law and sulfur dependent load ratio exponents are 3.07 and 1.0, respectively—parallel to fatigue behavior in air.

If none of the conditions that limit EAC are met, fatigue progresses as EAC. Consistent with laboratory experimentation results, the EAC behavior is differentiated between medium sulfur materials (0.004% to 0.013% sulfur content by weight) and high sulfur materials (>0.013% sulfur content by weight). For EAC in medium sulfur materials, the best-fit environmental factor is 1.17E-09 (m/cyc)/(MPa-√m)$^{-3.07}$, based on a conservative (95th percentile) curve derived from a combined set of EDEAC and United Kingdom (UK) data (934 points) from medium sulfur A508 forging materials tested in primary environments, with loading rise times exceeding one second, over a span of temperatures [35]. The conservative fit is appropriate as it better reflects the CGRs of medium sulfur specimens that did transition to EAC. Again, the best-fit Paris power-law and sulfur dependent load ratio exponents are 3.07 and 1.0, respectively—parallel to fatigue in air.

For EAC in high sulfur materials, the nominal environmental enhancement can be much greater and it will exhibit a greater dependence on load ratio (relative to air fatigue, TCF, or EAC in medium sulfur materials). Based on a conservative (95th percentile) curve derived from fatigue presenting as EAC in high sulfur material [36], the best-fit environmental factor is set to 1.42E-07 (m/cyc)/(MPa-√m)$^{-3.07}$, the Paris power-law constant is set to 3.07, and the sulfur dependent load ratio exponent is set to 2.166. Note that this is between 50 and 200 times greater than air fatigue CGRs, depending on load ratio.

---

[17] In reality, under very aggressive loading, the environmental fatigue behavior approaches air fatigue behavior. However, based on conservative N-643-2 recommendations, TCF behavior is used at the lower bound for fatigue CGR.

[18] A best-fit environmental factor for these data is approximately 1.1E-10 (m/cyc)/(MPa-√m)$^{-3.07}$.

As discussed previously, the importance of the environmental effect diminishes at progressively aggressive loading conditions, leading to a transition from EAC back to TCF. This transition is modeled to occur at a stress intensity factor range threshold defined below [36]:

$$\Delta K_b = C_{K_b} \cdot \theta^{0.326} \cdot (2.88 - R)^{2.69}$$

[Eqn. 2-26]

where the best-fit value of C_{Kb} is 0.498.

Between ΔK_b, at which the transition from EAC to TCF begins, and ΔK_c, at which TCF conditions are regained, the best-fit Paris power-law exponent is 0.948 and the sulfur-dependent load ratio exponent is 1.0. The environmental factor is the following function of loading rise time and load ratio (effectively yielding a linear transition):

$$C_{upper} = C_{EAC} \cdot (\Delta K_b)^{2.122} (2.88 - R)^{-5.702}$$

[Eqn. 2-27]

where C_{EAC} is the previously stated environmental factor for EAC of high sulfur material.
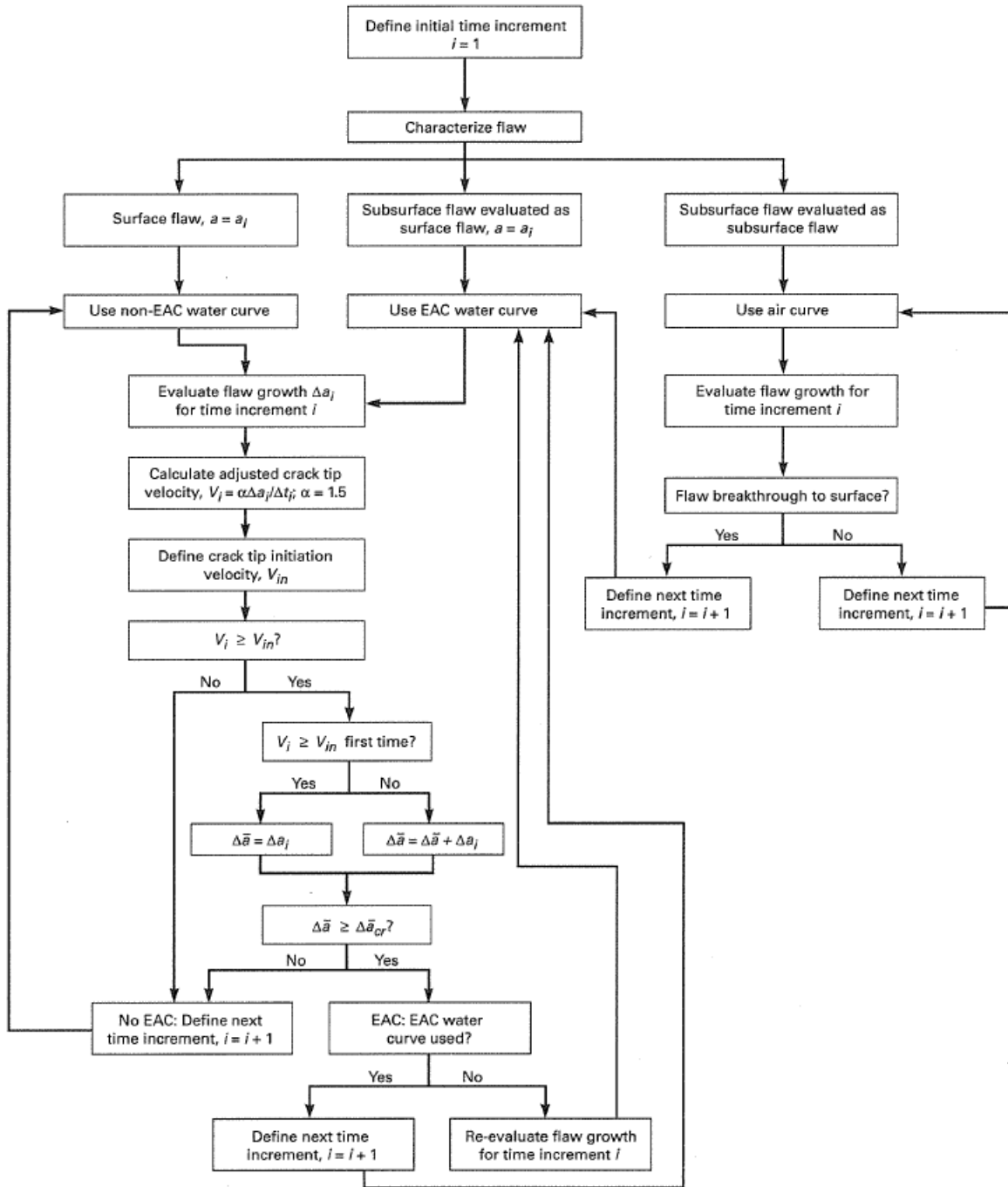
Figure 2-18. Flow Chart of Procedure Used in Determining Susceptibility to EAC for Fatigue Crack Growth in Ferritic Steels [23]
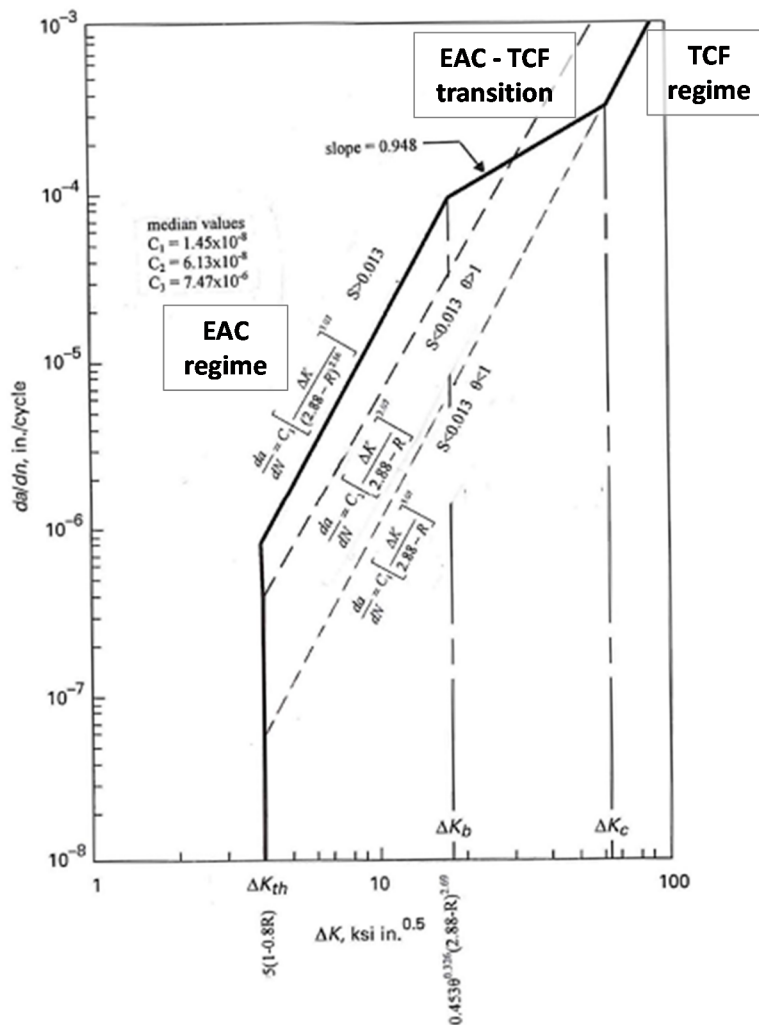
Figure 2-19.   Fatigue Crack Growth Relations for Ferritic Steels (in English units)

2.3.4.3   Treatment of Uncertainty

To account for uncertainty in the fatigue crack growth model prediction for ferritic steels, the environmental factor, C_{env}, in [Eqn. 2-23] can be characterized as a distributed random variable. The median values for the environmental factor at TCF conditions, EAC conditions in medium sulfur material, and EAC conditions in high sulfur material are taken to be the values given in the previous section: 2.76E-10, 1.17E-9, and 1.42E-7 (m/cyc)/(MPa-$\sqrt{m}$)$^{-3.07}$, respectively.

The uncertainty in the TCF environmental factor can then be represented by a log-normal distribution with 5th and 95th percentiles that are a factor of 0.46 and 2.16 relative to the median (or a log-σ parameter of 0.467). This uncertainty is based on scatter of low sulfur material fatigue CGR data about the TCF model, as presented in Reference [35].

The uncertainty in the EAC environmental factor can then be represented by a log-normal distribution with 5th and 95th percentiles that are a factor of 0.23 and 4.25 relative to the median (or a log-σ parameter of 0.88). This uncertainty is based on scatter of medium sulfur material

fatigue CGR data tested in simulated primary water environments with loading rise times exceeding one second, as presented in Reference [35].

Another critical parameter in the prediction of the EAC in high-sulfur material is the stress intensity factor range threshold at which environmental enhancement begins to moderate, ΔK_b. The best-estimate prediction for this threshold is attained with [Eqn. 2-26] by setting the scaling constant, C_{Kb}, to 0.498. To incorporate uncertainty in this quantity, results from Reference [36] (approximately 100 measurements, as shown in Figure 2-20) were used to develop a distribution for C_{Kb}. The recommended distribution for C_{Kb} is log-normally distributed with a median of 0.498, a 5th percentile of 0.35, and a 95th percentile of 0.70. In Reference [36], the author cites two unique sources of uncertainty (besides material and environmental differences) in this parameter estimate: a) that a large fraction of the data comes from tests not designed to determine the threshold and therefore may not be as reliable and b) a hysteresis between the different regimes of EAC growth (that is not explicitly modeled) has been observed in laboratory testing.
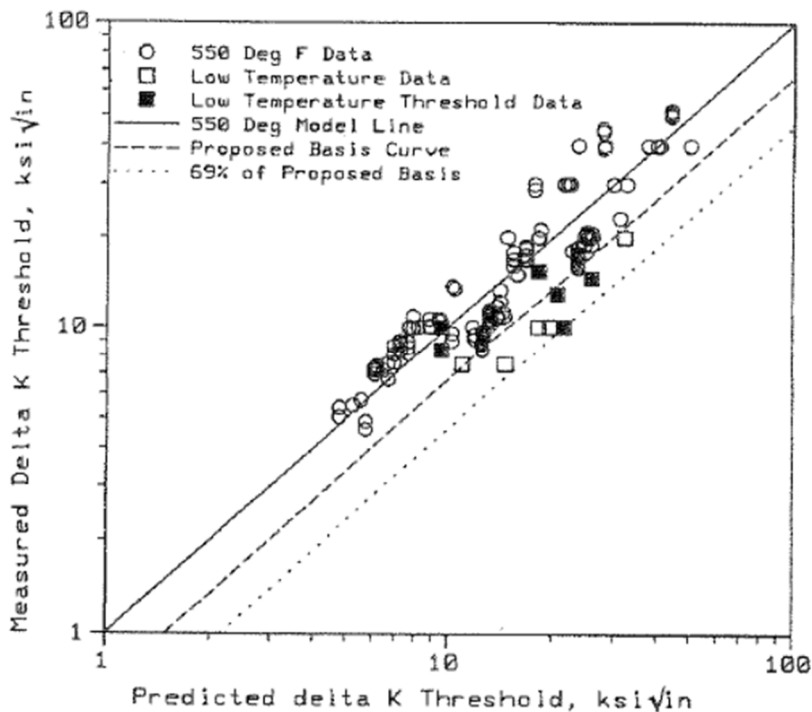
Figure 2-20.   Predicted vs. Measured ΔK_b For Ferritic Steels in Reactor Water Environment [36]

Discussion of sampling frequency and characterization of uncertainty (as epistemic or aleatory) given in Section 2.3.2.3 for the nickel-based alloy model is generally applicable to the ferritic steel fatigue CGR model uncertainties.

Finally, like the nickel-based alloy and austenitic SS models, uncertainty is not explicitly treated for other parameters in the ferritic steel model. Given the extensive data set reported in References [35] and [36], it is believed that additional analysis could be performed to estimate all parameter uncertainties in a unified and comprehensive manner. For now, however, all model uncertainty is consolidated in the environmental factor and ΔK_b.

2.3.4.4 Model Validation

The ferritic steel fatigue model was validated by comparison with an independently derived reference curve from ASME Boiler and Pressure Vessel Code, Section XI, Appendix A, Article A-4300 [40]. The A-4300 reference curve is a bounding curve relative to data that were available at the time it was developed. The A-4300 reference curve naïvely does not separate TCF from EAC, and in effect is considered a mixture of the two distinct growth modes because it is based on a combined dataset of fatigue crack growth tests from these two modes. At higher ΔK values, as expected, the TCF predictions of the xLPR model were consistent with or less than the A-4300 reference curve and the EAC predictions of the xLPR model were consistent with or greater than the A-4300 reference curve, e.g., see Figure 2-21 and Figure 2-22[19]. The Paris power-law exponents of the independent models were in good agreement. At lower ΔK values, the xLPR model is higher than the A-4300 reference curve irrespective of the growth regime.
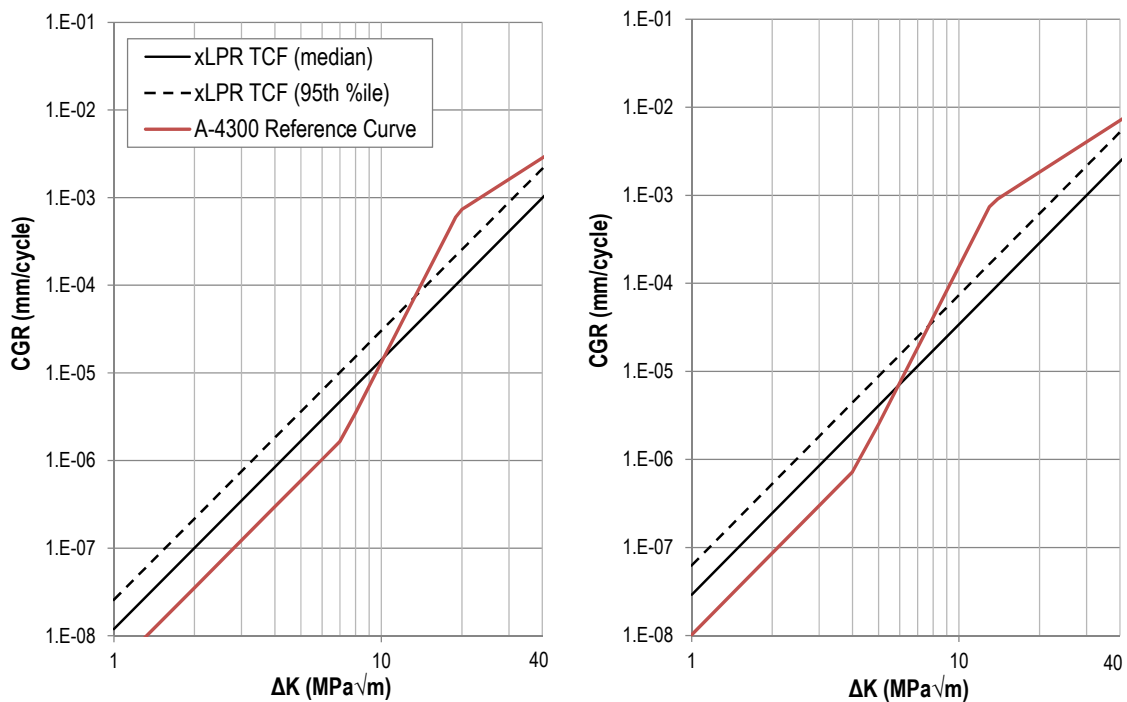
Figure 2-21.   Comparison of xLPR model and Section XI Article A-4300 [40]: TCF Predictions at a Load Ratio of 0.1 (left) or 0.8 (right)

---

[19] Note that the stress intensity factor range threshold is not depicted in these plots.
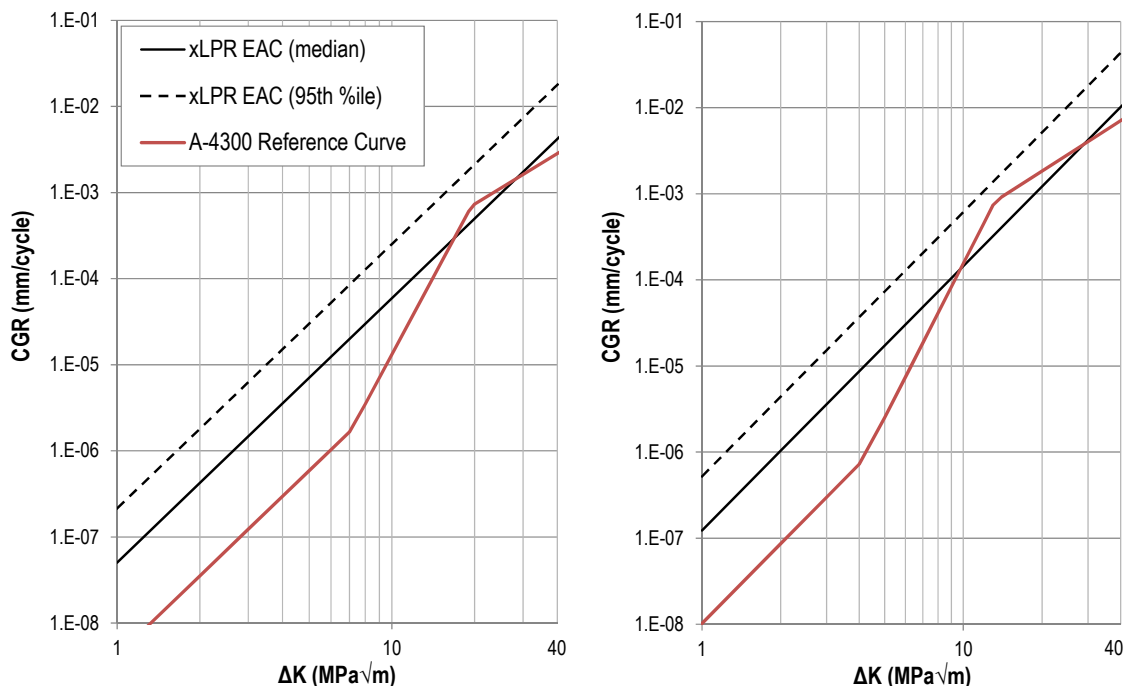
Figure 2-22. Comparison of xLPR model and Section XI Article A-4300 [40]: EAC Predictions in Medium Sulfur Material at a Load Ratio of 0.1 (left) or 0.8 (right)

2.4 General Crack Growth Requirements

Additional modeling steps are required to integrate CGR predictions over time and to apply the resulting crack advancement or extension to a finite number of crack locations in order to predict crack shape and size. This section details these modeling steps.

2.4.1 Time Integration

The mathematical models for PWSCC CGRs specified in [Eqn. 2-1] through [Eqn. 2-3] constitute non-linear ordinary differential equations (ODEs) for crack advancement. Nonlinearity arises from the stress intensity factor term, which is a nonlinear function of crack shape and size—not to mention the discrete coalescence and transition events that further couple and complicate the crack growth equations. These equations are solved numerically using an explicit fixed-time forward Euler method.[20] The nominal integration time step for solving the equations is user-defined. This value should be selected to result in converged statistics (within the tolerance needed for analysis) for the Monte Carlo simulation. The use of one effective full power month (1/12 of an effective full power year) has been found to be sufficient in other probabilistic crack simulations for PWR components, e.g., see Reference [6], but a satisfactory value depends on the exact input conditions including fatigue cycling frequencies.

---

[20] Implicit or adaptive numerical integration methods could yield more reliable ODE solutions at the cost of increased runtime. High precision ODE solution methods are not as essential for Monte Carlo simulations as for high fidelity deterministic simulations.

The mathematical models for fatigue CGRs specified for different material classes in [Eqn. 2-13], [Eqn. 2-19], and [Eqn. 2-23] give crack advancement on a per cycle basis. Crack advancement on a per cycle basis can be converted to the time rate of growth (e.g., *da/dt*) by multiplying by the number of cycles per unit time.[21] After this conversion, the same time integration method described above for PWSCC can be applied.

The net CGR at each integration time step is the sum of the PWSCC CGR and the fatigue CGRs for each active transient component. In general, it is this net CGR that is integrated over time.

The methods for time integration described above generally account for time-variant properties. That is, at each integration time step, the conditions relevant to crack growth are updated. This is especially important for stress intensity factor values, which change as a function of crack growth. The calculation of stress intensity factors is detailed in the K-Solutions and Transitioning Crack Subgroup Reports.

2.4.2 Crack Shape and Size

To permit a practical runtime, crack growth is modeled at only a few key locations (as opposed to semi-continuously over the entire crack profile as would be achieved with finite element models). Facilitating this approach, three general crack types are defined in the xLPR Version 2.0 Framework (all are depicted in Figure 2-23). These three crack types are discussed below:

- *Surface crack:* Surface cracks are constrained to have a symmetric semi-elliptical shape and a depth less than the component thickness. Cracks in xLPR conform to the surface crack type from the time of initiation until a) the crack grows through-wall[22], b) the crack is removed from service, or c) coalescence occurs (see Section 4).

  Surface cracks are defined by their center location, depth, and inner diameter (ID) length. The extension of surface cracks is solved at the deepest point and at surface points at each integration time step. Together, the extensions at these three locations are sufficient to update the crack shape.[23]

- *Transitioning through-wall crack:* Transitioning through-wall cracks are constrained to be symmetric and trapezoidal. By definition, for a transitioning crack, depth is equal to the component thickness and outer diameter (OD) length is less than ID length. Cracks in xLPR conform to the transitioning crack type from the time of through-wall growth until a) the ID and OD length become equivalent (in terms of radians for circumferential flaws and in terms

---

[21] The TIFFANY module and the xLPR Framework are responsible for resolving inputs defining patterns and time histories for fatigue cycles into the number of fatigue cycles during each integration time step.

[22] The Transitioning Crack Subgroup defines a surface crack depth less than the thickness at which ligament collapse rapidly occurs leading to a through-wall crack.

[23] Growth asymmetry (between surface tips) can occur in xLPR due to differing PWSCC susceptibility (e.g., different material). In these cases, the updated crack is assumed to remain symmetric, but its center location is shifted to account for the asymmetry. In the Computational Framework, this is implemented by evaluating growth at one general surface tip using an average of the conditions at the two surface tips (and scaling the result by two to attain total growth per integration time step).

of absolute length for axial flaws)[24], b) the crack is removed from service, or c) coalescence occurs.

Transitioning cracks are defined by their center location, ID length, and OD length. The extension of the transitioning crack is solved at the two ID surface tips and the two OD surface tips. Together, the extensions at these four locations are sufficient to update the crack shape.

- *Idealized through-wall crack:* Idealized through-wall cracks are constrained to be symmetric and to have equivalent ID and OD lengths (in terms of radians). Cracks in xLPR conform to the idealized through-wall crack type from the time at which a transitioning crack's ID and OD lengths become equivalent until a) the crack is removed from service or b) coalescence occurs.

  Idealized through-wall cracks are defined by their center location and length. The extension of the idealized through-wall crack is solved at the two ID surface tips and the two OD surface tips.[25] Together, the extensions at these two locations are sufficient to update the crack shape.

2.4.2.1 Special Considerations

Two instances have been identified for which growth is not well-approximated using the conventions established above. First, for dissimilar metal weld simulation, the surface tips of an axial surface crack can eventually reach the base metals (see Figure 2-24). When this occurs, the PWSCC growth mechanism at the surface tips is expected to slow drastically due to reduced susceptibility of the base metals. As the deepest point continues to advance, it can lead to a condition in which the depth becomes greater than the half-length, which is often beyond the range of applicability for existing stress intensity factor solutions. To achieve better agreement with natural crack growth (as predicted by finite element analysis studies) predictions for depth, the ratio of half-length to depth is limited to a minimum of one when calculating the stress intensity factor at the deepest point [41].

Likewise, the use of weld inlay or onlay or the use of stress improvement can result in low growth near the ID surface of a component. Natural crack growth predictions suggest that if a surface crack can escape this region of low growth, its growth can accelerate in both the depth and length direction under the resistant region, leading to a balloon crack shape. In contrast, conventional K-calculation and growth (e.g., at the deepest point tip and at the surface tips) can predict slow length growth and eventual declines in the stress intensity factor at the deepest point. Once more, to improve agreement with natural crack growth in this scenario, the ratio of half-length to depth is limited to a minimum of one when calculating the stress intensity factor at the deepest point.

---

[24] Since the OD length tends to approach the ID length asymptotically, the Transitioning Crack Subgroup defines an OD to ID length ratio at which the transition to the Idealized Through-Wall Crack occurs.

[25] In the Computational Framework, this is implemented by evaluating growth at one general ID surface tip using an average of the conditions at the two ID surface tips (and scaling the result by two to attain total growth per integration time step); likewise for the OD surface tip locations.
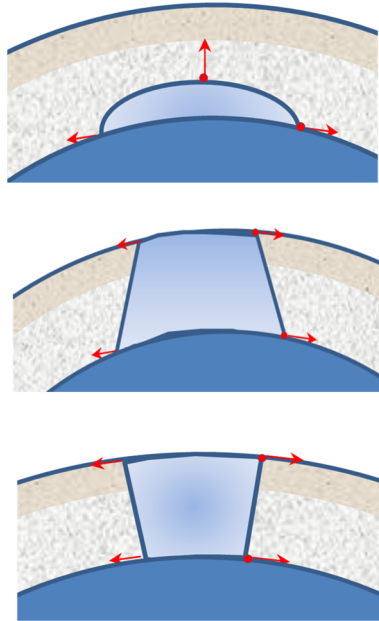
Figure 2-23. **Idealized Crack Types in xLPR Version 2.0: Surface Crack (top), Transitioning Crack (middle), and Idealized Through-Wall Crack (bottom)**
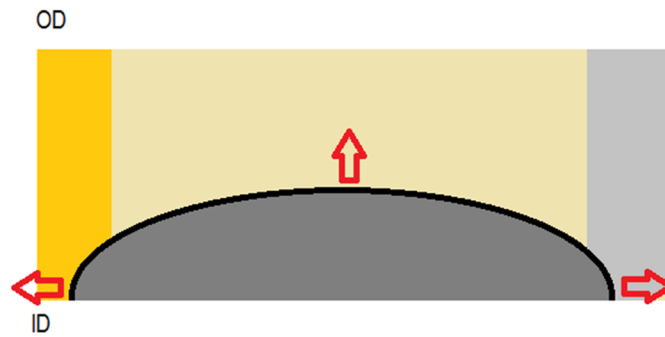
Figure 2-24. Example of Axial Crack Pinned Between Base Metals

2.5 Model Assumptions

This section identifies the assumptions, simplifications, and dependencies that are considered most important with respect to the CGR models.

- **Empirical modeling approach**: Probabilistic CGR model forms have been developed to accommodate laboratory growth data, allowing functional dependences on conditions that are known to have a strong impact on growth. These model parameters have been fit to laboratory data with regression techniques and have been validated against limited field experience.

  This approach to CGR modeling is preferred to fully mechanistic models given the relative complexity and the current state of knowledge associated with the physical process. Since the models are derived empirically, they are only as accurate and representative of field

conditions as the underlying data sets. The aforementioned investigations place particular emphasis on simulating representative conditions, combining the knowledge of laboratory and industry application experts. Further, screening processes are applied to data sets in the aforementioned investigations to ensure that data points adverse to quality representation of field conditions (e.g., obtained under improper conditions or with significant measurement error) are eliminated prior to model development. (Data screened from direct model development are often used for consistency comparisons to check for the implications if such data were not excluded.) Furthermore, laboratory studies that are considered reliable place tight controls on the measurement and characterization of growth rate and relevant conditions (e.g., stress intensity factor values, temperature, chemistry, etc.). Therefore, models are expected to contain limited bias with respect to real plant conditions.

- **Crack shape idealization:** Cracks are assumed to grow in one of three idealized planar shapes: semi-elliptical surface cracks, idealized through-wall cracks (same ID and OD length in terms of radians), or symmetric transitioning cracks. This convention is essential and is reflected in models throughout xLPR Version 2.0, including those that solve for local stress intensity factors. For the purposes of the xLPR program, these crack shapes are sufficiently representative of the physical stages of cracking.

- **Growth mechanism independence:** PWSCC and fatigue growth are assumed to be independent. Accordingly, in materials susceptible to both mechanisms, calculated PWSCC and fatigue growth rates are superimposed to obtain a total growth rate. This assumption aligns with Section XI guidance for flaw evaluation in Alloy 600/82/182/132 piping materials [3].

  Laboratory testing to determine PWSCC CGRs often involves a gradual transition from fatigue type loading to periodic partial unloading to steady loading conditions (see for example MRP-115 [9]). The growth observed during the transition in loading appears in general terms to be consistent with the independent treatment of fatigue and SCC growth (i.e., with the lack of significant synergistic effects).

- **Missing dependencies**: The CGR models allow a functional dependence of growth rate on the predominant drivers of growth: Mode (I) stress intensity factors, temperature, water chemistry (specifically, hydrogen concentration), material conditions (e.g., sulfur content for fatigue in ferritic steel), and load characteristics (e.g., loading rise time). Each of these dependencies has a strong technical basis.

  Modes (II) and (III) loading (in-plane and out-of-plane shear, respectively) are not directly considered in the CGR models, nor are they considered program-wide in xLPR Version 2.0. Mode I loading is considered to be the driving force for crack growth in PWR components applicable to xLPR Version 2.0. The effect of torsion loading on growth of circumferential cracks is modeled indirectly in xLPR Version 2.0 by including the torsion moment in the calculation of the effective bending moment [42], thus resulting in an increase in the calculated Mode (I) stress intensity factor.

  PWSCC growth is known to be dependent on orientation with respect to certain anisotropic material properties (e.g., direction of rolling, epitaxial weld crystallization, etc.). However, the CGR models do not include terms to account explicitly for orientation dependencies. This is partially because in practice orientation with respect to key material/manufacturing properties such as weld dendrite direction may not be known. Also, the xLPR computational framework does not track several anisotropic properties (e.g., material

banding). Note, however, that the data used to develop models are representative of susceptible directions of growth in each material.

PWSCC growth is known to be dependent on the level of material cold work. Cold work tends to introduce plasticity and grain misorientation, which may aid growth. The CGR models do not include functional terms to account for levels of cold work. This is partially because the components of interest do not include intentional cold work and because in practice cold work levels of specific components are not known. In the case of PWSCC of thick-wall Alloy 600 wrought material, cold work levels greater than that expected for most components of interest are necessary for the cold work to result in a substantial acceleration of the CGR (based on laboratory CGR data such as [43]). In addition, the xLPR computational framework does not track cold work. Note, however, that model uncertainties have in some cases been developed to capture experimental data from specimens spanning a range of feasible levels of cold work.

- **Range of applicability:** The PWSCC CGR models for thick-wall Alloy 600 and Alloys 82/182/132 have been validated over the range of conditions common during normal PWR plant operation including stress intensity factors from 10 to 80 MPa√m, temperatures from 280 to 350°C, and ECPs from -50 to 50 mV relative to the Ni/NiO transition (e.g., hydrogen concentration from 1 to 60 cc(STP)/kg at hot leg conditions). Extrapolation of the models at conditions far outside of these ranges is not recommended or at least should be substantiated (e.g., with data, sensitivity studies, etc.).

  The absence of independent validation for CGR at low stress intensity factors should have little effect within the xLPR framework because initial depths are representative of macroscopic flaws (e.g., ~1 mm or more) and therefore often begin with stress intensity factors near or greater than 10 MPa√m. Furthermore, the model for PWSCC growth implemented in xLPR 2.0 for Alloys 82/182/132 weld metal assumes a zero stress intensity factor threshold such that crack extension is predicted regardless of the magnitude of any stress intensity factor greater than zero. The absence of independent validation of high stress intensity factors should have little effect on leakage prediction within the xLPR framework because stress intensity factors exceeding 80 MPa√m are anticipated only for very deep cracks, which will grow through-wall relatively quickly regardless of the precise CGR prediction.

  The fatigue CGR models have been validated over the range of conditions common during normal PWR plant operation including stress intensity factor ranges between 0 and 60 MPa√m, load ratios between 0 and 1, loading rise times between 0.1 and 7200 seconds, temperatures between 160°C and 315°C, and sulfur contents from 0 to 0.02%. Extrapolation of the models at conditions far outside of these ranges is not recommended or at least should be substantiated (e.g., with data, sensitivity studies, etc.).

- **Material interfaces**: Crack growth prediction is complicated in regions near weld material interfaces due to thermally altered mechanical properties and potential material dilution. The xLPR Version 2.0 program does not account for the complex variation of material properties that exist at weld material interfaces. Instead, for example, the growth of a crack tip near the interface of a weld metal and a base metal, but still in the weld metal, would be predicted with the weld metal model; immediately after the crack tip extends into the base metal, growth would be predicted with the base metal model. Uncertainties for CGR models have in a limited number of cases been developed to capture the variability in experimental data taken near weld interfaces. No special considerations are made for crack growth along weld-base metal interfaces.

In reality, dissimilar metal butt weld geometries include dilution zones (e.g., for an Alloy 182 weld adjacent to a lower chromium material such as low-alloy steel). While a specific weld interface/dilution zone model has not been developed, plant PWSCC experience for piping butt weld locations has not indicated any apparent preference for cracking to occur in the Alloys 82/182 weld metal close to interfaces with lower-chromium materials. The nominal chromium level of Alloy 182 weld metal, which is very similar to that for Alloy 600, is sufficiently low to make Alloy 182 potentially susceptible to relatively high rates of PWSCC growth.

In addition, in reality, dissimilar metal and similar metal butt weld geometries are subject to heat-affected zones (HAZs) that extend over a portion of the base metal. While a specific model has not been developed for Alloy 600 HAZ material, a number of data points included in validation efforts and representing HAZ conditions were bounded by the nominal Alloy 600 model. In addition, Reference [44] concludes that CGRs recorded in Alloy 600 HAZ material are generally similar to those obtained in corresponding base metal.

- **Out of plane crack growth:** Out-of-plane crack growth is not considered by the growth models. Instead, cracks are assumed to be located in idealized axial or circumferential planes during crack initiation and growth. In reality, flaws may have a highly branched three-dimensional structure.

3. CRACK GROWTH RATE MODULE

The CGR module is incorporated within the xLPR Computational Framework to calculate the CGR for a given set of material, environmental, and loading conditions. A number of integration requirements are applied within the Framework to supply the correct inputs to the CGR module and to integrate the outputs of the CGR module to yield predictions for crack location, shape, and size versus time. The CGR module implements the CGR models detailed in Section 2: the MRP-55 [2], MRP-115 [9], and MRP-263 [5] studies published by EPRI are the bases for the PWSCC CGR calculations, while ASME Code Case N-643-2 [23], Code Case N-809 [45], and NUREG/CR-6721 [25] are the bases for fatigue CGR calculations.

This section presents the CGR module and is organized as follows:

- Section 3.1 provides an overview of the module, including a description of its scope and limitations

- Section 3.2 describes the requirements that are enforced in the implementation of the CGR models and the interfacing requirements to ensure proper usage of the module within the xLPR Computational Framework.

- Section 3.3 details the inputs to and outputs from the module.

- Section 3.4 summarizes the design and implementation of the module.

- Section 3.5 summarizes the V&V performed to ensure the correct implementation of the module-level requirements.

3.1 Module Scope and Limitations

Figure 3-1 provides a diagram describing how the CGR module is incorporated by the xLPR Computational Framework for a single point in time. While not depicted in the diagram, the Framework discretizes time and implements a numerical time integration method to solve for crack growth versus time. This time integration takes into consideration other processes including crack and component stability, leakage, and non-destructive examination. These other processes are outside of the scope of this report.

For a given point in simulation time, the Framework performs the input selection to ensure that all physical conditions, some of which are time-varying, are appropriately communicated to the CGR module. The Framework performs this input selection not only on a crack-specific basis—to account for crack-to-crack differences and within-component variation—but also a crack location-specific basis—to account for varying stress intensity factor on the advancing crack front. CGR prediction is carried out at a finite number of characteristic locations on each crack (e.g., deepest point and surface tips for surface cracks) to allow reasonable updates to crack size, shape, and location. The interfacing requirements for the Framework to perform the operations described above and depicted in Figure 3-1 are discussed in Section 3.2.2.

The operations of the CGR module are summarized within the enclosed section in Figure 3-1. Each time the module is called, it first verifies that the inputs are within acceptable ranges (as defined in Section 3.3); if not, the module returns control to the Framework with an error flag to specify the input that is out of range. If all inputs are within acceptable ranges, the next set of

operations selects the correct material-specific and mechanism-specific model parameters and routes to the material-specific and mechanism-specific CGR functions.

Immediately preceding the call to the CGR functions, a number of pre-calculations are performed. These include, for instance, calculation of the stress intensity factor range, ΔK, or load ratio from minimum and maximum stress intensity factor inputs for each active transient component.

The cornerstone of the CGR module is the set of CGR functions that implement the CGR models described in Section 2. These functions return PWSCC and fatigue CGRs for the given material and physical conditions. The fatigue CGR function is called once for each active transient component. The sum of all CGRs is returned to the Framework for integration.
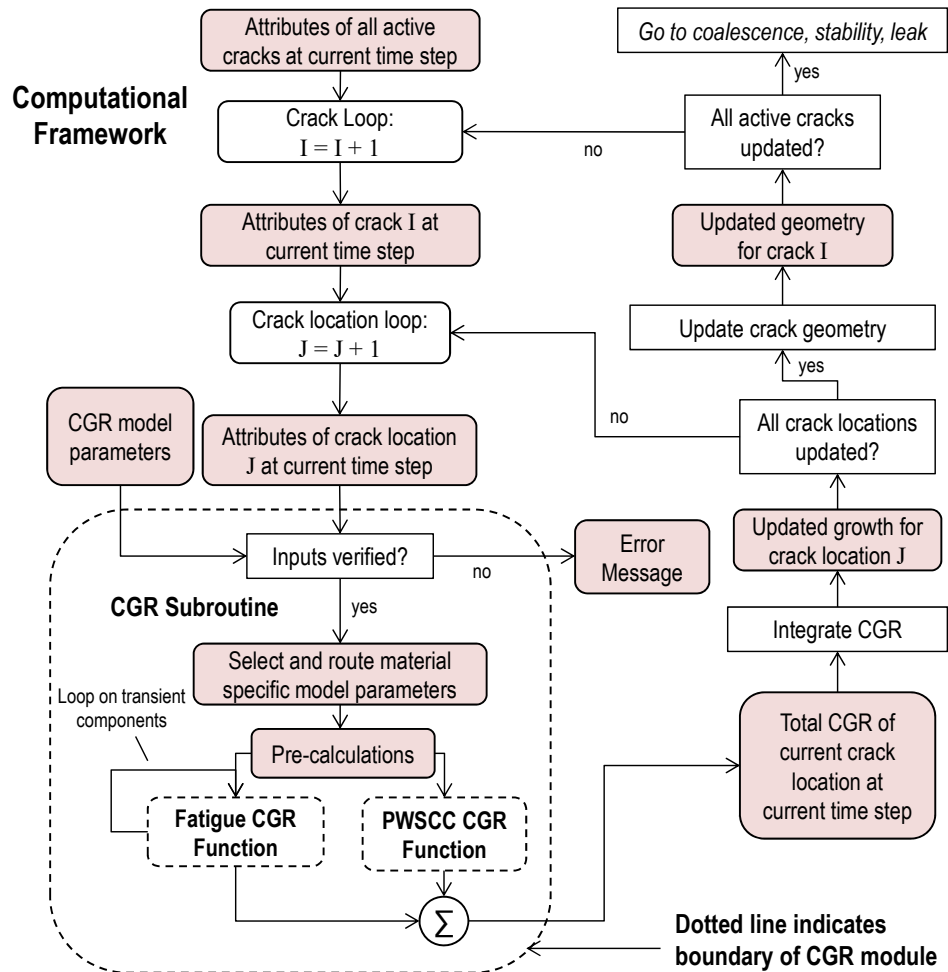
Figure 3-1.   Flow Diagram of the Version 2.0 xLPR CGR Module for a Single Integration Time Step

The scope of the CGR module is limited to the calculation of PWSCC and fatigue *CGRs*. CGR integration over time and over different locations on the crack front require bookkeeping operations performed by the Computational Framework. Stress intensity factor calculation requires the use of the Thermal Stress Intensity Factor for Any Coolant History (TIFFANY) module and the K-Solution modules. Crack interaction and stability calculations require the use of the

Crack Coalescence module (see Sections 4 and 5), the Transitioning Crack module, and the Stability modules.

The CGR equations implemented within the CGR module are semi-empirical model forms developed from laboratory studies, as introduced in Section 2. Numerous parameters of these model forms are user inputs to the xLPR program (i.e., they are not hardwired into the source code). So, while several combinations of material type, crack growth mechanism, and environment are not explicitly addressed in this report (namely, those not directly relevant to the present scope of xLPR Version 2.0 to focus on dissimilar metal and similar metal butt weld locations in PWR primary system piping), the module is believed to provide enough flexibility to accommodate new data or updated analyses.

Finally, a comprehensive list of assumptions and limitations associated with the crack growth and CGR *models* is given in Section 2.5.

3.2 Module Requirements

Software requirements for the CGR module were documented rigorously in the xLPR Software Requirements Description for the PWSCC and Fatigue CGR Module. Requirements were either module-level requirements, specific to the implementation of the CGR module, or interfacing requirements for the xLPR Computational Framework or other modules to ensure correct integration of the CGR module within xLPR. In total, there were 62 requirements—47 module-level requirements and 15 interfacing requirements.

3.2.1 Module-Level Requirements

This section summarizes module-level requirements related to input allocation and verification, pre-processing, CGR calculation, post-CGR calculation, and performance.

3.2.1.1 Input Allocation and Verification

A number of requirements relate to the allocation of memory for inputs and input verification, for example:

- The CGR module is capable of addressing multiple transient components. Attributes that are defined on a transient-specific basis—e.g., loading rise time or maximum stress intensity factor—are stored in vector arrays dynamically allocated by the module based on the input argument that defines the number of transient components.

- Prior to any other operations, all arguments to the module are confirmed to be within acceptable ranges, as identified in Section 3.3. If not, the module returns control to the calling entity with an error flag to indicate which input was first found to be out of range.

- A number of model parameters may be manipulated by expert users to disable or toggle certain functionality of the module, e.g., for sensitivity studies. For a number of model parameters, the module identifies non-standard inputs and returns a 300-level error. By definition within xLPR, a 300-level error does not result in termination of the program instance, but is logged to a run file for the benefit of the user or reviewers.

3.2.1.2 Routing and Pre-CGR Calculation

Various different sub-modules (or CGR functions) are included in the CGR module to calculate PWSCC or fatigue CGRs. This modularity facilitates multiple developers or software updates in the future. Prior to CGR calculation, the CGR module performs logical and mathematical operations to prepare to call the appropriate CGR function(s) with the appropriate inputs, for example:

- The CGR module interprets the material of the current crack location with the material code input, as given in Table 3-1. Furthermore, the module interprets the active degradation mechanism(s) for growth (PWSCC, fatigue, or both) with the mechanism type flag input. The module calls the CGR functions pertaining to the appropriate combination of material and degradation mechanisms.

- In preparation for the fatigue CGR function, the module calculates stress intensity factor range, load ratio, temperature, and stress intensity factor range threshold in accordance with the descriptions given in Section 2.3.1.

- The module implements a looping structure to call the fatigue CGR function multiple times in the case of multiple transient components. Within this loop, the module selects the inputs that are appropriate for the current transient component.

Table 3-1. Material Groups Recognized by CGR Module

Material Group	Numeric Code
Alloy 600	1
Alloy 182 or Alloy 132	2
Alloy 82	3
Alloy 690	4
Alloy 52 or Alloy 152	5
304 or 316L SS and associated weld metals	6
316 and associated weld metals	7
304L or 304LE SS and associated weld metals	8
ferritic steel (CS/LAS) and associated weld metals and base metal HAZ	9
custom material	10

3.2.1.3 CGR Calculation

Individual CGR functions are implemented for material- and mechanism-specific degradation, for example:

- If the PWSCC degradation mechanism is active, the following functional form is used to calculate PWSCC CGR for all materials besides the custom material (Material Group 10):

$$\dot{a}_{PWSCC} = \begin{cases} \dfrac{1}{IF}\alpha f_{comp} f_{flaw} e^{-\frac{Q_g}{R_{gas}}\left(\frac{1}{T}-\frac{1}{T_{ref}}\right)}\left(K-K_{th}\right)^{\beta} \\ \qquad \left[\dfrac{1}{P}+\dfrac{(P-1)}{P}\exp\left(-0.5\left(\dfrac{\Delta ECP_{Ni/NiO}}{c}\right)^{2}\right)\right] \qquad K>K_{th} \\[2em] \qquad\qquad 0 \qquad\qquad\qquad\qquad\qquad\qquad\qquad\qquad K\le K_{th} \end{cases} \qquad \text{[Eqn. 3-1]}$$

$$\Delta ECP_{Ni/NiO} = 29.58\left(\frac{T}{298.15}\right)\log_{10}\left(\frac{[H_2]}{10^{(0.0111(T_C)-2.59)}}\right)$$

$$T = T_C + 273.15$$
$$T_{ref} = T_{ref,C} + 273.15$$

where input parameters are defined in Section 3.3. This functional form is flexible to accommodate all PWSCC CGR models presented in Section 2.2. Specifically, f_{comp} and f_{flaw} in [Eqn. 3-1] are equivalent to f_{weld} and f_{ww} in [Eqn. 2-3], respectively, and the improvement factor, IF, term in [Eqn. 3-1] may be used to mimic the f_{alloy} and f_{orient} terms from [Eqn. 2-3]. For materials that are not susceptible, PWSCC can be deactivated using the mechanism type flag or by setting the scaling constant, α, to zero.

- For custom materials (Material Group 10), by which xLPR users can specify their own growth characteristics, the following functional form is used to calculate PWSCC CGR:

$$\dot{a}_{PWSCC} = \begin{cases} \alpha f_{comp} f_{flaw} e^{-\frac{Q_g}{R_{gas}}\left(\frac{1}{T}-\frac{1}{T_{ref}}\right)}\left(K-K_{th}\right)^{\beta} & K>K_{th} \\ 0 & K\le K_{th} \end{cases} \qquad \text{[Eqn. 3-2]}$$

This model form is similar to [Eqn. 3-1], but does not include an improvement factor or a hydrogen effect.

- If the fatigue degradation mechanism is active and the material is a nickel-based alloy (Material Groups 1 through 5), the fatigue CGR is calculated with the CGR model given in Section 2.3.2.

- If the fatigue degradation mechanism is active and the material is austenitic SS (Material Groups 6 through 8), the fatigue CGR is calculated with the CGR model given in Section 2.3.3.

- If the fatigue degradation mechanism is active and the material is ferritic steel (Material Group 9), the fatigue CGR is calculated with the CGR model given in Section 2.3.4. Additional considerations for the implementation of the ferritic steel fatigue CGR function are discussed below:

  - Because the susceptibility to EAC depends on time-dependent characteristics and the CGR module nominally has information only for the current time step, the CGR module stores in permanent memory information about the crack tip advancement and whether or not EAC has engaged for all locations of active cracks. A later interfacing requirement requires the Framework to provide a crack location index so that the CGR module can select from crack location-specific information.

  - A 300-level error is issued if the threshold for the transition from EAC to TCF (ΔK_b in Section 2.3.4) is less than the stress intensity factor range threshold for fatigue growth (ΔK_{th} in Section 2.3.1). This behavior is not considered physically representative. This error does not terminate the program instance, but is logged for the information of the user and reviewers.

- If the fatigue degradation mechanism is active and the material is in a custom material (Material Group 10), the fatigue CGR is calculated in accordance with the following equation:

$$\frac{da}{dN} = C_{cstm}\tau_R^{p_{cstm}}\left(\frac{\Delta K}{\left(1 - a_{cstm}R\right)^{b_{cstm}}}\right)^{m_{cstm}}$$

[Eqn. 3-3]

where all variables with the subscript *cstm* are user-defined custom CGR model parameters.

3.2.1.4   Post-CGR Calculation

A number of post-calculation operations are required to compile the outputs of the individual calls to the CGR functions, for example:

- The output of the fatigue CGR functions is in terms of crack advancement per fatigue cycle. To convert this to a time rate, the per-cycle rate is scaled by the ratio of the number of cycles during the current integration time step to the duration of the current integration time step.

- The primary output of the CGR module to the calling entity is the sum of the CGRs calculated for PWSCC and fatigue across all transient components.

- As a preventive measure, if either the PWSCC or fatigue component is negative or non-numerical (e.g., NaN in Fortran), the module returns a 200-level error.

3.2.1.5 Performance Requirements

To motivate efficient module design, the following runtime and memory requirements were imposed:

- The CGR module memory does not exceed 20 kB during runtime.

- The CGR module can complete 21,600[26] calls in less than 30 seconds using various material groups, both degradation mechanisms, and with at least five transient components.

3.2.2 Interfacing Requirements

This section identifies interfacing requirements for the xLPR Computational Framework and other xLPR modules.

3.2.2.1 Computational Framework

Several interfacing requirements are imposed on the xLPR Computational Framework to ensure appropriate utilization of the CGR module and to implement the crack growth models described in Section 2.4, for example:

- Communication of inputs to and outputs from the CGR module is performed with explicit passing of variables. The order of arguments to the module is specified in the Software Design Description discussed in Section 3.4.

- Communication of inputs is performed with the required units and data types given in Section 3.3.

- Random sampling is performed for inputs defined as distributed random variables. Random sampling is performed either on a per-simulation basis (e.g., component-to-component variation) or a per-subunit[27] basis (e.g., within-component variation), as determined by sampling frequencies specified in Section 3.3.

- Calculation of the material group identification number is performed in accordance with Table 3-1.

- All time-varying inputs—including stress intensity factors, temperatures, hydrogen concentrations, and the number of fatigue cycles per unit time—are updated such that they represent the current time step.

---

[26] This number is based on a conservative estimate of the number of CGR module calls required for a "roughly" industry-representative set of 1,000 Monte Carlo realizations of a component: 1,000 MC realizations * (1 active crack / 50 MC realizations) * (3 tracked crack tips / active crack) * (20 operating cycles / tracked crack tip) * (18 time steps / operating cycle)

[27] A "subunit" refers to one of many circumferential sections resulting from the spatial discretization of the component surface required for initiation modeling. (A subunit is also referred to as a "segment" in xLPR documentation.) The subunits provide a useful spatial discretization that may be used to simulate spatial variation of properties such as within-component material susceptibility.

- The CGR calculation is managed at each defined location of each active crack. The different crack types and defined locations for these different crack types are detailed in Section 2.4.

- A crack index is assigned to each unique crack location. This index is supplied to the module for the purpose of retrieving crack location-specific quantities required to calculate fatigue CGR in ferritic steels.[28]

- Time-integration of CGRs is performed to calculate crack front extension.

- The growth calculation conventions described in Section 2.4 are applied to update crack sizes, shapes, and locations as a function of time.

3.2.2.2 K-Solutions, TIFFANY, and Transitioning Crack Modules

Several other modules are essential to enable the prediction of crack growth. The stress intensity factors needed for the PWSCC CGR calculation are calculated by the K-Solutions module. The minimum and maximum stress intensity factors, minimum and maximum temperatures, and loading rise times needed for the fatigue CGR calculation are looked up from tables generated by the TIFFANY module. The Transitioning Crack module calculates scaling factors to apply to stress intensity factor calculations (for idealized through-wall cracks) so that they are appropriate for the transitioning crack shape. The xLPR Version 2.0 Stress Requirements [42] provide detailed instructions for these calculations, including which loads or stresses are factored in depending on crack orientation and crack type.

3.2.2.3 Initiation Modules

The sources of uncertainty of the initiation models may be correlated with those of the growth models, for analogous mechanisms (e.g., PWSCC initiation in Alloy 182 and PWSCC growth in Alloy 182). Such correlation allows the ability to simulate the expectation that material that has relatively high susceptibility to initiation also is susceptible to relatively high CGRs [9]. In general, material conditions and microstructures that tend to increase the CGR are also expected to increase the susceptibility to crack initiation. For example, a heat of CRDM nozzle material known to have an especially high incidence of PWSCC in the field displayed in laboratory testing CGRs near the upper end of expected behavior for thick-wall Alloy 600 material [46]. However, cases in which relative material susceptibility to both initiation and growth are available are rare, and thus a correlation value relating these two material susceptibilities was not developed. Instead, this correlation may be used for the purpose of sensitivity studies.

3.3 Module Inputs and Outputs

Table 3-2 and Table 3-3 describe all inputs to the CGR module, including their required unit, range of verification, data type, and sample frequency. These attributes are discussed in turn below:

- *Required unit:* Assumed units are built into the growth module calculations and therefore must be upheld by input arguments.

---

[28] Conventions have been specified for how crack index is assigned if a crack transitions to a different crack type or if two cracks coalesce. These conventions are discussed in the Framework report.

- *Range of verification:* A critical error (requiring program termination) is generated for inputs outside of the range of verification. In general, these ranges prevent unrealistic or non-meaningful inputs. This range is different from the range over which model validation was performed.

- *Data type:* For memory allocation purposes, the user inputs are to be entered as specific data types, all of which are interpreted by common programming languages. No requirement is made for bit precision, but double-precision was used in design of the source code.

- *Sample frequency:* The Framework performs all sampling of distributed random variables. The sample frequency conveys to the Framework interfacing requirements defining the periodicity of sampling.

  - A "per heat" frequency refers to a sample taken once for each distinct material group, for each independent simulation.

  - A "per subunit" frequency refers to sample taken once for each spatial discretization of the component.

  - A "per heat / per subunit" is a derived random variable that has the ability to be the product of one "per heat" random variable and one "per subunit" random variable.

The remainder of this section provides additional discussion about the inputs and outputs to the CGR module.

Table 3-2. PWSCC CGR Subroutine Inputs

Description	Symbol	Required Units	Range of Verification	Data Type	Sample Frequency
Material group	$I_{material}$	-	1 - 10 (inclusive)	integer	-
Mechanism type flag	$I_{mechanism}$	-	1, 2, 3	integer	-
Operating stress intensity factor	K_I	MPa√m	-	real	-
Operating temperature	T	°C	>0	real	-
Reference temperature	T_{ref}	°C	>0	real	-
Power-law constant	α	$(m/s)(MPa\sqrt{m})^{-\beta}$	≥ 0	real	-
Power-law exponent	β	-	-	real	-
Threshold stress intensity factor	K_{th}	MPa√m	≥ 0	real	-
Component-to-component CGR variation factor	f_{comp}	-	>0	real	per heat
Within-component CGR variation factor	f_{flaw}	-	>0	real	per subunit
Thermal activation energy	Q_g	kJ/mol	>0	real	per heat
Hydrogen concentration	$[H_2]$	cc/kg	>0	real	-
Peak-to-valley ratio	P	-	>0	real	per heat
Peak width	c	mV	>0	real	per heat
Improvement factor	IF	-	>0	real	per heat

Table 3-3. Fatigue CGR Subroutine Inputs

Description	Symbol	Required Units	Range of Verification	Data Type	Sample Frequency
Material group	$I_{material}$	-	1 - 10 (inclusive)	integer	-
Mechanism type flag	$I_{mechanism}$	-	1, 2, 3	integer	-
Number of transient components	NTS	-	1 - 20 (inclusive)	integer	-
Duration of time step	Δt	EFPY	> 0	real	-
Number of cycles per transient component	N_{cyc}	-	≥ 0	real array	-
Minimum stress intensity factor per transient component	K_{min}	MPa√m	$\leq K_{max}$	real array	-
Maximum stress intensity factor per transient component	K_{max}	MPa√m	$\geq K_{min}$	real array	-
Rise time per transient component	τ_R	s	>0	real array	-
Threshold stress intensity factor range scaling factor	C_{Kth}	-	≥ 0	real	per heat
Minimum temperature per transient component	T_{min}	°C	0 - T_{max} (inclusive)	real array	-
Maximum temperature per transient component	T_{max}	°C	$\geq T_{min}$	real array	-
Nominal temperature flag	I_{Temp}	-	1, 2, 3	integer	-
Ni-based alloy scaling factor	C_{Ni}	-	≥ 0	real	per heat / per subunit
Ni-based alloy Paris power-law exponent	n_{Ni}	-	≥ 0	real	-
Ni-based alloy weld factor	$f_{Ni,weld}$	-	>0	real	-
Ni-based alloy environment factor	A_{env}	$(m/cyc\text{-}s)^{1-nenv}$	≥ 0	real	per heat / per subunit
Ni-based alloy environment exponent	n_{env}	-	≥ 0	real	-
SS scaling factor	C_{SS}	-	≥ 0	real	per heat / per subunit
SS Paris power-law exponent	n_{SS}	-	≥ 0	real	-
Ferritic true corrosion fatigue environmental factor	C_1	$(m/cyc)(MPa\ \sqrt{m})^{-3.07}$	≥ 0	real	per heat / per subunit
Ferritic medium-sulfur EAC environmental factor	C_2	$(m/cyc)(MPa\ \sqrt{m})^{-3.07}$	≥ 0	real	per heat / per subunit
Ferritic high-sulfur EAC environmental factor	C_3	$(m/cyc)(MPa\ \sqrt{m})^{-nfer}$	≥ 0	real	per heat / per subunit
Ferritic upper EAC threshold scaling factor	C_{Kb}	-	>0	real	per heat
Crack depth	a	m	>0	real	-
Crack tip index	I_{tip}	-	1 - 1000 (inclusive)	integer	-
Sulfur content	S	%wt	≥ 0	real	-
Custom model scaling constant	C_{cstm}	$(m/cyc)s^{-pcstm}(MPa\ \sqrt{m})^{-mcstm}$	≥ 0	real	per heat / per subunit
Custom model rise time exponent	p_{cstm}	-	≥ 0	real	-
Custom model load ratio constant	a_{cstm}	-	≥ 0	real	-
Custom model load ratio exponent	b_{cstm}	-	≥ 0	real	-
Custom model Paris law exponent	m_{cstm}	-	≥ 0	real	-

3.3.1 Physical Inputs

Several geometrical, material, loading, and environmental properties are required for prediction of PWSCC and fatigue CGRs. This section describes module inputs representing these physical quantities, including their source within the xLPR Computational Framework (e.g., user-input, calculated by another module, etc.).

- *Material group:* A numerical code specifying the material at the crack location being evaluated (see Table 3-1). Different materials exhibit different PWSCC and fatigue behaviors and therefore are treated with different model forms.

- *Operating stress intensity factor:* The Mode (I) stress intensity factor calculated at the crack location being evaluated, neglecting fatigue transient cycles. The operating stress intensity factor is a primary determinant of PWSCC growth. This input is calculated by the K-

Solutions modules and (over the course of multiple Monte Carlo realizations) incorporates uncertainties in the component load conditions.

- *Operating temperature:* The temperature at the component of interest, neglecting transient cycles. Operating temperature is a second primary determinant of PWSCC growth. Operating temperature is a user input that may be specified as a random variable to account for temporal variation, spatial variation (e.g., thermal stratification), measurement uncertainty, etc.

- *Hydrogen concentration:* The dissolved hydrogen concentration in the reactor coolant. The resistance to PWSCC of some materials is influenced by hydrogen concentration—or, more accurately, electrochemical potential of the environment that is influenced by hydrogen concentration. Hydrogen concentration is a user input that may be specified as a random variable to account for chemistry excursions or control tolerances.

- *Number of transient components:* The number of active transient components that are treated independently in the calculation of fatigue CGR. The number of transients is a deterministic user input. The user specifies the characteristics of each transient component, as discussed further below.

- *Duration of time step:* The duration of the time discretization used by the Framework to perform time integration required to simulate growth and coalescence of cracks. This value is used together with the number of cycles (discussed next) to infer the number of cycles per unit time, which is used to adjust predictions for growth on a per cycle basis to predictions on a per time basis.

- *Number of cycles:* The number of cycles that occur during the current time step (for each transient component). The user specifies the frequency of occurrence and duty cycle of transient components. The Framework uses these inputs to schedule the transient cycles within each integration time step resulting from discretization. Cycles are scheduled deterministically, reflecting the belief that transient components represent scheduled or predictable transients.

- *Minimum and maximum stress intensity factor:* The stress intensity extrema (for each transient component) calculated at the crack location being evaluated. These values are used by the CGR module to calculate the stress intensity factor range and load ratio that are primary determinants of fatigue growth. These values are calculated as the sum of the operating stress intensity factors and the alternating stress intensity factors calculated with the TIFFANY module. These inputs (over the course of multiple Monte Carlo realizations) incorporate uncertainties in the transient load conditions.

- *Loading rise time:* In accordance with ASME Code Case N-643-2, the span of time over which the rate of change of surface stress exceeds 1000 psi/hr during a cycle at the component of interest (for each transient component). Loading rise time is a primary determinant of environmental factors for fatigue growth. Loading rise times are calculated by the TIFFANY module based on user input defining the transient cycle.

- *Minimum and maximum temperature:* The temperature extrema at the component of interest (for each transient component). These values are used together to determine the temperature at which the fatigue CGR calculations are carried out. Higher temperatures

tend to increase fatigue modestly. Temperature extrema are calculated by the TIFFANY module based on user input defining the transient cycle.

- *Crack depth:* The depth of the crack being evaluated. The depth of the crack plays a role in predicting the susceptibility to EAC for ferritic steels. The depth of each crack is maintained as a state variable by the Framework.

- *Sulfur content:* The percent of sulfur by weight in the material at the crack location being evaluated. Sulfur content is a primary determinant of the susceptibility to EAC for ferritic steels. Sulfur content is a user input that may be specified as a distributed random variable to account for heat-to-heat variation, within-heat variation, etc.

3.3.2 PWSCC CGR Model Parameters

The PWSCC CGR model comprises numerous model parameters that define its trends and uncertainties. The CGR module applies the same PWSCC CGR model form irrespective of the material. Therefore, it is the model parameters that are varied in order to simulate PWSCC behavior of different materials. The xLPR Inputs Database allows the user to specify PWSCC CGR model parameters for each distinct material group involved in the simulation and the Framework performs the bookkeeping to ensure that the CGR module is called with the appropriate parameters for the different crack tip locations.

Extensive efforts to derive best-estimate quantities and uncertainties for model parameters for Alloys 600, 82, and 182 are detailed in Section 2.2. Table 3-4 summarizes these values. The values of Table 3-4 for each specified material are inter-dependent and should only be modified in parallel with careful assessment. PWSCC CGR model parameters for other materials are not provided in this report.

Each PWSCC CGR model parameter is defined below:

- *Reference temperature*: The PWSCC CGR model uses a reference temperature to normalize the temperature effect such that it is near unity. A fixed deterministic reference temperature of 325°C was selected based on the precedent set in MRP-55 and MRP-115 that 325°C represents a common test temperature near the middle of the range of test temperatures applied. The reference temperature value does not affect the predicted PWSCC CGR as long as the power-law constant is adjusted to the specific reference temperature value using the value of the thermal activation energy. However, the reference temperature value does have an effect in the sense that the thermal activation energy is statistically sampled from an uncertainty distribution while the reference temperature and power-law constant values are taken as constants. Hence, it is appropriate that a reference temperature most representative of the test data used to develop the MRP-55 and MRP-115 models is applied.

- *Power-law constant*: The power-law constant scales the overall PWSCC CGR model. In deterministic applications, it is typically set to a value such that the nominal CGR prediction corresponds with the 75th percentile of the variability exhibited due to material heat for wrought material or weld for weld metal material; in probabilistic applications, like xLPR, the power-law constant should be set to correspond with the median of the variability exhibited due to material heat for wrought material or weld for weld metal material as the median of the recommended *component-to-component CGR variation factor* is normalized to be one. The best-estimate values for the power-law constant for Alloy 600 and Alloys 82/182/132

are based on analyses presented in MRP-55, MRP-115, and MRP-263. The power-law constant may be set to zero for materials simulated as having no susceptibility to PWSCC growth (in which case no other model parameters are used).

- *Power-law exponent*: The power-law exponent quantifies the sensitivity of PWSCC CGR relative to stress intensity factor (as quantified through a power-law modeling term). By convention, uncertainty is not typically allocated for the stress intensity factor effect. Instead, the uncertainty in PWSCC CGR is allocated principally to the *component-to-component CGR variation factor* and the *within-component CGR variation factor*. The best-estimate values for the power-law exponent for Alloy 600 and Alloys 82/182/132 are based on the dependencies originally developed in MRP-55 and MRP-115. These values are between one and two, suggesting a super-linear, sub-quadratic effect. The power-law exponent may be set to zero to remove the stress intensity factor dependency.

- *Threshold stress intensity factor*: The threshold stress intensity factor quantifies a minimum threshold at which constant loading conditions are assumed to be not sufficient to support PWSCC growth. The theoretical rationale for such a threshold is tenuous and little data are available for validation of this effect in thick-section material. The use of a stress intensity factor threshold is a topic under investigation for future PWSCC modeling efforts. At this time, the best-estimate values for the threshold stress intensity factor are based on the dependencies originally developed in MRP-55 and MRP-115—the Alloys 82/182/132 model includes no threshold while the Alloy 600 model includes a threshold at 9 MPa√m. Caution should be taken when applying a nonzero threshold as the PWSCC CGR data for Alloy 600 used to develop the MRP-55 model reflected K values no less than about 15 MPa√m.

- *Component-to-component CGR variation factor*: The component-to-component CGR variation factor is a value that is sampled for each distinct material group within xLPR[29] and is used to scale the PWSCC CGR prediction for crack tips located in that material group. The uncertainty of this term should reflect variability in growth susceptibility from weld-to-weld or from heat-to-heat due to unmodeled influences, e.g., due to differences in material processing, heat treatment, weld techniques, etc. The selected distributions for the component-to-component CGR variation factor are based on heat-to-heat and weld-to-weld variation analyzed in MRP-55, MRP-115, and MRP-263. One notable characteristic of all selected distributions is the use of a log-μ parameter of zero. This yields a median of one, such that the central tendency of the model is not altered by the component-to-component variation.

- *Within-component CGR variation factor*: The within-component CGR variation factor is a value that is sampled for each spatial discretization of each contiguous material group within xLPR and is used to scale the PWSCC CGR prediction for a crack tip located in that spatial discretization. The uncertainty of this term should reflect variability in growth susceptibility from location to location on the same weld or heat of material due to unmodeled influences, e.g., due to microstructural variation or variation in mechanical properties. The selected distributions for the within-component CGR variation factor are based on specimen-to-specimen variation analyzed in MRP-115 and MRP-335 [6] for specimens fabricated from the same heat of wrought material or from the same test weld.

---

[29] The xLPR Version 2.0 framework uses multiple discrete material groups to model the different materials present at a dissimilar metal weld.

- *Thermal activation energy*: The thermal activation energy defines the sensitivity of the PWSCC CGR to temperature variation via an Arrhenius modeling term.

  If the hydrogen effect model is invoked, the activation energy input should account only for thermal activation of reaction kinetics (and not for changes in electrochemical potential relative to the Ni/NiO transition). This activation energy—termed here "actual activation energy"—can be estimated with testing performed at or normalized to a fixed ECP relative to the Ni/NiO transition.

  If the hydrogen effect model is not invoked, the activation energy input should account for all temperature-dependencies. This activation energy—termed here "apparent activation energy"—can be estimated with testing performed at a fixed hydrogen concentration.

  The selected distributions for the activation energy are based on different estimates provided by different investigators and analyzed in MRP-55, MRP-115, MRP-263, and the CGR Module Validation Report. These distributions represent the uncertainty in the best-estimate value of activation energy as opposed to the total variation in activation energy from heat to heat or weld to weld. The activation energy may be set to zero to remove the temperature dependency.

- *Peak-to-valley ratio*: The peak-to-valley ratio quantifies the modeled factor of improvement between the PWSCC CGR at the Ni/NiO transition and PWSCC CGR asymptotically far from the Ni/NiO transition. The peak-to-valley ratio (and the peak width below) should be derived from controlled studies in which all independent conditions are held constant besides the electrochemical potential relative to the Ni/NiO transition. The uncertainty in this parameter in practice may be due to various sources including specimen-to-specimen variation, within-specimen variation, sensitivity of estimates to outliers, or imprecision because of small data sets. The estimate given for the peak-to-valley ratio for Alloys 82/182/132 is based on analysis performed in MRP-263. No hydrogen model for Alloy 600 was selected here; in lieu of such a model, the peak-to-valley ratio should be set to unity to omit the hydrogen effect on the model prediction.

- *Peak width*: The peak width quantifies the sensitivity of the PWSCC CGR relative to electrochemical potential in the region around the Ni/NiO transition. At one peak width ($\Delta ECP_{Ni/NiO} = c$) from the Ni/NiO transition, CGR is reduced by approximately 40% relative to the difference between the maximum CGR at the Ni/NiO transition and the asymptotic CGR far from the Ni/NiO transition. The estimate given for peak width for Alloys 82/182/132 is based on analyses performed in MRP-263 specifically for Alloys 182/132.

- *Improvement factor*: The improvement factor is an input that may be used to scale down the PWSCC CGR model prediction, usually to credit improved PWSCC resistance of a certain alloy, without altering other model trends. For instance, it is often convenient to make overall adjustments to growth predictions for like materials that are expected to behave similarly. One such example is the adjustment recommended in MRP-115 to account for the increased PWSCC resistance of Alloy 82 relative to Alloy 182 due to increased chromium content. The improvement factor may also be useful for later models of Alloys 690/52/152, although no specifics were selected at this time. The improvement factor may be set to one to omit its effect on the model prediction.

Table 3-4. Recommended Values and Distributions for PWSCC CGR Subroutine Inputs

Description	Units	Characterization of Uncertainty	Distribution Parameters	Material Model		
				Alloy 600	Alloy 82/182/132 without H$_2$ effect	Alloy 82/182/132 with H$_2$ effect
Reference temperature	°C	deterministic	best-estimate	325	325	325
Power-law constant	(m/s)/(MPa√m)$^\beta$	deterministic	best-estimate	1.34E-12	9.82E-13	2.01E-12
Power-law exponent	-	deterministic	best-estimate	1.16	1.6	1.6
Threshold stress intensity factor	MPa√m	deterministic	best-estimate	9	0	0
Component-to-component CGR variation factor	-	distributed (epistemic)	type	Log-Normal	Log-Normal	Log-Normal
			log-norm μ	0.00	0.00	0.00
			log-norm σ	1.0160	0.5892	0.4895
			lower truncation	0.143	0.313	0.44
			upper truncation	5.32	2.64	2.24
Within-component CGR variation factor	-	distributed (aleatory)	type	Log-Normal	Log-Normal	Log-Normal
			log-norm μ	0.00	0.00	0.00
			log-norm σ	0.5695	0.4807	0.3742
			lower truncation	0.208	0.309	0.335
			upper truncation	3.68	3.24	2.04
Thermal activation energy	kJ/mol	distributed (epistemic)	type	Normal	Normal	Normal
			mean	130	130	104
			stdev	5	20	20
Peak-to-valley ratio (see Notes 1 and 2)	-	distributed (epistemic)	type			Log-Normal
			log-norm μ	1	1	4.52
			log-norm σ			2.75
Peak width (see Note 1)	mV	distributed (epistemic)	type			Normal
			mean	not used	not used	18.2
			stdev			5.5
			lower truncation			0.0
Improvement factor	-	deterministic	best-estimate	1	1 (for Alloy 182/132) 2.6 (for Alloy 82)	1 (for Alloy 182/132) 2.6 (for Alloy 82)

Notes:

(1) The underlying normal deviates used to sample peak-to-valley ratio and peak width should be correlated by a Pearson correlation coefficient of 0.714

(2) The log-norm μ and log-norm σ parameters for the peak-to-valley ratio are specified for P-1. The determinstic values shown are for P itself.

3.3.3 Fatigue CGR Model Parameters

The CGR module comprises three independent material-specific models for fatigue CGR predictions, each with their own model parameters. The CGR module applies the model that is appropriate for the material at the current crack tip location, as specified in the material group input described in Section 3.3.1. The model parameters are varied in order to simulate fatigue behavior of different materials within a material group.

The xLPR Inputs Database allows the user to specify fatigue CGR model parameters for each distinct material group involved in the simulation, and the Framework performs the bookkeeping to ensure that the CGR module is called with the appropriate parameters for the different crack tip locations.

Extensive efforts to derive best-estimate quantities and uncertainties for model parameters for the fatigue CGR models are detailed in Section 2.3. Table 3-5 summarizes these values.

Each fatigue CGR model parameter is defined below:

- *Threshold stress intensity factor range scaling factor*: The stress intensity factor range defines a mechanical threshold below which the fatigue CGR is negligible. This parameter, which is used for all material groups, scales the stress intensity factor range equation from ASME Code Case N-643-2, as given in [Eqn. 2-11]. This value may be used to shift the otherwise conservative estimate for stress intensity factor range. It may also be a distributed input in order to represent uncertainty, e.g., due to component-to-component variation on account of manufacturing and heat treatment differences that are not modeled explicitly. The recommended dispersion for this scaling factor is based on differences observed in several different heats of ferritic and austenitic steels [22]; however, the median is held at one to remain conservative.

- *Fatigue CGR scaling factor for Ni-based alloys*: This parameter scales the air fatigue CGR prediction for any material within the Ni-based alloy material group (it is not used for materials outside of the Ni-based alloy material group). This input should be distributed to introduce uncertainty in the prediction of air fatigue CGR in Ni-based alloys. This uncertainty may account for component-to-component variation, within-component variation, or possible differences in air fatigue behavior for different Ni-based alloys. The recommended distribution for this parameter is a best-estimate based on analysis of data scatter for tests performed with Alloy 600 [25].

- *Weld factor for Ni-based alloys:* This parameter defines any systematic difference in fatigue behavior in Ni-based alloy welds versus Ni-based alloy base metals. A best-estimate value of 2.0 is recommended based on analysis presented in NUREG/CR-6721 [25]. Uncertainty of this term is consolidated in the fatigue CGR scaling factor.

- *Paris power-law exponent for Ni-based alloys*: This parameter defines the sensitivity of air fatigue to the stress intensity factor range for any material within the Ni-based alloy material group. A best-estimate value of 4.1 is recommended based on analysis presented in NUREG/CR-6721 [25]. Uncertainty of this term is consolidated in the fatigue CGR scaling factor.

- *Environmental factor for Ni-based alloys*: Together with the environmental exponent discussed next, this parameter quantifies the enhancement of fatigue caused by environmental conditions for any material within the Ni-based alloy material group. The use of zero, for instance, neglects environmental enhancement, while larger values lead to proportionally more enhancement for a given loading condition. This input should be distributed to introduce uncertainty in the prediction of environmental enhancement in Ni-based alloys. This uncertainty may account for component-to-component variation, within-component variation, possible differences in air fatigue behavior for different Ni-based alloys, or environmental variation. The recommended distribution for this parameter is conservatively high relative to data for different heats of Alloy 600 and Alloy 690 in a simulated PWR environment [25]; for instance, many heats of Alloy 600 and Alloy 690 exhibit no environmental enhancement. It also is an upper bound on the input uncertainty described in Section 2.3.2.[30]

---

[30] Section 2.3.2 describes a log-normal standard deviation that varies as a function of the loading condition. This cannot be accomplished in the current xLPR program and therefore a bounding input is recommended.

- *Environmental exponent for Ni-based alloys*: This parameter defines a power-law relationship between fatigue rate in air and fatigue rate in PWR environments for any material within the Ni-based alloy material group. A best-estimate value of 0.33 is recommended based on analysis presented in NUREG/CR-6721 [25]. However, validation of the model with an independent data set [26] suggests a value of approximately 0.25.

- *Fatigue CGR scaling factor for austenitic SS*: This parameter scales the fatigue CGR prediction for any material within the austenitic SS material group (it is not used for materials outside of the austenitic SS material group). This input should be distributed to introduce uncertainty in the prediction of fatigue CGR in SS. This uncertainty may account for component-to-component variation, within-component variation, possible differences in fatigue behavior for different SS, or environmental variation. The recommended distribution for this parameter is a best-estimate based on analysis of data scatter for tests performed with 304, 304L, 304LE, 316, and 316L SS in simulated PWR environments [24].

- *Paris power-law exponent for austenitic SS*: This parameter defines the sensitivity of fatigue to the stress intensity factor range for any material within the austenitic SS material group. A best-estimate value of 2.25 is recommended based on analysis to support the forthcoming ASME Code Case for fatigue CGRs in austenitic SS [27]. Uncertainty of this term is consolidated in the fatigue CGR scaling factor.

- *TCF environmental factor for ferritic steels*: This parameter scales the fatigue CGR prediction for instances of cracking in ferritic steel for which EAC is not engaged or cannot be maintained, i.e., it scales the TCF prediction. This input should be distributed to introduce uncertainty in the prediction of TCF in ferritic steels including component-to-component variation, within-component variation, possible differences in fatigue behavior for different ferritic steels, or environmental variation. The recommended median for this parameter is an approximately 99th percentile bounding value based on analysis of data for tests performed with ferritic steel with bulk sulfur content less than 0.004% by weight in simulated PWR environments [39].[31] The recommended distribution is based on the scatter of this same data about a best-fit model.

- *Medium-sulfur EAC environmental factor for ferritic steels:* This parameter scales the fatigue CGR prediction for instances of EAC in medium-sulfur (between 0.004% and 0.013% sulfur by weight) ferritic material. This input should be distributed to introduce uncertainty in the prediction of EAC in ferritic steels. The recommended median for this parameter is a 95th percentile value based on analysis of data for tests performed with medium sulfur A508 forging materials in simulated PWR environments [35].[32] The recommended distribution is based on the scatter of this same data about a best-fit model. Finally, logic is implemented within the CGR module to use the sampled TCF environmental factor in the unlikely event that it exceeds the sampled EAC environmental factor.

- *High-sulfur EAC environmental factor for ferritic steels:* This parameter scales the fatigue CGR prediction for instances of EAC in high-sulfur (> 0.013% sulfur by weight) ferritic material. Again, this input should be distributed to introduce uncertainty in the prediction of EAC in ferritic steels. The recommended median for this parameter is a 95th percentile value

---

[31] To use a best-fit model, the log-μ parameter is set to -22.93.

[32] To use a best-fit model, the log-μ parameter is set to -22.4.

based on analysis of data presenting EAC at aggressive loading conditions (in the "second slope region" [36]). The recommended distribution is based on the scatter of data from medium sulfur ferritic steel as presented in the previous bullet. The relative variation of EAC is similar for medium and high sulfur materials.

- *Upper EAC threshold scaling factor for ferritic steels*: The upper EAC threshold defines a stress intensity factor range above which the rate of EAC growth versus stress intensity factor range begins to decline in high-sulfur steels, reflecting a loading aggressive enough that the environment begins to have less of a relative impact. This parameter scales the upper EAC threshold equation form from ASME Code Case N-643-2, as shown in [Eqn. 2-27]. This parameter can be set to a value of 0.498 to recover the N-643-2 equation. This parameter may also be distributed to represent uncertainty. The recommended distribution for this scaling factor is based on measurements of the upper EAC threshold for tests in A508 forging materials [36].

- *Custom fatigue CGR model parameters:* Five parameters are available to define a fatigue CGR model for a custom material using [Eqn. 3-3]. These include a scaling factor applied to the net CGR prediction that may be distributed to represent uncertainty and other parameters to define stress intensity factor range, load ratio, and loading rise time dependencies. The user of xLPR may choose to develop these parameters for any material if the given models for Ni-based alloy, austenitic SS, and ferritic steel are not satisfactory.

Table 3-5. Recommended Values and Distributions for Fatigue CGR Subroutine Inputs

Description	Units	Characterization of Uncertainty	Distribution Parameters	Value
General fatigue CGR model parameters				
Threshold stress intensity factor range scaling factor	-	distributed (epistemic)	type	log-normal
			log-μ	0.239
			log-σ	0.139
			upper truncation	1.927
Ni-based alloy model parameters				
Scaling factor	-	distributed (epistemic)	type	log-normal
			log-μ	0.0
			log-σ	0.408
Paris power-law exponent	-	deterministic	best-estimate	4.1
Weld factor	-	deterministic	best-estimate	2.0
Environmental factor	$(m/cyc\text{-}s)^{1\text{-}nenv}$	distributed (epistemic)	type	log-normal
			log-μ	-14.6
			log-σ	1.2
Environmental exponent	-	distributed (epistemic)	type	uniform
			min	0.25
			max	0.33
Austenitic stainless steel model parameters				
Scaling factor	-	distributed (epistemic)	type	log-normal
			log-μ	0.0
			log-σ	0.420
Paris power-law exponent	-	deterministic	best-estimate	2.25
Ferritic steel model parameters				
True corrosion fatigue environmental factor	$(m/cyc)(Mpa\sqrt{m})^{-3.07}$	distributed (epistemic)	type	log-normal
			log-μ	-22.01
			log-σ	0.467
Medium-sulfur EAC environmental factor	$(m/cyc)(Mpa\sqrt{m})^{-3.07}$	distributed (epistemic)	type	log-normal
			log-μ	-20.6
			log-σ	0.88
			lower truncation	sampled value for true corrosion fatigue environmental factor
High-sulfur EAC environmental factor	$(m/cyc)(Mpa\sqrt{m})^{-nfer}$	distributed (epistemic)	type	log-normal
			log-μ	-15.8
			log-σ	0.88
			lower truncation	sampled value for true corrosion fatigue environmental factor
Upper EAC threshold scaling factor	-	distributed (epistemic)	type	log-normal
			log-μ	-0.697
			log-σ	0.210

3.3.4 Other Input Parameters

A few flags are required by the CGR module to communicate run mode. These are described below:

- *Mechanism type flag:* This flag indicates whether the CGR module invokes both (1), the PWSCC (2), or the fatigue (3) component(s) of degradation. In general, this flag should be

set to 1. However, the user of xLPR may opt to use 2 or 3 to study the effects of PWSCC and fatigue independently; for instance, to determine the predominant driver of risk.

- *Nominal temperature flag:* This flag indicates how minimum and maximum temperatures for transient cycles are used to arrive at a temperature used in fatigue CGR calculation. The options are to take the average (1), the minimum (2), or the maximum (3) temperature. In general, this flag should be set to 1. However, the user of xLPR may opt to use 2 or 3 to study the sensitivity of this approximation.

3.3.5 Outputs

The primary output of the CGR module is the net CGR (versus time) for the material, loading, and environmental conditions communicated via inputs. This output includes both PWSCC and fatigue components, if applicable. As discussed in Section 3.2.2, these outputs are used by the xLPR Computational Framework to simulate the progression of one or more cracks as a function of time and time-dependent conditions.

A second output of the CGR module is an error flag communicating any errors or anomalies encountered during the call to the CGR module. The error codes are described below:

- The default error code is 0, indicating no errors or anomalies.

- Error codes 101 through 144 communicate an input that is out of its range of validity. For these error codes, the calling entity should terminate the run and notify the user which input is out of range. These error codes may indicate an unknown error in the Computational Framework or an error in the user input.

- Error codes 201 and 202 communicate that calculated PWSCC or fatigue CGR, respectively, is below zero or non-numerical. For these error codes, the calling entity should terminate the run and notify the user of an anomalous CGR module condition.

- Error code 203 is issued if the calculated upper EAC threshold is less than the threshold stress intensity factor range. While a CGR is nonetheless calculated in accordance with module requirements, this is an unexpected condition and should therefore be evaluated. Within the xLPR Framework, the user should be notified if this condition occurs, including the fraction of Monte Carlo realizations in which this condition occurs. If this error condition is prevalent, the user may reevaluate the stress intensity range threshold or upper EAC threshold scaling factors.

- Error codes 301 through 305 communicate that certain modes of degradation have been disabled by the choice of model parameters. Modes of degradation may be disabled by expert users, so the run is not terminated, but it is considered prudent to log these instances for user and reviewer consideration.

3.4 Module Design and Implementation

This section gives a brief overview of the design and implementation of the CGR module. The design of the CGR module, including presentation of all applicable interfaces and operations, is detailed in the xLPR Software Design Description for the PWSCC and Fatigue CGR Module.

The architecture of the CGR module is depicted in Figure 3-2. The CGR module is deployed as a dynamic link library (DLL), making it generally accessible to other Windows programs, e.g., the GoldSim software in which the Computational Framework is developed. The CGR DLL wrapper code, developed by the Framework Group, defines the input and output allocation for the DLL and appropriately routes this information to and from the CGR module. This wrapper code also implements the bookkeeping required to calculate CGR at each relevant crack location at a given time step. The CGR DLL source code is contained in a file called *growth_DLL_source.f90* maintained in accordance with xLPR configuration control.

The *CGR* subroutine is the driver of the CGR module. The operations of the *CGR* subroutine are summarized in Figure 3-3. This subroutine executes logic to allocate memory, validate inputs, determine whether to call the *GrowthPWSCC* subroutine and/or the *GrowthFatigue* subroutine, route inputs appropriately, and calculate the total CGR.

The *GrowthPWSCC* subroutine is simply composed of the mathematical equations that implement PWSCC CGR model. The *GrowthFatigue* subroutine executes logic to determine which material-specific function to call and routes inputs accordingly. The *GrowthFatigue* subroutine performs a number of other operations including the calculation of general fatigue parameters that apply to all models (e.g., load ratio), the execution of a loop over all transient components, the summation of the transient component fatigue CGRs, and the conversion from a per cycle rate to a per time rate (as summarized in Figure 3-4). The individual fatigue CGR functions implement the Ni-based alloy, austenitic SS, ferritic steel, or custom material fatigue CGR models.

The final source code for the *CGR* subroutine and its subordinate subroutines and functions are contained in a file called *grower_v3.3.f90* maintained in accordance with xLPR configuration control.[33] The verification of this source code against module requirements is discussed in the next section.

---

[33] Developed on a Windows 7 64-bit operating system with an Intel Core i7 CPU M620 2.67 GHz processor. The source code should be compiled with Intel(R) Visual Fortran Composer XE 2011 or an equivalent compiler. The following compiler options should be used: /nologo /debug:full /Od /warn:interfaces /real_size:64 /module:"Debug\\" /object:"Debug\\" /Fd"Debug\vc100.pdb" /traceback /check:bounds /libs:static /threads /dbglibs /c
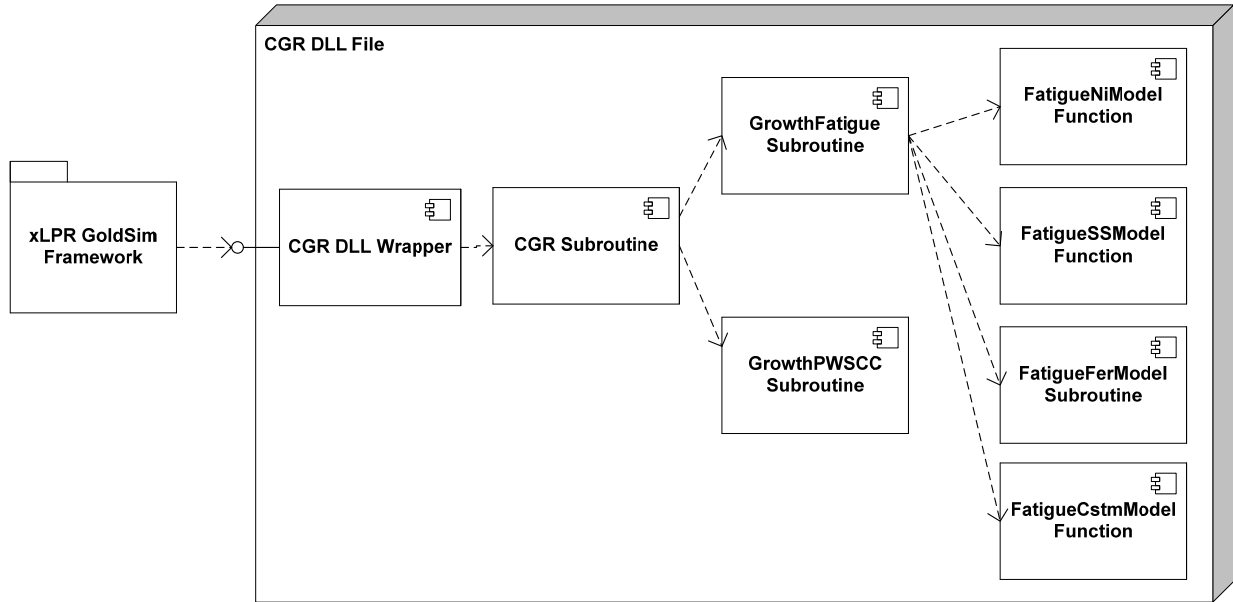
Figure 3-2.   Component Diagram of CGR Logical and Deployment Architecture
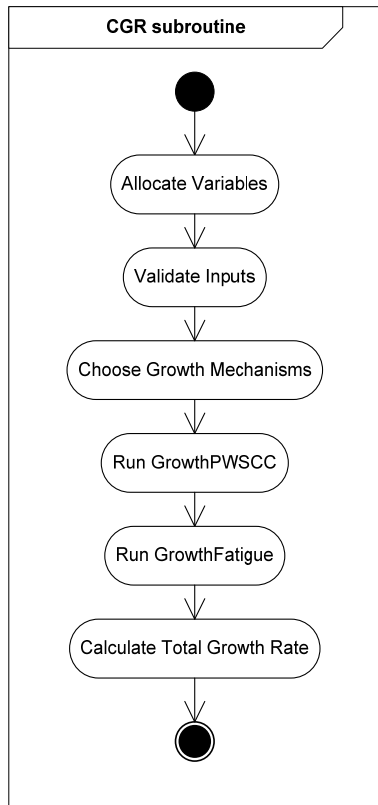
Figure 3-3.   Activity Diagram of CGR Subroutine Process Flow

GrowthFatigue subroutine

ii = transient component index
Ncyc(ii) = number of cycles for transient ii
NTS = total number of transient components
delK = stress intensity factor range
delKth = threshold stress intensity factor range

Allocate Variables

Validate Inputs

Calculate Transient-Specific Inputs

ii = ii + 1

[Ncyc(ii)=0]

[Ncyc(ii)>0]

[delK ≥ delKth]

[delK < delKth]

Run Growth Model

[ii < NTS]

[ii = NTS]

Evaluate Ferritic EAC Criteria

Figure 3-4.   Activity Diagram of GrowthFatigue Subroutine Process Flow

3.5 Module V&V

3.5.1 Module Verification

Module verification refers to the process of determining that the computational model accurately represents underlying requirements and accurately performs or solves any mathematical equations. The test plan for verification of module-level requirements is given in the xLPR

Software Test Plan for the PWSCC and Fatigue CGR Module. The results of executing the test plan are given in the xLPR Software Results Report for the PWSCC and Fatigue CGR Module.

In summary, all module-level requirements were assigned at least one corresponding test case. Additionally, test cases were developed such that all logic branches in the code were verified. In total, 46 (static) tests were performed by directly comparing source code to written requirements to verify verbatim compliance. In addition, 101 (dynamic) tests were performed in which module input-output combinations were compared against independent calculations performed in accordance with requirements. The first 56 dynamic tests were performed to verify error codes for out-of-range inputs. An additional 35 dynamic tests were designed to test mathematical or logical requirements. The remaining 10 dynamic tests were designed to test run time performance of the module. In addition to these static and dynamic tests, the source code was manually inspected to verify conformance with a set of recommended programming practices. Five anomalous events were found during the testing activities, all of which were resolved and closed.

Finally, interfacing requirements were not verified as part of module-level verification. Interfacing requirements are instead verified as part of the Framework verification.

3.5.2 Module Validation

Module validation refers to the process of determining the degree to which the model is an accurate representation of the real world from the perspective of the intended uses of the model. Module validation is discussed on a model-specific basis in Sections 2.2 and 2.3. Module validation is further detailed in the xLPR Module Validation Report for PWSCC CGR Models and the xLPR Module Validation Report for Fatigue CGR Models.

4. CRACK COALESCENCE MODEL

This section describes the model that enables the prediction of crack coalescence within the xLPR Version 2.0 framework. In this context, crack coalescence refers to the combining of multiple cracks of engineering scale, provided each is one of the three xLPR crack types defined in Section 2.4.2. This section is organized as follows:

- Section 4.1 presents an overview of the coalescence model.

- Section 4.2 describes the mathematical conventions and technical bases that serve as the foundation for the crack coalescence model.

- Section 4.3 catalogues the primary assumptions and simplifications built into the crack coalescence model.

Section 5 complements this section with a description of the coalescence module that implements the coalescence model.

4.1 Model Overview

The coalescence model is a set of conventions for simulating the combination of cracks based on their sizes, shapes, and locations. These conventions are a substitute for higher order fracture mechanics calculations that are not amenable to the xLPR probabilistic framework or that were not made a priority for Version 2.0 of xLPR. Specifically, coalescence conventions may simulate two distinct modes by which cracks in proximity to one another may combine on a time scale faster than is predicted by treating growth of each crack separately:

- Crack interaction, whereby stress intensity experienced at crack front locations are amplified due to local stress fields radiating from a nearby crack, resulting in accelerated growth;

- Ligament collapse, whereby the span of material separating two through-wall cracks experiences high stresses to the point of fully plastic failure.

It is emphasized that the coalescence model of Version 2.0 of xLPR is not applicable to model the earlier stages of crack development that often involve coalescence of multiple short cracks (i.e., micro-fissures). Instead, the purpose of the coalescence model is to account for the situation when two adjacent macro-cracks of engineering significance (e.g., 1 to 3 mm or more) that are already growing via a subcritical crack growth regime (i.e., PWSCC or fatigue crack growth) controlled by fracture mechanics (i.e., crack-tip stress intensity factor) are predicted to merge into a single, larger crack of engineering significance. Hence, the distinct research area of short crack coalescence (e.g., Parkins et al. [47] and Calonne et al. [48]) is not directly relevant.

While the coalescence model is rooted in a simple rule-based methodology, these modeling conventions were developed to be physically viable and have been validated against laboratory experimentation and higher order fracture mechanics modeling.

4.2 Coalescence Model Development

This section describes the development and technical bases for the coalescence modeling conventions. Coalescence modeling conventions are applicable to coplanar macro-cracks of engineering significance characterized as one of the three xLPR crack types: semi-elliptical surface crack, transitioning through-wall crack, or idealized through-wall crack. The conventions are generally applicable irrespective of material.

4.2.1 Model Form Development

This section describes the prediction of imminent coalescence and the prediction of crack shape, size, and location after coalescence. All coalescence conventions are based on pairwise coalescence between only two cracks. For rare instances of more than two cracks coalescing at the same time at the same location, pairwise coalescence conventions are applied in series. For reference, coalescence between two cracks and key terminology are illustrated in Figure 4-1.

Similar coalescence conventions are commonly applied for deterministic and probabilistic analyses throughout the nuclear power industry and are appropriate for xLPR. Furthermore, the use of a simple convention-based approach, with overall fidelity with respect to the physical coalescence process, is justified within a Monte Carlo framework, for which a single prediction is of minor importance (due to the many other sources of significant uncertainty).
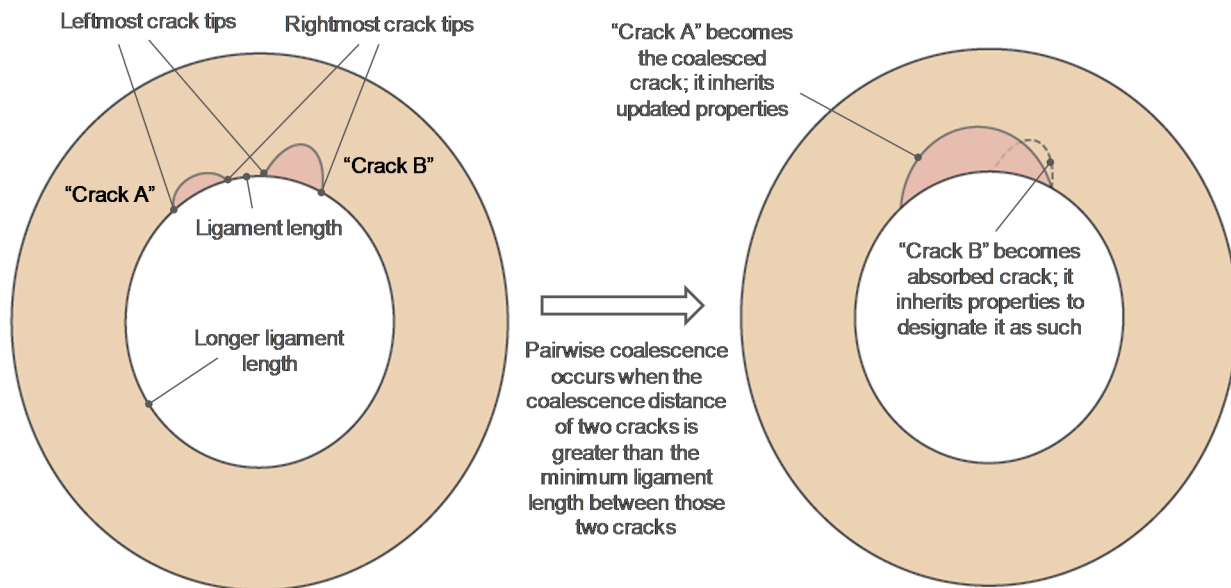
Figure 4-1.   Illustration of Key Terminology for Coalescence Model

4.2.1.1 Prediction of Imminent Coalescence

The prediction of coalescence is contingent on the length of the smallest ID ligament (see Figure 4-1) separating two cracks. When this ligament length becomes less than some value—termed the coalescence distance—coalescence is said to be imminent, resulting in the replacement of the two original cracks with a single coalesced crack in the xLPR Framework.

The common physical driver of coalescence for two surface cracks is crack interaction, whereby stress intensities experienced at crack front locations are amplified due to local stress fields radiating from a nearby crack, resulting in accelerated growth. This complex process is not treated in the K-calculation and growth predictions of Version 2.0 of xLPR and instead can be simulated with a positive coalescence distance. Two conventions have been selected to determine the coalescence distance for surface cracks: in the first, the coalescence distance is set to some user-defined value, irrespective of crack sizes; in the second, the coalescence distance is calculated by scaling the maximum crack depth by some user-defined value. The second convention is recommended to approximate the known dependency between crack interaction and crack depth [49].[34] Furthermore, this convention is consistent with ASME Boiler and Pressure Vessel Code Section XI IWA-3000, which requires cracks separated by less than half of the maximum depth to be combined prior to stability assessment. Provided the second modeling convention, the best-fit scaling factor is half (0.5) of the maximum depth of the cracks involved in coalescence.

For two through-wall cracks, the common physical driver of coalescence is ligament collapse, whereby the span of material separating the cracks experiences high stresses to the point of fully plastic failure. These complex processes are not treated in the K-calculation, growth, or stability predictions of Version 2.0 of xLPR and instead can be simulated with a positive coalescence distance. The coalescence distance in this case is set to a user-defined value. In actuality, this distance may systematically depend on crack length; however, this dependency is not implemented in the coalescence module for xLPR Version 2.0. Through-wall crack coalescence distances between 0 and 20 inches are possible for components of interest in xLPR, depending on the sizes of the flaws involved.

For the crack pair made up of one surface crack and one through-wall crack, the coalescence distance is set to zero by default. This crack arrangement has no known ASME Code considerations (as for two surface cracks) and no true ligament formation (as for two through-wall cracks).

4.2.1.2 Coalesced Crack Geometry

The crack resulting from the coalescence of two original cracks requires updated geometrical attributes including type, depth, length, and location. The various conventions for modeling the updated attributes are discussed below. These conventions are also summarized in Figure 4-2 and Figure 4-3.

Regarding crack type after coalescence, two surface cracks form a surface crack; two transitioning cracks form a transitioning crack; two idealized through-wall cracks form an idealized through-wall crack; and the combination of cracks with dissimilar type results in a transitioning crack. These transitioning rules were developed based on physical expectations and logical considerations when constrained to the three crack types recognized within the Version 2.0 xLPR Framework. In reality, the crack resulting from one surface crack and one through-wall crack would possess significant asymmetry upon coalescence. The importance of this asymmetry is not

---

[34] Recent finite element analysis work presented by Azuma et al. [50] suggests that crack interaction might more appropriately be characterized by the *lengths* of the cracks involved in coalescence. This work predicts a near-constant ratio between the crack interaction distance (i.e., coalescence distance) and the maximum length of the cracks involved in coalescence, irrespective of crack depths. In this manner, it predicts that the ratio between the crack interaction distance and the maximum crack depth fluctuates depending on crack length. This work is considered further in Section 6.3.

well known, but a fourth crack shape (based on an asymmetric trapezoid) could mitigate this concern for later versions of xLPR.

Consistent with physical expectations, the depth of the new crack is the component thickness for instances of coalescence involving one or more through-wall cracks. A number of options were selected for the depth of the coalesced crack resulting from two surface cracks: the minimum, maximum, or average depth of the original two cracks. These different options may be used to understand xLPR prediction sensitivity to the coalescence depth modeling convention. However, from these selected options, the maximum depth is recommended based on the physical expectation that stress intensity factors in the "re-entrant sector" between the two original cracks will be amplified from the time crack interaction becomes significant until the coalesced crack regains a roughly symmetric shape (e.g., see Figure 4-4 from laboratories studies presented in Reference [49]).

The center of the new crack is set to the center of the arc that circumscribes the ID lengths of the original cracks. For through-wall cracks, this convention is physically consistent with ligament collapse. For coalescence involving one or more surface cracks, this convention is based on the physical expectation that stress intensity factors will tend to be amplified in regions of reduced depth, resulting in rapid growth toward symmetry. This convention is believed to be logical when constrained to the three crack types recognized within the Version 2.0 xLPR Framework.

The OD length of the new crack is set to the length of the arc that circumscribes the OD lengths of the original cracks. For two surface cracks, this length is zero. For one surface crack and one through-wall crack, this length is the OD length of the original through-wall crack. This convention is consistent with physical expectations and should result in acceptable leakage continuity immediately before and after coalescence. Also, this convention is believed to be logical when constrained to the three crack types recognized within the Version 2.0 xLPR Framework.

For two surface cracks or two through-wall cracks, the ID length of the new crack is set to the length of the arc that circumscribes the ID lengths of the original cracks. This is physically consistent with the simulated modes of coalescence and is believed to be logical when constrained to the three crack types recognized within the Version 2.0 xLPR Framework. For the coalescence of one through-wall crack and one surface crack, the ID length is set such that the area of the coalesced crack is equivalent to the sum of the areas of the original two cracks. This promotes continuity of the component stability prediction immediately before and after coalescence.

Red line indicates arc circumscribing ID lengths of original cracks

Surface Crack + Surface Crack
Coalescence distance = various options

Surface Crack
Center = centerline of arc circumscribing ID lengths of original cracks
Depth = various options for calculation
ID Length = length of arc circumscribing ID lengths of original cracks
OD length = zero

Surface Crack + Idealized Through-Wall Crack
Coalescence distance = zero (must overlap)

Transitioning Crack
Center = centerline of arc circumscribing ID lengths of original cracks
Depth = thickness
ID length = calculated to preserve area equivalence with original cracks
OD Length = OD length of original idealized through-wall crack

Surface Crack + Transitioning Crack
Coalescence distance = zero (must overlap)

Transitioning Crack
Center = centerline of arc circumscribing ID lengths of original cracks
Depth = thickness
ID length = calculated to preserve area equivalence with original cracks
OD length = OD length of original transitioning crack

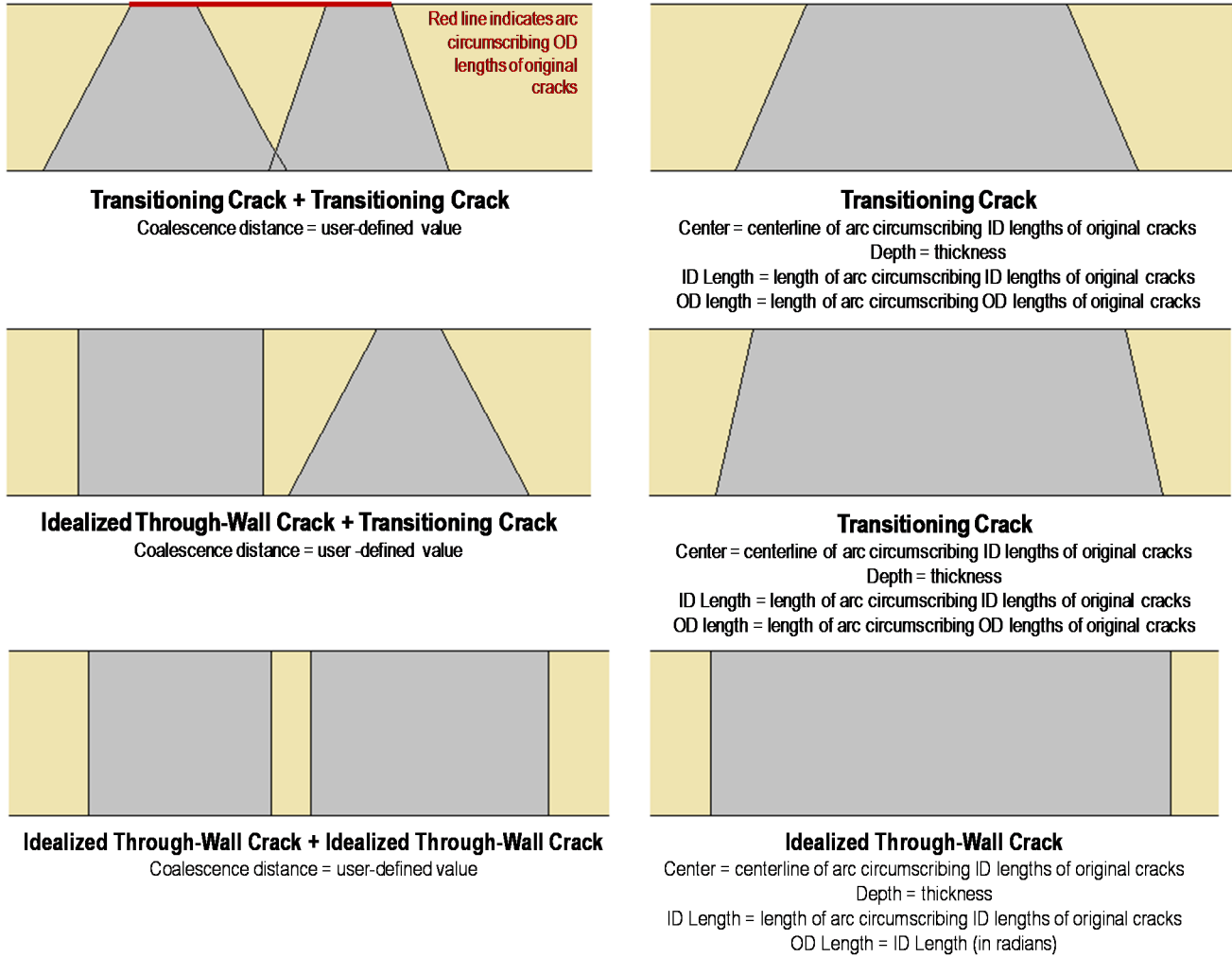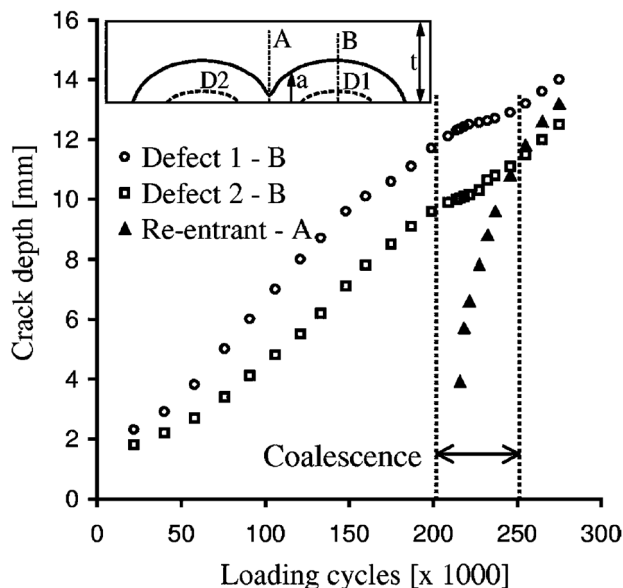**Figure 4-2.   Illustration of Coalescence Conventions (Surface Crack)**

Figure 4-3.   Illustration of Coalescence Conventions (Through-Wall Cracks)

Figure 4-4. **Crack Depth in the Re-Entrant Sector (position A) and at Deeper Segments (position B) for Semi-Elliptical Cracks Extending by Fatigue [49]**

4.2.2 Treatment of Uncertainty

Uncertainty in the coalescence prediction may be incorporated through the use of distributed coalescence distances. This uncertainty may reflect variability in the complex processes that lead to coalescence as well as model error (e.g., the lack of a systematic dependency with respect to crack length). It is recommended that these uncertainties be designated as epistemic given that more detailed models would be expected to result in more precise estimates.

For surface cracks, the ratio of the crack interaction distance (i.e., coalescence distance) to the maximum depth of the two cracks is between zero (i.e., no crack interaction) and roughly 0.75, with a best-estimate of 0.5. In the absence of more detailed investigation, a triangular distribution is recommended with extremes at 0.0 and 0.75 and a mode at 0.5.

The coalescence distance for through-wall cracks should be roughly consistent with the lengths of cracks at the time at which coalescence is simulated. This reflects analytical findings (after the time of model development) that the coalescence distance has a roughly one-to-one relationship with crack length [51].[35]

The other coalescence modeling conventions are fully deterministic. That is, for any given pair of cracks undergoing coalescence, the type, location, depth, ID length, and OD length of the resulting crack is fully determined. The modeling conventions for type, location, ID length, and OD length are logically rooted and are therefore not considered subject to significant uncertainties. The convention of using the maximum depth of the original cracks for coalescence

---

[35] Alternatively, the coalescence distance for through-wall cracks may be assumed to be deterministic for individual program runs and then varied for the purpose of sensitivity studies to understand its influence on xLPR predictions.

of surface cracks is based on physical expectation; this convention may be varied for individual program runs to understand its influence on xLPR predictions.

4.2.3 Model Validation

The coalescence modeling conventions were originally developed a) to reflect logical and physical expectations and b) to be flexible to accommodate the findings of more advanced analytical and experimental investigations. Through application of published research, the coalescence modeling conventions were generally validated. For instance, Bezensek et al. [49] examined crack interaction effects for surface cracks experimentally and analytically. A study by Huh et al. [52] supported these crack interaction effects through an alternate model. Chang et al. [51] provided an analytical model for local ligament collapse of idealized through-wall cracks, while global stability of two through-wall cracks was modeled by Suga et al. [53]. Specific instances of model validation are noted below:

- Experimental evidence suggests that the onset of the intensification of stress intensity factor for surface cracks is well-predicted using a coalescence distance that is some fraction— e.g., somewhere between 0.0 and 0.75—of crack depth, validating the selected modeling convention.

- Higher order modeling suggests low likelihood of rapid tearing leading to ligament collapse until the ligament between two cracks is less than the length of the cracks. This supports the use of some positive coalescence distance for through-wall cracks[36]. However, this finding beckons the implementation of more detailed coalescence modeling for through-wall cracks to account for length-dependency.

- The maximum depth convention for a crack resulting from two surface cracks is supported by the rapid growth of the "re-entrant sector" at the intersection of the two coalescing cracks due to elevated stress intensity factors in that region until the bounding crack shape is obtained. This rapid growth is predicted with higher order analytical modeling and has been observed experimentally.

- The conventions for establishing the crack type after coalescence—i.e., transitioning rules— are generally validated with experimental results and higher order modeling.[37]

- The convention for establishing location, ID length, and OD length of the coalesced crack is generally validated with experimental results and higher order modeling.

This module validation applies for the full range of crack and component geometries expected within xLPR Version 2.0.

---

[36] This study assumed equal length for two flaws. It is believed reasonable to employ the results of this study where the flaw length represents the maximum flaw length for the two interacting cracks.

[37] While there is not experimental data involving the coalescence of a surface crack and a through-wall crack, the established convention to transition to a transitioning through-wall crack shape is considered the most appropriate given the three crack type options in xLPR Version 2.0.

4.3 Model Assumptions

This section identifies the assumptions, simplifications, and dependencies that are considered to be the most important with respect to the coalescence model:

- **Convention-based modeling:** The foremost simplification of the coalescence model is the use of simplified convention-based modeling in lieu of mechanistic or phenomenological modeling of coalescence (e.g., modeling derived from fracture mechanics or first principles). The goal of the convention-based modeling is to approximate physical coalescence in an average and physically viable sense; and, indeed, higher order analytical modeling and experimental investigations validate the modeling conventions (e.g., see sections above). This type of modeling is often used in association with probabilistic methods where the result of any single deterministic simulation is not of primary significance. The model includes a range of different conventions, or rules, for coalescence so that the sensitivity to these simplifications can be explored.

- **Crack shape idealization:** As described earlier, cracks are idealized as one of three crack types: semi-elliptical surface cracks, idealized through-wall cracks (same ID and OD length in terms of radians), or transitioning through-wall cracks. This is an xLPR-wide approximation for Version 2 used to allow tractable development of analytical models, e.g., for stress intensity factor calculation, crack opening displacement calculation, etc. In reality, of course, PWSCC and fatigue cracks possess complex geometries with spatial variation on multiple different scales. Despite the simplified crack shapes required, applying the coalescence module to make predictions for complex crack geometries is believed to yield reasonable results for observed time to coalescence and observed depth / length subsequent to coalescence, provided parameters are selected appropriately.

- **Coplanar crack assumption:** All circumferential cracks are assumed to be coplanar within the xLPR Version 2.0 framework. This means that circumferential cracks that more realistically might remain offset axially and independent are combined. The conservatism of this approach varies depending on the crack configuration (e.g., see Figure 4-5). For cracks with little to no circumferential overlap (Configuration A in Figure 4-5), this assumption will lead to a single large crack at the expense of two axially offset cracks. This would increase probability of leakage somewhat, increase leakage rates significantly, and increase susceptibility to rupture significantly depending on the degree of axial offset. For cracks with substantial circumferential overlap (Configuration B in Figure 4-5), this assumption would tend to result in a slightly reduced probability of leakage as one of two cracks may grow more quickly than the other, decrease leakage rates by approximately one half, and decrease susceptibility to rupture somewhat. Further analysis would be required to quantify the effects of the coplanar assumption more rigorously.
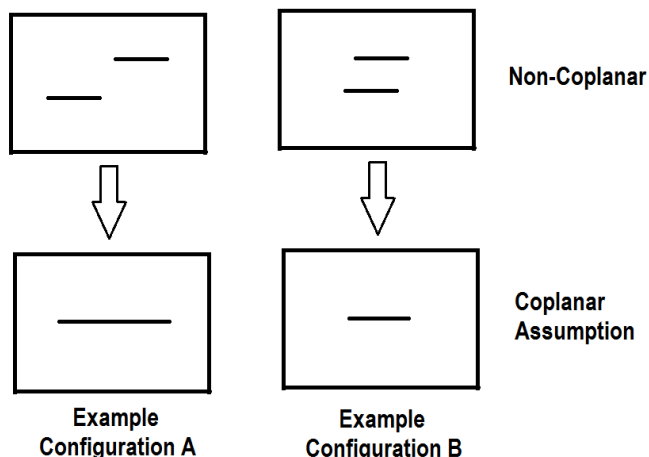
Figure 4-5. **Example of Configurations Illustrating Impact of Coplanar Crack Assumption**

- **Neglecting interaction between axial and circumferential cracks:** Axial cracks are neglected when applying coalescence rules. In reality, the intersection of perpendicular cracks may result in crack blunting that arrests one of the cracks. Therefore, this is a conservative assumption relative to probability of leakage and stability.

  Coplanar axial cracks are not modeled in Version 2.0 of xLPR. A maximum of one axial crack of engineering significance is modeled at each circumferential discretization of the component. For dissimilar weld modeling, this is consistent with the expectation that weld residual stresses will peak (and therefore initiation will be most likely) over a relatively narrow axial extent.

- **Neglecting systematic variation in coalescence distance:** Higher order analytical predictions suggest that coalescence distance may be sensitive to crack length and component thickness, especially for coalescence of very large cracks where the ligament stress between the cracks is substantially elevated relative to the intact condition. This systematic variation is not addressed in the coalescence model. This is expected to result in generally early coalescence for short-length cracks and generally late coalescence for long-length cracks. The overall conservatism of these biases depends on the selection of the coalescence distance inputs and may be studied with sensitivity studies performed within the xLPR framework.

- **Extension of coalescence validation to annular geometries:** All validation data available concern coalescence of cracks in flat plate geometries. In many applicable components, the characteristic length of ID curvature is much longer than typical crack lengths and therefore the extension of flat plate data is reasonable. For smaller radius components, such as pressurizer nozzles, or for particularly large cracks, the ID curvature may affect crack interaction and susceptibility to ligament collapse. Uncertainty in this effect can be considered in the coalescence distance distributions.

5. CRACK COALESCENCE MODULE

The coalescence module is incorporated within the xLPR Computational Framework to handle the combination of independent cracks. The coalescence module, which may be called by the Computational Framework at any given time, updates the crack configuration (i.e., location, shape, and size for all active cracks) to reflect processes that lead to rapid crack combination (e.g., accelerated growth due to crack interaction or plastic collapse of separating ligaments). The module implements the coalescence modeling conventions detailed in Section 4.

This section presents the coalescence module and is organized as follows:

- Section 5.1 provides an overview of the module, including a description of its scope and limitations.

- Section 5.2 describes the requirements that are enforced in the implementation of the coalescence model and the interfacing requirements to ensure proper usage of the module within the xLPR Computational Framework.

- Section 5.3 details the inputs to and outputs from the module.

- Section 5.4 summarizes the design and implementation of the module.

- Section 5.5 summarizes the V&V performed to ensure the correct implementation of the module-level requirements.

5.1 Module Scope and Limitations

Figure 5-1 provides an overview of the basic structure of the coalescence module and how it is incorporated by the Computational Framework. While not depicted in the diagram, the Framework discretizes time and implements a numerical time integration method to solve for crack growth versus time. At each time discretization, the Framework may call the coalescence module to update the crack configuration (i.e., location, shape, and size for all active cracks). For each update, the Framework provides information about the crack configuration, component geometry, and coalescence model parameters via inputs that are detailed in Section 5.3.

To update the crack configuration, the coalescence module implements an iterative procedure whereby each pair of active cracks is assessed against coalescence criteria. If any pair of cracks does satisfy coalescence criteria, the coalescence module updates the attributes associated with this pair of cracks to result in a) a coalesced crack with attributes determined as a function of the attributes of the two original cracks and b) an absorbed crack, which is effectively ignored throughout the remainder of simulation. The iterative procedure continues until no pair of active cracks satisfies coalescence criteria, at which point the coalescence module returns control to the calling entity.
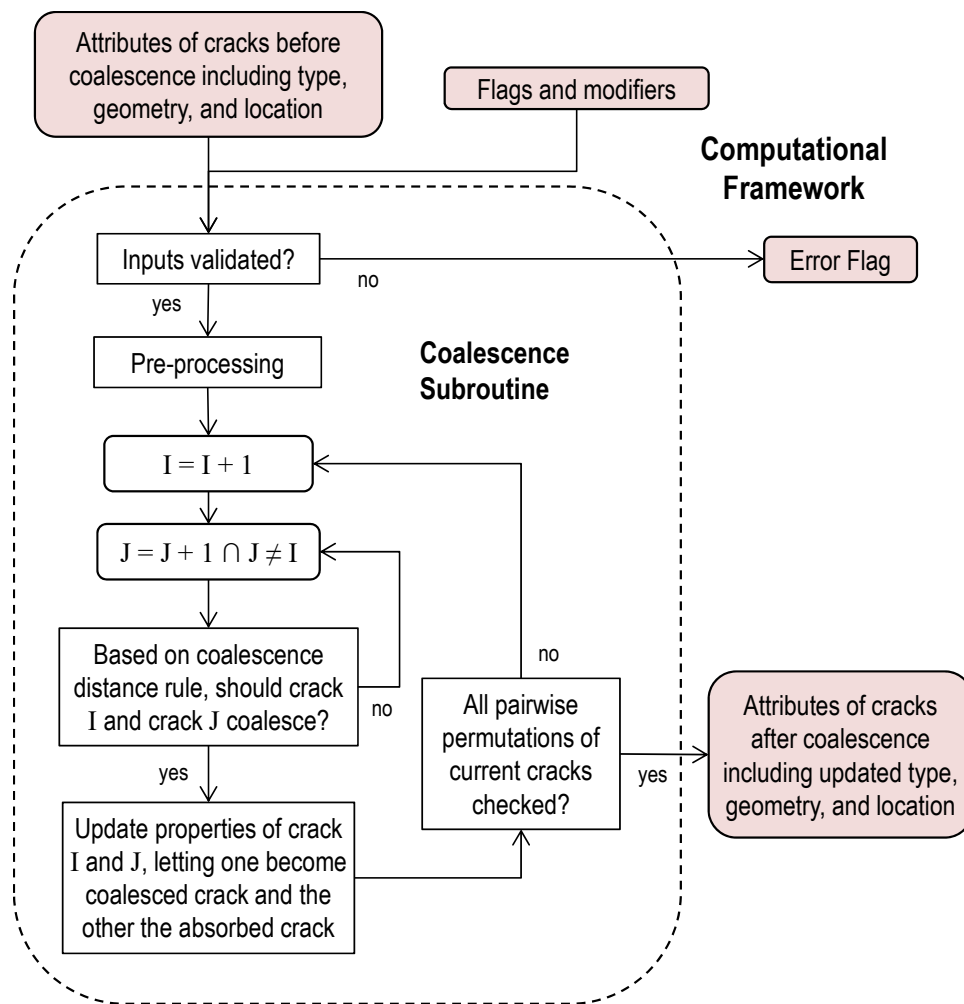
Figure 5-1.   Flow Diagram of the Version 2.0 xLPR Crack Coalescence Module

The scope of the coalescence module is limited to coplanar circumferential cracks. Axial cracks are neglected with respect to coalescence considerations. All circumferential cracks are assumed to be coplanar (an xLPR-wide assumption).

Furthermore, the coalescence module assumes that all cracks comply with one of three idealized crack types, as detailed in Section 2.4.2. These three idealized crack types are assumed throughout the xLPR Version 2.0 Framework and are necessary for other calculations including stress intensity factors, growth evolution, and crack opening displacements.

A comprehensive list of assumptions and limitations associated with the coalescence *model* is given in Section 4.3.

5.2 Module Requirements

Software requirements for the coalescence module were documented rigorously in the xLPR Software Requirements Description for the Coalescence Module. In total, there were 51 requirements—45 module-level requirements and six interfacing requirements. This section summarizes these requirements.

5.2.1 Module-Level Requirements

This section summarizes module-level requirements related to input allocation and verification, pre-processing, implementation of the iterative application of coalescence procedures, defining coalescence distance, updating crack attributes, post-processing, and performance.

5.2.1.1 Input Allocation, Input Verification, and Output Requirements

A few requirements relate to the allocation of memory for inputs and input verification, for example:

- The coalescence module requires attributes for multiple cracks each time it is called. Attributes that are defined on a crack-specific basis—e.g., crack type, crack depth—are stored in vector arrays dynamically allocated by the module based on the input argument that defines the number of cracks.

- Prior to any other operations, all arguments to the module are confirmed to be within acceptable ranges, as identified in Section 5.3. If not, the module returns control to the calling entity with an error flag to indicate which input was first found to be out of range.

5.2.1.2 Pre-Processing Requirements

Before application of the iterative procedure, a number of pre-processing requirements are enforced to improve efficiency and limit complexity:

- All vector arrays corresponding to crack-specific attributes are reordered in terms of circumferential location.[38] Enforcement of this requirement and others discussed in Section 5.2.1.3 guarantees that pairwise coalescence will only occur between adjacent cracks. This condition is helpful for verifying the coalescence module.

- Cracks that have not yet initiated or that have been absorbed by earlier coalescence (at the time of the call to the coalescence module) are neglected in the consideration of coalescence.

- Axial cracks are neglected in the consideration of coalescence.

- If fewer than two circumferential cracks are active (at the time of the call to the coalescence module), all coalescence module arguments are returned unmodified.

5.2.1.3 Iterative Application of Coalescence Rules

A number of highly specific requirements are enforced for the iterative application of the coalescence rules. These requirements put a burden on the coalescence module design but were intended to be helpful for module-level verification. These requirements rely on the designation of "Crack A" and "Crack B", as detailed below:

- In general, the crack coalescence criteria are satisfied when the leftmost tip (relative to an observer standing on the origin of the pipe cross-section) of "Crack B" is between the tips of "Crack A" or if the leftmost tip of "Crack B" is less than the coalescence distance from the

---

[38] This requirement is facilitated by the Index Transformation array described later.

rightmost tip of "Crack A" in the clockwise direction. The coalescence distance depends on the crack types and geometries of "Crack A" and "Crack B". See Section 5.2.1.4.

- The crack that initiated in subunit 1 is the first crack designated as "Crack A".

- Each time a crack is designated as "Crack A", each other crack is iteratively designated as "Crack B", beginning immediately clockwise of "Crack A" and proceeding in the clockwise direction.

- If the current "Crack A" does not satisfy the coalescence criteria with any other crack, the crack immediately clockwise of the current "Crack A" is designated as the new "Crack A".

- If the coalescence criteria are satisfied, "Crack A" receives updated attributes corresponding with the coalesced crack and "Crack B" receives updated attributes corresponding with the absorbed crack. See Section 5.2.1.5.

- The above requirements for the iterative procedure are repeated until there is no pair of cracks that satisfies the coalescence criteria.

- The directionality of the iterative coalescence procedure (as stated above) may be reversed using a module flag (the Coalescence Direction flag). This capability was built-in to investigate the concern that—for configurations requiring more than one instance of pairwise coalescence—the iterative coalescence rules may give different updated crack configurations depending on directionality of the iterative procedure.

5.2.1.4 Defining Coalescence Distance

A number of requirements are enforced to define the coalescence distance—the distance between two cracks below which those cracks will coalesce—in accordance with the modeling conventions of Section 4.2, for example:

- If both cracks are surface cracks, two possible conventions have been implemented: in the first, the coalescence distance is set to a user-defined input, irrespective of crack sizes; in the second, the coalescence distance is calculated by scaling the maximum crack depth by a user-defined input. Either option may be invoked by varying a model flag (the Surface Crack Coalescence Distance Rule flag).

- If both cracks are through-wall cracks, the coalescence distance is set to a user-defined input.

- If one crack is a surface crack and the other is a through-wall crack, the coalescence distance is set to zero.

5.2.1.5 Updating Crack Attributes

A number of requirements are enforced to update crack attributes in accordance with the coalescence modeling conventions of Section 4.2, for example:

- Absorbed cracks—those neglected after coalescence—are assigned as such using the crack type value. By convention in xLPR Version 2.0, positive integers designate absorbed cracks.[39]

- A coalesced crack resulting from coalescence between any two dissimilar crack types is a Transitioning Crack.

- A coalesced crack resulting from coalescence between cracks of the same type maintains this type.

- The center location of a coalesced crack is set to the center of the ID arc that circumscribes both original cracks.

- The OD length of a coalesced crack is set to the length of the OD arc that circumscribes the OD lengths of both original cracks. For two surface cracks, the OD length is zero.

- If both original cracks are surface cracks or both original cracks are through-wall cracks, the ID length of the coalesced crack is set to the length of the ID arc that circumscribes both original cracks.

- If one original crack is a surface crack and the other is a through-wall crack, the ID length of the coalesced crack is set such that the area of the coalesced crack is the same as the sum of the individual areas of the original cracks.

- If either original crack is through-wall, the depth of the coalesced crack is set equal to the component thickness.

- If both original cracks are surface cracks, the depth of the coalesced crack may be set to the minimum, average, or maximum of the original depths. These options are invoked by varying a model flag (the Depth Rule flag).

5.2.1.6 Output Requirements

Several requirements pertain to the output of the coalescence module, for example:

- Cracks not involved in coalescence do not have their attributes updated by the coalescence module.

---

[39] Specifically, absorbed cracks are given a crack type equal to the initiation time index of the crack with which it coalesces (i.e., "Crack A"). This information can be diagnostically helpful at the end of program execution.

- Prior to returning control to the calling entity, all arguments from the module are confirmed to be within acceptable ranges, as identified in Section 5.3. If not, the module returns control to the calling entity with an error flag to indicate which output was found to be out of range.

- If the number of pairwise coalescences exceeds one during a single call to the coalescence module, the error flag is set to 301. By definition within xLPR, a 300-level error does not result in termination of the program instance, but is logged to a run file for the benefit of the user or reviewers.

- All vector array outputs containing crack-specific attributes are reordered and returned with the order corresponding to crack initiation times.

5.2.1.7   Performance Requirements

To motivate efficient module design, the following runtime and memory requirements were imposed:

- The coalescence module memory does not exceed 30 kB during runtime.

- For a case with the existence of at least five cracks of arbitrary type, depth, and length—subject to at least two instances of overlapping cracks—the coalescence module shall be capable of execution 1000 times in less than 10 seconds.

5.2.2   Interfacing Requirements

Several interfacing requirements are imposed on the xLPR Computational Framework to ensure appropriate utilization of the coalescence module:

- Communication of inputs to and outputs from the coalescence module is performed with explicit passing of variables. The order of arguments to the module is specified in the Software Design Description discussed in Section 5.4.

- Communication of inputs is performed with the required units and data types given in Section 5.3.

- Random sampling is performed for inputs defined as distributed random variables.

- All vector array inputs containing crack-specific attributes contain information for at least each active circumferential crack. The vector array inputs have the same length, defined by the number of cracks input argument.

- All vector array inputs containing crack-specific attributes are indexed with order corresponding to crack initiation time.

- The Index Transformation array contains the subunit number associated with the center of each crack, allowing reordering based on circumferential location within the coalescence module.

5.3 Module Inputs and Outputs

Table 5-1 describes all inputs to the coalescence module, including their required unit, range of verification, and data type. These attributes are discussed in turn below:

- *Required unit:* Assumed units are built into the coalescence module calculations and therefore must be upheld by input arguments.

- *Range of verification:* A critical error (requiring program termination) is generated for inputs outside of the range of verification. In general, these ranges prevent unrealistic or non-meaningful inputs. This range is different from the range over which model validation was performed.

- *Data type:* For memory allocation purposes, the inputs are to be entered with specific data types, all of which are interpreted by common programming languages.

The remainder of this section provides additional discussion about the inputs and outputs to the coalescence module.

Table 5-1. Coalescence Subroutine Arguments

Description	Required Units	Range of Verification
Number of cracks represented	-	$0 \le x \le 200$
Crack type array	-	$-3 \le x < 100$
Depth array	m	$0 < x \le \text{thickness}$
Center location array	rad	$0 \le x < 2\pi$
ID half-length array	m	$0 < x \le \pi*\text{inner radius}$
OD half-length array	m	$0 \le x \le \pi*\text{outer radius}$
Crack orientation array	-	$1 \le x \le 2$
Index transformation array	-	$1 \le x < 100$
Component inside radius	m	$x > 0$
Component thickness	m	$x > 0$
Coalescence direction	-	$1 \le x \le 2$
Surface crack coalescence distance rule value (*DistanceRule*)	-	$1 \le x \le 2$
Surface crack coalescence distance rule modifier	meter if *DistanceRule* =1 unitless if *DistanceRule* =2	$x \ge 0$
Through-wall crack coalescence distance rule modifier	m	$x \ge 0$
Coalescence depth rule value	-	$1 \le x \le 3$
Error flag	-	-
Number of pairwise coalescences	-	-

5.3.1 Physical Arguments

Several arguments corresponding to physical quantities are required to define the crack configuration, as detailed below:

- *Number of cracks:* The number of cracks argument specifies how many independent cracks of engineering significance are to be assessed for coalescence. This number of cracks must include all active circumferential cracks. This input also defines the sizes for vector arrays supplying crack-specific attributes. The number of cracks is determined at each time step by the Computational Framework.

- *Crack type:* The crack type array gives the crack type associated with each crack. By convention of the xLPR Computational Framework, 0 corresponds to a crack that has not yet initiated; -1 corresponds to a surface crack; -2 corresponds to a transitioning crack; -3 corresponds to an idealized through-wall crack; and any positive integer corresponds to a crack that was previously absorbed by coalescence. The coalescence rules are dependent on crack type, and crack type may be updated as part of the coalescence prediction. This array is constructed and updated[40] at each time step by the Computational Framework.

- *Crack geometry:* The crack depth, center location, ID half-length, and OD half-length arrays define the geometry of each crack. The coalescence rules are dependent on crack geometry and crack geometry may be updated as part of the coalescence prediction. These arrays are constructed and updated[41] at each time step by the Computational Framework.

- *Crack orientation:* The crack orientation array designates cracks as either circumferential (1) or axial (2). Axial cracks are neglected in the assessment of coalescence. This array is constructed by the Computational Framework.

- *Index transformation array:* The index transformation array specifies the subunit in which each crack initiated. This information is used to map between order of initiation time (as is input) and order of circumferential location (as is required to perform the iterative coalescence procedure). This array is constructed by the Computational Framework.

- *Component geometry:* The component radius and thickness are used to verify the range of crack geometries at both the input and output of the coalescence module. These parameters are user-defined.

5.3.2 Coalescence Model Parameters and Flags

The implemented coalescence models are parameterized to improve flexibility. The following parameter inputs fully define the behavior of the coalescence module:

- *Coalescence direction*: The coalescence direction flag determines whether the iterative coalescence procedure is applied in a clockwise (1) or counter-clockwise direction (2). The

---

[40] The coalescence module performs updates to crack type due to coalescence. The Framework performs updates to crack type due to other transitioning rules.

[41] The coalescence module performs updates to geometry due to coalescence. The Framework performs updates to geometry due to growth.

direction in which the coalescence procedure is applied is irrelevant so long as no more than two cracks coalesce at the same instance in time. Coalescence of three or more cracks can lead to dependence on the direction of the coalescence procedure. Cases of three or more cracks coalescing during the same time step is believed to be rare for the one month time step that is the default in xLPR Version 2.0. In any case, the user may choose to rerun the xLPR program an additional time as a sensitivity study to explore this deterministic input.

- *Surface crack coalescence distance rule*: This input selects the rule applied to determine if the coalescence distance is defined as an absolute distance (1) or as a ratio of the maximum depth of the cracks involved in potential coalescence (2). The latter convention is recommended in order to capture the depth-dependence of crack interaction discussed in Section 4.2.

- *Surface crack coalescence distance rule modifier:* For a distance rule value of 1, this value is the coalescence distance—absolute distance between two surface cracks at the time that they are predicted to coalesce. For a distance rule value of 2, this value is the ratio of the coalescence distance to the maximum crack depth.

  The coalescence distance for surface cracks is used predominantly to simulate crack interaction resulting in accelerated growth. As discussed in Section 4.2, provided a distance rule of 2, the surface crack coalescence distance rule modifier should be sampled from a triangular distribution with extremes at 0.0 and 0.75 and a mode at 0.5 to represent variability observed in laboratory studies.

- *Through-wall crack coalescence distance rule modifier*: This value is the coalescence distance for two through-wall cracks. The coalescence distance for through-wall cracks is used predominantly to mimic ligament collapse. As discussed in Section 4.2, the through-wall crack coalescence distance rule modifier should be sampled from a distribution roughly consistent with the lengths of cracks at the time at which coalescence is simulated to represent a dependence on crack length that is otherwise unmodeled. For components of interest, this distribution might be achieved roughly with a uniform distribution between zero and 20 inches.

- *Coalescence depth rule*: The coalescence depth rule specifies whether the depth of the coalesced surface crack is the maximum (1), minimum (2), or average (3) of the original crack depths. A value of 1 is recommended based on findings presented in Section 4.2.

5.3.3 Other Output Arguments

In addition to the updated crack type and geometry arrays, two other output arguments are used to convey additional information about the call to the coalescence module. First, the number of pairwise coalescences is returned. Second, an error flag is returned to communicate any errors or anomalies encountered during the call of the coalescence module. The error codes are described below:

- The default error code is 0, indicating no errors or anomalies.

- Error codes 101 through 115 communicate an input that is out of its range of verification. For these error codes, the calling entity should terminate the run and notify the user which input is out of range. These error codes indicate an unknown error in the Computational Framework.

- Error codes 201 and 210 communicate that a calculated output of the coalescence module is out of its range of verification. For these error codes, the calling entity should terminate the run and notify the user which input is out of range. These error codes indicate an unknown error in the coalescence module.

- Error code 301 communicates that the number of pairwise coalescences exceeded one during a single call to the coalescence module. This error code does not terminate the realization, but should be tracked by the Framework to ensure that the condition is relatively rare across all realizations. If it occurs frequently, the run should be repeated with the Coalescence Direction input set to apply the coalescence procedure in the reverse direction to ensure that there was no bias during the run.

5.4 Module Design and Implementation

This section gives a brief overview of the design and implementation of the coalescence module. The design of the coalescence module, including presentation of all applicable interfaces and operations, is detailed in the xLPR Software Design Description for the Coalescence Module.

The coalescence module is deployed as a DLL, making it generally accessible to other Windows programs, e.g., the GoldSim software in which the Computational Framework is developed. The coalescence DLL wrapper code, developed by the Framework Group, defines the input and output allocation for the DLL and appropriately routes this information to and from the coalescence module. The coalescence DLL source code is contained in a file called *coalescence_DLL_source.f90* maintained in accordance with xLPR configuration control.

The *Coalesce2* subroutine is the driver of the coalescence module. The operations of the *Coalesce2* subroutine are illustrated in Figure 5-2 and are summarized below:

- Inputs are verified.

- Crack indices are reordered in terms of circumferential position (not shown in the diagram).

- The nominal implementation applies the iterative coalescence procedure in a clockwise direction. If the Coalescence Direction flag is 2, the crack configuration is mirrored and re-indexed prior to entering the iterative procedure.

- An outer loop is used to apply the "Crack A" designation to all active circumferential cracks iteratively, in a clockwise direction.

- For each outer loop iteration, an inner loop is used to apply the "Crack B" designation to all other active circumferential cracks iteratively, in a clockwise direction.

- The location of "Crack B" in polar coordinates is redefined so it is greater than the location of "Crack A" in polar coordinates. For instance, if "Crack A" is situated at 350° and "Crack B" is situated at 20°, the "Crack B" location is temporarily assigned as 380°. This is a necessary condition for checking the coalescence criteria.

- It is checked whether the current "Crack A" and "Crack B" satisfy the coalescence criteria in accordance with requirements given in Section 5.2. If not, the inner loop is incremented. If so, the coalescence modeling conventions described below are applied.

- Position, ID length, and OD length of the coalesced crack ("Crack A") are calculated in accordance with requirements given in Section 5.2.

- Depth of the coalesced crack is calculated in accordance with requirements given in Section 5.2.

- Crack type of the coalesced crack is assigned in accordance with requirements given in Section 5.2.

- The other crack ("Crack B") is assigned as a positive integer to designate it as absorbed.

- Once no pair of cracks satisfies the coalescence criteria, the outer loop is exited.

- If the Coalescence Direction flag is 2, the crack configuration is re-mirrored and re-indexed.

- Crack indices are reordered in terms of initiation time.

- Outputs are validated.

- The subroutine returns control to calling entity.

The final source code for the *Coalesce2* subroutine are contained in a file called *Coalesce_v1.6.f90* maintained in accordance with xLPR configuration control.[42] The verification of this source code against module requirements is discussed in the next section.

---

[42] Developed on a Windows 7 64-bit operating system with an Intel Core i7 CPU 27600QM 2.40 GHz processor. The source code should be compiled with Intel(R) Visual Fortran Compiler XE Version 14.0.1 or an equivalent compiler. The following compiler options should be used: Options: /OUT:"Debug\Coal.exe" /INCREMENTAL:NO /NOLOGO /MANIFEST /MANIFESTFILE:"C:\Coal\Coal\Debug\Coal.exe.intermediate.manifest" /MANIFESTUAC:"level='asInvoker' uiAccess='false'" /DEBUG /PDB: "C:\Coal\Coal\Debug\Coal.pdb" /SUBSYSTEM:CONSOLE /IMPLIB: "C:\Coal\Coal\Debug\Coal.lib" /module:"Debug\\" /object:"Debug\\" /Fd"Debug\vc100.pdb" /traceback /check:bounds /libs:static /threads /dbglibs /c
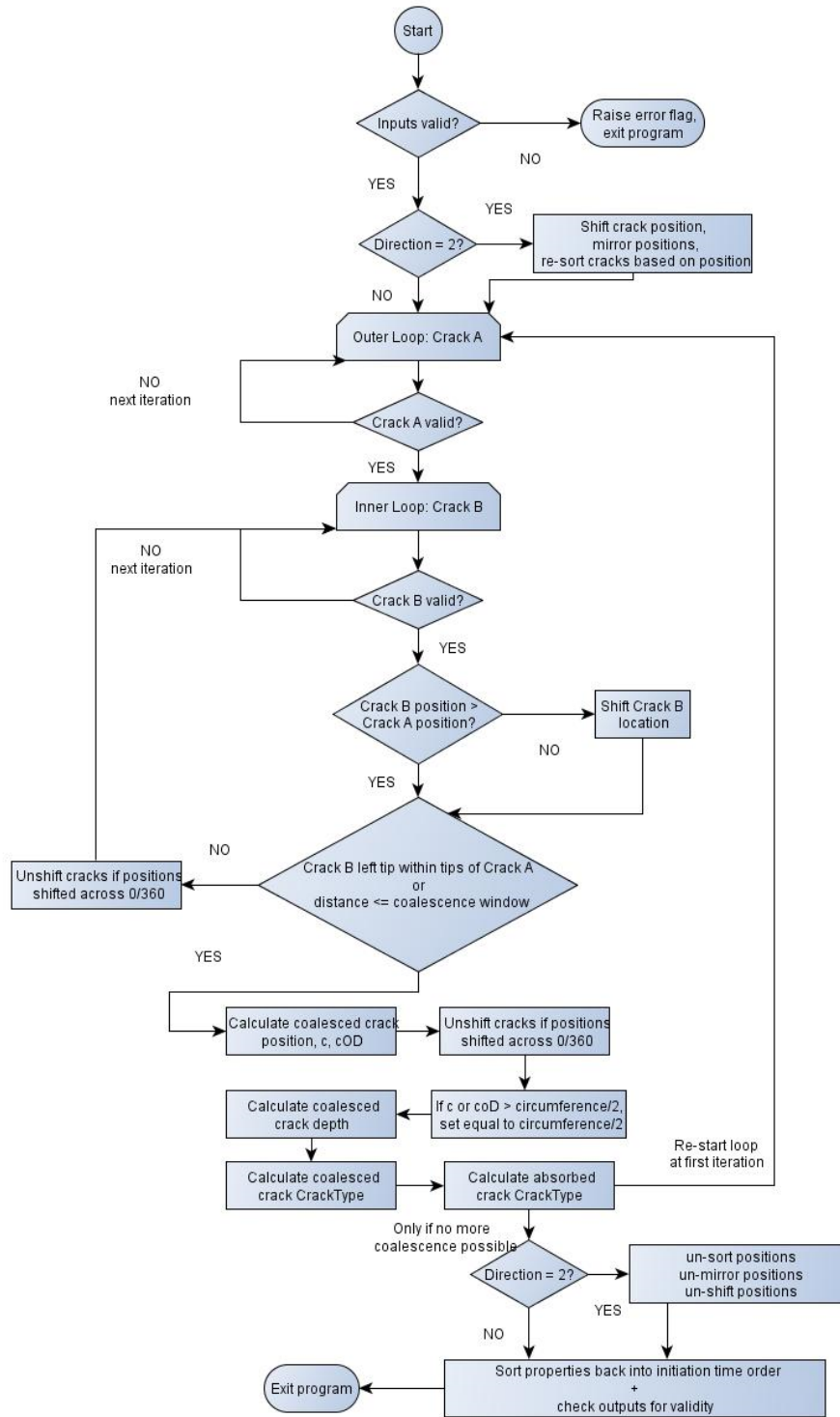
Figure 5-2.   Logic Flowchart for the Coalescence Module

5.5 Module V&V

5.5.1 Module Verification

The test plan for verification of module-level requirements is given in the xLPR Software Test Plan for the Coalescence Module. The results of executing the test plan are given in the xLPR Software Test Results Report for the Coalescence Module.

In summary, all module-level requirements were assigned at least one corresponding test case. Additionally, test cases were developed such that all logic branches in the code were verified. In total, 51 (static) tests were performed by directly comparing source code to written requirements to verify verbatim compliance. In addition, 72 (dynamic) tests were performed in which module input-output combinations were compared against independent calculations performed in accordance with requirements. The first 45 dynamic tests involved the coalescence solution for different crack configurations, designed to test the various requirements. Results from these test cases were compared against an alternative solution implemented in MATLAB. An additional 26 dynamic tests were performed to verify error codes for out-of-range inputs. The remaining dynamic test was designed to test run time performance of the module. In addition to these static and dynamic tests, the source code was manually inspected to verify conformance with a set of recommended programming practices. Fourteen anomalous events were found during the testing activities, all of which were resolved and closed.

5.5.2 Module Validation

Module validation is discussed on a model-specific basis in Section 4.2.3. Table 5-2 lists inputs for the coalescence module, along with ranges of applicability for validation and the corresponding technical bases for those values. Module validation is further detailed in the xLPR Module Validation Report for Coalescence.

Table 5-2. Range of Applicability for Coalescence Inputs

Input Description	Range of Applicability	Technical Basis
Number of cracks represented	0-200	Engineering judgment; any number of cracks can be evaluated by the coalescence module, provided other configuration inputs satisfy those ranges described below.
Crack Type array	All crack types	Two surface cracks as well as two idealized TW cracks are explicitly validated in the coalescence MVR. Engineering judgment applied to extend validity to all crack type combinations.
Crack Depth array	0 – thickness [m]	Laboratory data for surface crack interaction; higher-order analytical modeling for TW crack ligament collapse; engineering judgment to fill in ranges required for use of coalescence module in xLPR framework.
Crack Center Location array	0-2π [rad]	
Half-Crack ID Length array	0-π*inner radius [m]	
Half-Crack OD length array	0-π*outer radius [m]	
Crack Orientation array	1 (circumferential cracks)	Only circumferential cracks are addressed by the coalescence MVR.
Component Inside Radius	Positive values	Component geometry used in module validation, extended using engineering judgment as crack interaction effects depend on relative crack and pipe dimensions, not absolute values for inside radius or wall thickness.
Component Thickness	Positive values	
Coalescence Direction	1 or 2	Engineering judgment; as long as no more than two adjacent cracks coalesce at any given integration step, both values are guaranteed to produce the same answer. Multiple coalescences of adjacent cracks during a single integration step are rare, as can be confirmed with the 300-class warning of the coalescence module.
Surface Crack Coalescence Distance Rule Value	2 (Coalescence distance to maximum depth ratio)	Engineering judgment; crack interaction effects should be a function of crack depths.
Surface Crack Coalescence Distance Rule Modifier	0.0 - 0.75	Derived from laboratory data presented in [49]. Valid within the precision of available information.
TW Crack Coalescence Distance Rule Modifier	0 – 20 [in]	Derived from analytical model presented in [51]. Valid within the precision of available information.
Coalescence Depth Rule Value	1 (use maximum depth)	Rule for combining two surface cracks as per ASME Boiler and Pressure Vessel Code Section XI [3].

6. RECOMMENDATIONS FOR FUTURE WORK

This section identifies several areas for improvement within the context of crack growth and coalescence that may be considered as part of efforts to develop future versions of xLPR.

6.1 PWSCC Growth Rates

6.1.1 Refinements to Alloy 600/82/182 PWSCC Models

Refinements and extensions of the existing Alloy 600/82/182 PWSCC CGR models are desired for several areas. Many of these areas are being investigated as part of the EPRI Expert Panel on PWSCC Growth. For instance:

- *Stress intensity factor dependency*: The currently implemented stress intensity factor dependency has been developed from data that do not generally represent low (<15 to 20 MPa√m) or high (>80 MPa√m) values. Additional data may lead to insights that require a different model form, e.g., a plateau in CGR above a certain threshold. Alternatively, additional data may simply help refine the parameter values for the currently implemented model forms, e.g., data may refute the stress intensity factor threshold currently recommended for Alloy 600.

- *Hydrogen dependency*: Currently, the Alloy 82 hydrogen model parameters recommended are based on a database consisting of mostly Alloy 182 data. Additional laboratory data and/or further analysis could improve the representation of hydrogen dependency for Alloy 82. Furthermore, additional analysis is required to recommend a hydrogen dependency for the Alloy 600 CGR (including how other parameters and uncertainties should vary with the inclusion of the hydrogen dependency).

- *Mechanical properties*: The "hybrid model" published by EPRI includes explicit treatment of material yield stress for PWSCC CGR prediction. Provided yield stress can be estimated sufficiently accurately for in-service components, it may reduce overall uncertainty to implement the hybrid model (and refit PWSCC CGR model parameters and uncertainties).

- *Cold work*: PWSCC growth is known to be dependent on the level of material cold work. Cold work tends to introduce plasticity and grain misorientation that may aid growth. As such, it may be appropriate to develop a cold work dependency or develop different models for different ranges of cold work. However, in the case of PWSCC of thick-wall Alloy 600 wrought material, based on laboratory CGR data such as [43], cold work levels greater than that expected for most components of interest are necessary for the cold work to result in a substantial acceleration of the CGR.

- *Heat treatment*: It may be useful to include the effect of post-weld heat treatment of adjacent carbon/low-alloy steel material on the material dependence of the CGR of Alloys 600/82/182. For instance, French researchers (Le Hong et al. [54]) have recommended an improvement factor of 2.0 when modeling the PWSCC CGR for Alloy 182 exposed to post-weld heat treatment of adjacent carbon/low-alloy steel material.

- *Material interfaces*: Crack growth prediction is complicated in regions near weld material interfaces due to thermally altered mechanical properties and the potential for dilution in composition. The xLPR Version 2.0 program does not account for the complex variation of

material properties that exists at weld material interfaces, e.g., base metal heat affected zone (HAZ) and weld metal dilution zone. Instead, for example, the growth of a crack tip near the interface of a weld metal and a base metal, but still in the weld metal, would be predicted with the weld metal model; immediately after the crack tip extends into the base metal, growth would be predicted with the base metal model. While a specific weld interface / dilution zone model has not been developed, plant PWSCC experience for piping butt weld locations has not indicated any apparent preference for cracking to occur in the Alloys 82/182 weld metal close to interfaces with lower-chromium materials. The nominal chromium level of Alloy 182 weld metal, which is very similar to that for Alloy 600, is sufficiently low to make Alloy 182 potentially susceptible to relatively high rates of PWSCC growth.

- *Initiation-growth correlation*: Currently, xLPR Version 2.0 includes the ability to correlate susceptibility to PWSCC initiation and PWSCC growth; however, with the current state of knowledge, no precise value is recommended for this correlation. This correlation can be important for assessing plant risks because it tends to result in relatively high CGRs for the earliest initiating cracks. Carefully planned laboratory experiments may help quantify this correlation.

6.1.2 Other SCC Models

In addition to refinement of the CGR models for PWSCC of Alloys 600/82/182/132 in PWR environments, it may be useful to develop CGR models for other materials and other environments. The hope is that such models would be accommodated by the currently implemented model form ([Eqn. 3-1]), but alternative model forms may be required. Some specific conditions of interest are noted below:

- *Alloy 690 and associated weld metals*: After Alloy 600 and its associated weld metals, PWSCC CGR models are desired for Alloy 690 and its associated weld metals (e.g., Alloy 52, 152, and variants). There are efforts underway within the EPRI Expert Panel on PWSCC Growth to develop such models.

- *BWR environments*: As xLPR progresses to take on a more diverse set of component types, it may be required to implement SCC CGR models for BWR environments. For instance, IGSCC CGR models for SS have been developed from laboratory data and could be implemented.

6.2 Fatigue Crack Growth Rates

6.2.1 Updated Fatigue Crack Growth Relations for Austenitic SS

The fatigue CGR relations for austenitic SS discussed in Section 2.3.3 are largely based on work by Mills [24] and Rev. 2 of Code Case N-809 [55]. Code Case N-809 [55] has been revised further [45] since the implementation of the fatigue CGR module for xLPR Version 2.0, and the resulting updates in the module are described here.

The material groupings for the SS alloy effect were changed to:

$$f_{alloy} = \begin{cases} 9.10*10^{-9} & \text{304 and 316} \\ 1.39*10^{-8} & \text{304L, 316L, and 304LE} \end{cases}$$

[Eqn. 6-1]

Also, the upper limit of 2000 seconds for loading rise time in [Eqn. 2-22] was eliminated.

6.2.2 Enhancements to Probabilistic Model for Nickel-Based Alloys

As discussed in Section 2.3.2, there is considerable scatter in the environmental effects on fatigue CGR for nickel-based alloys in reactor environments. The fatigue CGR module developed for xLPR Version 2.0 accounts for uncertainty in the environmental effect using a distributed input for the environmental factor. This model could be improved in a later version of xLPR by implementing an environmental factor whose dispersion could vary with the fatigue CGR prediction in air. Specifically, good agreement with data scatter has been achieved using a log-normal distribution with a median of 4.4×10^{-7} $(m/cyc\text{-}s)^{1\text{-}0.33}$ and a log-σ parameter determined as follows:

$$\log\text{-}\sigma = \begin{cases} 0 & CGR_{air} > 10^{-8} \\ -2.4 - 0.3 \log_{10}(CGR_{air}) & 10^{-12} < CGR_{air} < 10^{-8} \\ 1.2 & CGR_{air} < 10^{-12} \end{cases}$$

[Eqn. 6-2]

6.2.3 Material-Specific Stress Intensity Factor Range Threshold

The current xLPR model uses the same fatigue stress intensity factor range threshold model, irrespective of material. While this model has been validated as acceptable across different materials, there are efforts underway to develop models from material-specific stress intensity factor range threshold testing for ASME Section XI. These models should be consulted for future revisions of the xLPR program.

6.2.4 Future Validation Efforts

The validation performed for the fatigue CGR models was based predominantly on alternative equation or software predictions. In some cases, these alternative predictions were not independent from the development efforts underlying the xLPR fatigue CGR models. For future validation efforts, additional laboratory fatigue CGR data—independent from model development—is needed for validation that is more thorough.

Alternatively, review of in-service examination reports may lead to instances in which cracks verified to be advancing by fatigue were left in service for one or more cycles, thus allowing some estimation of fatigue CGR in field conditions. To the extent that these can be identified, they should be used to bolster the fatigue CGR model validation.

6.3 Crack Growth and Coalescence

6.3.1 Complex Growth Prediction

Crack growth predictions—not to mention stress intensity factor, crack opening displacement, and stability predictions—within xLPR Version 2.0 rely on a set of simplified crack and component geometries. More complex geometries constitute extensive development efforts, but could improve the overall fidelity of xLPR. For instance:

- *Component geometry*: xLPR Version 2.0 focuses on a dissimilar metal weld geometry, represented by three material groups, each an annular shape, adjacent to one another. Weld overlay or onlay may be modeled with a fourth material group. It is expected that later versions of xLPR will introduce more complicated geometries, e.g., to allow for through-wall material gradients. Furthermore, geometries are expected to be developed to represent other susceptible components such as J-groove welds used for head penetration nozzles.

- *Asymmetric crack growth:* All three idealized crack shapes in xLPR Version 2.0 are symmetric, precluding the possibility of asymmetric growth that may arise, for instance, from off-axis bending loads, within-weld growth susceptibility variation, etc. While idealized (non-complex) crack shapes will probably remain necessary in later versions, it is recommended that asymmetric variations be developed.

- *Non-coplanar cracks*: All circumferential cracks in Version 2.0 of xLPR are assumed to be coplanar, while in reality, circumferential cracks may be offset. As discussed in Section 4.3, the conservatism of this modeling convention is difficult to determine for any given case. While a coordinated effort between the Computational Framework and Models Groups would be required to eliminate the coplanar assumption, this would improve the predictive fidelity of xLPR.

- *Subsurface flaws:* xLPR Version 2.0 does not include initiation, growth, coalescence, or stability predictions for subsurface flaws. Subsurface flaws may arise from various mechanisms (e.g., lack of fusion of an overlay) and can influence plant risks. A coordinated effort between the Computational Framework and Models Groups would be required to introduce treatment for subsurface flaws.

6.3.2 Crack Coalescence

The prediction of crack coalescence in later versions of xLPR could be improved, for instance:

- *Crack interaction*: Currently, the K-solutions modules do not account for the interaction of stress fields for adjacent cracks, which can lead to increased stress intensity factors. Instead, this interaction, which can lead to accelerating crack growth for cracks in close proximity, is simulated by the coalescence module using simple modeling conventions. More precise predictions would be achieved using fracture mechanics based solutions implemented in the K-solutions modules.

  Alternatively, recent validation work [50] has suggested that the secondary determinant for crack interaction (after ligament length) is crack length. Revisions to the simple modeling conventions implemented by the current coalescence module to introduce crack length-dependence could significantly improve the simulation of crack interaction.

- *Ligament collapse*: Currently, the stability modules do not account for the collapse of ligaments between two cracks. Instead, this collapse is simulated by the coalescence module using a distributed input variable to define the ligament length at the time of collapse. More precise predictions would be achieved using fracture mechanics based solutions implemented in the stability or coalescence modules.

  Alternatively, recent validation work (based on analytical modeling) has suggested that ligament length at the time of collapse is roughly one-to-one with crack length (for cracks of roughly the same size). Revisions to the simple modeling conventions implemented by the current coalescence module to introduce crack length-dependence could significantly improve the simulation of ligament collapse.

- *Axial crack coalescence*: The interaction of axial and circumferential cracks is ignored by the current coalescence module. Coalescence modeling could be updated to account for the effects of the intersection of orthogonal cracks; however, the treatment of mixed orientation cracks is likely more of a challenge for other modules.

- *Micro-fissure coalescence*: The current coalescence module accounts for the combination of macro-sized cracks of engineering significance. It is not applicable to simulation of micro-fissure coalescence, a step commonly considered to be part of the initiation process. The simulation of micro-fissure coalescence is considered a potential area of future work for the Initiation Subgroup.

7. REFERENCES

1. G. White, *xLPR Crack Growth Subgroup Work Plan,* xLPR-WP-MG-CG Version 1.0, March 2012.

2. *Materials Reliability Program (MRP) Crack Growth Rates for Evaluating Primary Water Stress Corrosion Cracking (PWSCC) of Thick-Wall Alloy 600 Materials (MRP-55) Revision 1*, EPRI, Palo Alto, CA: 2002. 1006695. [available at www.epri.com]

3. ASME Boiler and Pressure Vessel Code, Section XI, Rules for Inservice Inspection of Nuclear Power Plant Components, 2010 Edition.

4. P. M. Scott, "An Analysis of Primary Water Stress Corrosion Cracking in PWR Steam Generators," Presented at *NEA/CSNI Specialist Meeting on Operating Experience with Steam Generators*, Brussels, Belgium, September 16-20, 1991.

5. *Materials Reliability Program: Technical Bases for the Chemical Mitigation of Primary Water Stress Corrosion Cracking in Pressurized Water Reactors (MRP-263)*, EPRI, Palo Alto, CA: 2009. 1019082. [Proprietary]

6. *Materials Reliability Program: Topical Report for Primary Water Stress Corrosion Cracking Mitigation by Surface Stress Improvement (MRP-335, Revision 1)*. EPRI, Palo Alto, CA: 2013. 3002000073. [available at www.epri.com]

7. xLPR-MVR-CGR-SCC, *xLPR Module Validation Report for PWSCC CGR Models*, Version 1.0, 2015.

8. B. Alexandreanu, et al., *Crack Growth Rates in a PWR Environment of Nickel Alloys from the Davis-Besse and V.C. Summer Power Plants*, NUREG/CR-6921, Argonne National Laboratory, ANL-05/55, November 2006. [NRC ADAMS Accession No. ML063520366]

9. *Materials Reliability Program: Crack Growth Rates for Evaluating Primary Water Stress Corrosion Cracking (PWSCC) of Alloy 82, 182, and 132 Welds (MRP-115)*, EPRI, Palo Alto, CA: 2004. 1006696. [available at www.epri.com]

10. *Models and Inputs Selected for Use in the xLPR Pilot Study*. EPRI, Palo Alto, CA: 2011. 1022528.

11. *Materials Reliability Program: Probabilistic Assessment of Chemical Mitigation of Primary Water Stress Corrosion Cracking in Nickel-Base Alloys (MRP-307): Zinc Addition and Hydrogen Optimization to Mitigate Primary Water Stress Corrosion Cracking in Westinghouse Reactor Vessel Outlet Nozzles and Babcock & Wilcox Reactor Coolant Pump Nozzles*. EPRI, Palo Alto, CA: 2011. 1022852. [available at www.epri.com]

12. *Materials Reliability Program: Mitigation of PWSCC in Nickel-Base Alloys by Optimizing Hydrogen in the Primary Water (MRP-213)*, EPRI, Palo Alto, CA: 2007. 1015288. [available at www.epri.com]

13. D. S. Morton, S. A. Attanasio, E. Richey, and G. A. Young, "In Search of the True Temperature and Stress Intensity Factor Dependencies for PWSCC," *Proceedings of the 12th International Conference on Environmental Degradation of Materials in Nuclear Power Systems – Water Reactors*, Edited by T. R. Allen, P. J. King, and L. Nelson, TMS (The Minerals, Metals & Materials Society), 2005.

14. S. A. Attanasio and D. S. Morton, "Measurement of the Nickel/Nickel Oxide Transition in Ni-Cr-Fe Alloys and Updated Data and Correlations to Quantify the Effect of Aqueous Hydrogen on Primary Water SCC," *Proceedings of the 11th International Conference on*

Environmental Degradation of Materials in Nuclear Power Systems – Water Reactors, ANS, 2003.

15. *Materials Reliability Program: Mitigation of Stress Corrosion Crack Growth in Nickel-based Alloys by Optimization of Hydrogen in Primary Water (MRP-252)*, EPRI, Palo Alto, CA: 2008. 1016603. [Proprietary]

16. S. M. Bruemmer, J. S. Vetrano, and M. B. Toloczko, "Microstructure and SCC Crack Growth of Nickel-Base Alloy 182 Weld Metal in Simulated PWR Primary Water," *Proceedings of the 13th International Conference on Environmental Degradation of Materials in Nuclear Power Systems – Water Reactors*, Paper 0140, NACE, 2007.

17. *Materials Reliability Program: Resistance of Alloys 690, 52 and 152 to Primary Water Stress Corrosion Cracking (MRP-237, Rev. 1): Summary of Findings From Completed and Ongoing Test Programs Since 2004.* EPRI, Palo Alto, CA: 2008. 1018130. [available at www.epri.com]

18. *Materials Handbook for Nuclear Plant Pressure Boundary Applications (2010)*. EPRI, Palo Alto, CA: 2010. 1022344. [Proprietary]

19. P. L. Andresen, "SCC of Stainless Steels in Hot Water," *Contribution of Materials Investigations to Improve the Safety and Performance of LWRs, Proceedings of the International Symposium, Fontevraud VII*, SFEN, Avignon, France, Sep. 26-30, 2010.

20. *Materials Reliability Program: Stress Corrosion Cracking of Stainless Steel Components in Primary Water Circuit Environments of Pressurized Water Reactors (MRP-236)*, EPRI, Palo Alto, CA: 2007. 1015540. [Proprietary]

21. *Materials Reliability Program: Assessment of the Current Status and Completeness of Work on Inner and Outer Diameter Stress Corrosion Cracking of Austenitic Stainless Steels in PWR Plants (MRP-352)*, EPRI, Palo Alto, CA: 2013. 3002000135. [Proprietary]

22. J. M. Barsom and S. T. Rolfe, *Fracture and Fatigue Control in Structures, Applications of Fracture Mechanics*, 2nd Edition, Prentice-Hall, 1987.

23. ASME Boiler and Pressure Vessel Code Case N-643-2, *Fatigue Crack Growth Rate Curves for Ferritic Steels in PWR Water Environment,* Section XI, Division 1, Approved 5/4/2004.

24. W. J. Mills, as reported in "Fatigue Crack Growth Curves for Austenitic Materials in Water Environments," Task Group on Reference Crack Growth Curves, ASME Section XI Meeting, Seattle, Washington, February 2, 2011.

25. O. K. Chopra, W. K. Soppet, and W. J. Shack, *Effects of Alloy Chemistry, Cold Work, and Water Chemistry on Corrosion Fatigue and Stress Corrosion Cracking Alloys and Welds,* U.S. Nuclear Regulatory Commission Report, NUREG/CR-6721, April 2001.

26. Y. Nomura, H. Kanasaki, and K. Sakaguchi, "Fatigue Crack Growth Rate Curve for Nickel Based Alloys in PWR Environment," *Proceedings of the ASME 2007 Pressure Vessels and Piping Division Conference*, PVP2007-26186, San Antonio, Texas, July 2007.

27. R. C. Cipolla and W. H. Bamford, "Technical Basis for Code Case N-809 on Reference Fatigue Crack Growth Curves for Austenitic Stainless Steels in Pressurized Water Reactor Environments," *Proceedings of the ASME 2015 Pressure Vessels & Piping Conference*, PVP2015-45884, 2015.

28. W. J. Shack, *Material Science and Technology Division Light-Water Reactor Safety Research Program. Volumes 1-4*. U.S. Nuclear Regulatory Commission Report, NUREG/CR-3689, July 1984 – October 1984.

29. W. J. Shack, et al., *Environmentally Assisted Cracking in Light Water Reactors. Annual Report October 1983 – September 1984*. U.S. Nuclear Regulatory Commission Report, NUREG/CR-4287, June 1985.

30. W. J. Shack, O. K. Chopra, et al., *Environmentally Assisted Cracking in Light Water Reactors Semiannual Reports*. U.S. Nuclear Regulatory Commission Report, NUREG/CR-4667.

31. W. J. Shack, *Light-Water Reactor Safety Materials Engineering Research Programs. Quarterly Progress Report. Volumes 1-3*. U.S. Nuclear Regulatory Commission Report, NUREG/CR-3998, October 1984 – October 1985.

32. W. J. Shack, *Light-Water Reactor Safety Materials Engineering Research Programs. Quarterly Progress Report. Volume 1*. U.S. Nuclear Regulatory Commission Report, NUREG/CR-4490, March 1986.

33. B. C. Syrett and R. Pathania, "EDEAC-PC Cracking of Structural Materials in Nuclear Environments. User's Manual," EPRI Project 8002-19, December 1992.

34. D. O. Harris, E. Y. Lim, and D.D. Dedhia, "Probability of Pipe Fracture in the Primary Coolant Loop of a PWR Plant, Vol. 5: Probabilistic Fracture Mechanics Analysis," U.S. Nuclear Regulatory Commission Report, NUREG/CR–2189, Vol. 5, August 1981.

35. E. D. Eason, E. E. Nelson, and G.B. Heys, "Fatigue Crack Growth Rate of Medium and Low Sulfur Ferritic Steels in Pressurized Water Reactor Environments," *Pressure Vessel and Piping Codes and Standards 2003*, PVP1003-1776, pp.123-134, 2003.

36. E. D. Eason, E. E. Nelson, and J. D. Gilman, "Report No. 3: Technical Basis for a Revised Fatigue Crack Growth Rate Reference Curve for Ferritic Steels in Light Water Reactor Environments," Welding Research Council Bulletin 404, August 1995.

37. E. D. Eason and E. E. Nelson, *Analysis of Fatigue Crack Growth Rate Data for A508 and A533B Steels in LWR Environments*, EPRI TR-102793, August 1993.

38. L. A. James, "Report No. 1: Environmentally-Assisted Cracking of Ferritic Steels in Aqueous Environments: An Interpretive Review," *Welding Research Council Bulletin 404*, August 1995.

39. E. D. Eason, E. E. Nelson, and J. D. Gilman, "Modeling of Fatigue Crack Growth Rate for Ferritic Steels in Light Water Reactor Environments," *Nuclear Engineering and Design*, Vol. 184, pp. 89-111, 1998.

40. ASME Boiler and Pressure Vessel Code, Section XI, Rules for In-service Inspection of Nuclear Power Plant Components, 2004 Edition, Appendix A, Article A-4300.

41. D. Rudland, D.J. Shim, and S. Xu, "Simulating Natural Axial Crack Growth in Dissimilar Metal Welds due to Primary Water Stress Corrosion Cracking," *Proceedings of the ASME 2013 Pressure Vessels & Piping Division Conference*, PVP2013-97188, Paris, France, July 2013.

42. D. Rudland, *xLPR Version 2.0 Stress Requirements,* xLPR-TR-Stress.docx, 2015.

43. W. C. Moshier and C. M. Brown, "Effect of Cold Work and Processing Orientation on Stress Corrosion Cracking Behavior of Alloy 600," *Corrosion*, Vol. 56, No. 3, NACE International, 2000.

44. D. Gomez-Briceño, J. Lapeña, M. Garcia-Redondo, L. Castro, F. J. Perosanz, K. Ahluwalia, and J. Hickling, "Crack Growth Rate in the HAZ of Alloy 600/182," *Proceedings of the*

International Symposium Fontevraud 7 on Contribution of Materials Investigations and Operating Experience to LWRs' Safety, Performance and Reliability, SFEN, 2010.

45. ASME Boiler and Pressure Vessel Code Case N-809, *Reference Fatigue Crack Growth Rate Curves for Austenitic Stainless Steels in Pressurized Water Reactor Environment*, Rev. 6, Approved 12/8/2014.

46. B. Alexandreanu, O. K. Chopra, and W. J. Shack, *Crack Growth Rates and Metallographic Examinations of Alloy 600 and Alloy 82/182 from Field Components and Laboratory Materials Tested in PWR Environments*, U.S. Nuclear Regulatory Commission Report, NUREG/CR-6964, May 2008.

47. R. Parkins and P. Singh, "Stress Corrosion Crack Coalescence," *Corrosion*, Vol. 46, No. 6, 1990.

48. O. Calonne, L. Fournier, P. Combrade, P. Scott, and P. Chou, "Experimental Study of Short Crack Coalescence in Nickel-Base Alloys in PWR Primary Water," *Proceedings of the 15th International Conference on Environmental Degradation of Materials in Nuclear Power Systems – Water Reactors*, TMS, 2011.

49. B. Bezensek, and J. W. Hancock, "The Re-characterization of Complex Defects Part I: Fatigue and Ductile Tearing," *Engineering Fracture Mechanics*, Vol. 71, 2004.

50. K. Azuma, Y. Li, and K. Hasegawa, "Evaluation of Stress Intensity Factor Interactions between Adjacent Flaws with Large Aspect Ratios," *Proceedings of the ASME 2015 Pressure Vessels & Piping Conference*, PVP 2015, July 2015.

51. D. Chang, and A. Kotousov, "A Strip Yield Model for Two Collinear Cracks in Plates of Arbitrary Thickness," *International Journal of Fracture*, Vol. 176, Issue 1, pp. 39-47, 2012.

52. N. Huh, et al., "Guidance on a Defect Interaction Effect for In-Plane Surface Cracks Using Elastic Finite Element Analysis," *Proceedings of the ASME 2008 Pressure Vessels and Piping Division Conference*, PVP2008-61405, Chicago, Illinois, July 2008.

53. K. Suga, K. Miyazaki, et al., "Interaction Effect Evaluation of Multiple Through Cracks in Ductile Fracture Process," *Proceedings of the ASME 2012 Pressure Vessels and Piping Conference*, PVP2012-78208, Toronto, Canada, July 2012.

54. S. Le Hong, J. M. Boursier, C. Amzallag, and J. Daret, "Measurements of Stress Corrosion Cracking Growth Rates in Weld Alloy 182 in Primary Water of PWR," *10th International Conference on Environmental Degradation of Materials in Nuclear Power System - Water Reactors*, NACE International, 2002.

55. ASME Boiler and Pressure Vessel Code Case N-809, *Reference Fatigue Crack Growth Rate Curves for Austenitic Stainless Steels in Pressurized Water Reactor Environment*, Rev. 2, Approved 11/7/2012.